THE
PHYSICAL REVIEW
A Journal of Experimental and Theoretical Physics Established by E. L. Nichols in 1893
VOL. 54, NO. 3 AUGUST 1, 1938 SECOND SERIES

The Cosmic-Ray Intensity at High Elevations in Northern Latitudes

T. H. JOHNSON
Bartol Research Foundation of the Franklin Institute, Swarthmore, Pennsylvania
(Received May 27, 1938)

Balloon flights with vertical coincidence counters for cosmic-ray measurements have been made at geomagnetic latitudes 56°N and 69°N. Within the accuracy of the measurements there is no further increase of intensity above 56°N at atmospheric depths greater than 2 meters of water.

THE airplane flights with an unshielded electroscope made by Bowen, Millikan and Neher[1] up to an elevation corresponding to an atmospheric depth of 4.5 meters of water showed about a twenty percent increase in cosmic-ray intensity between the magnetic latitudes 41°N and 54°N but from there on up to 63°N there was no further increase. Their failure to find a dependence upon latitude at these highest latitudes could have been interpreted either as an inability of rays of energy less than the 2.2 billion volt limit corresponding to 54° latitude to penetrate to the depth of 4.5 meters, or as an absence of such low energy rays in the primary cosmic-ray spectrum. If the knee at 40°N in the curve representing intensity at sea level *vs.* latitude were due to the stopping of the corresponding 6-billion volt rays in ten meters, and if range were proportional to energy, one would have expected the stopping power of the atmosphere at 4.5 meters depth to produce a knee at 50°N, and therefore no variation of intensity above 54°N could have been expected on either hypothesis. The same conclusion is reached by considering the effect of the soft component at this depth in the theory of Bhabha and Heitler.[2]

In view of the interesting suggestion of Vallarta[3] and Janossy[4] that the magnetic field of the sun might be sufficient to exclude these low energy radiations from the region within the earth's orbit, with the consequence that the cosmic-ray spectrum would possess a low energy limit other than that imposed by the earth's magnetic field, a series of balloon flights were planned and carried out in August and September 1937 in central Minnesota, 56°N, and in Churchill, Manitoba, 69°N. Vertical coincidence counters were used for the cosmic-ray measurements in order to realize shorter path lengths through the atmosphere, and the ultra-high frequency radio technique was employed for transmission of the data.[5] Each coincidence was transmitted as a dot and at regular intervals a series of dashes counted off the number of immersed taps on a mercurial barometer so that the exact times when the balloon passed through definite pressure intervals were recorded. The counters were 6 cm long by 1.2 cm in diameter and were placed horizontally

[1] I. S. Bowen, R. A. Millikan and H. V. Neher, Phys. Rev. **46**, 641 (1934).
[2] H. J. Bhabha and W. Heitler, Proc. Roy. Soc. **A159**, 432 (1937). A convenient table for calculation is given by L. W. Nordheim Phys. Rev. **53**, 694 (1938). The probability of a ray of energy greater than 10^8 ev appearing at a depth of 4.5 meters when one ray of 2.2×10^9 ev enters the atmosphere is about 0.05.
[3] M. S. Vallarta, Nature **139**, 839 (1937).
[4] L. Janossy, Zeits. f. Physik **104**, 430 (1937).
[5] For a fuller description of the experimental technique see T. H. Johnson, J. Frank. Inst. **223**, 218 (1937).

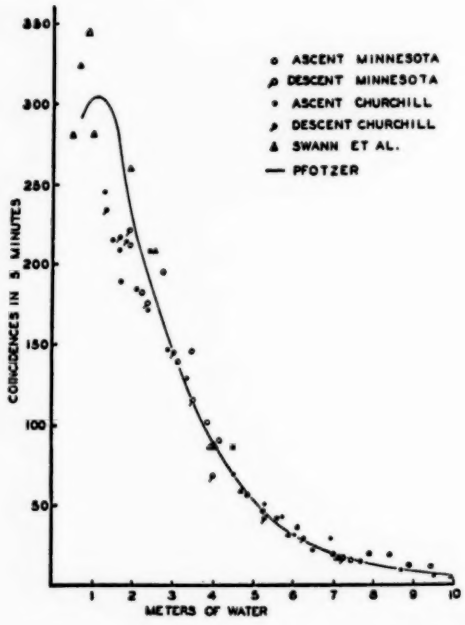

FIG. 1. Cosmic-ray intensities measured with vertical coincidence counters. Results in Churchill mag. lat. 69°N are compared with similar data at lower latitudes.

one above the other with a 2.5 cm separation between axes. In this configuration the coincidence rate at sea level was about 2 per minute. The counters were filled with 25 cm of a one to one mixture of neon and hydrogen and operated at about 1100 volts. The discharges were quenched with 300 megohm resistors and the plateau of uniform counting rate extended over such a wide range of overvoltage that it was possible to use a capacity multiplication of the B voltage for the operation of the counters without trouble from counter voltage variations. A multivibrator type of feedback circuit[6] was used for prolongation of the pulses from the coincidence selecting stage and this could be tripped off with such a small input of power that exceedingly short resolving times were realized; with the radiation intensity equal to that encountered in the stratosphere there was no appreciable alteration of the coincidence rate either from accidentals or from the inefficiency resulting from the high counting rate.

The shaded points in Fig. 1 indicate the numbers of coincidences recorded in five minute intervals on a flight made in Churchill, plotted against the mean pressure during the interval. The open points are the corresponding data for a flight in Minnesota with exactly similar apparatus. The curve represents the corrected data of G. Pfotzer[7] obtained at the latitude 52°N and the triangles represent the data of Swann, Locher and Danforth.[8] Both these and Pfotzer's data were obtained with triple coincidence counters in the vertical direction. They have been adjusted by suitable factors to bring about agreement in the central part of the curve.

The results indicate no increase of intensity with latitude north of Minnesota (56°N) up to an atmospheric depth of two meters of water. If the sea-level knee were attributable to absorption of rays of energy less than 6 billion volts then with proportionality between range and energy a knee at two meters depth could be expected at 60°N where, according to Lemaitre and Vallarta, 1.2-billion volt rays are excluded by the earth's field. Thus it would have been reasonable to expect an increase of intensity at Churchill over that found at Minnesota equal to the contribution of rays in the energy range between 1.2 and 1.5 billion volts. The fact that no such increase was found favors the interpretation that there is very little intensity in the primary spectrum within this range of energies,[9] but in view of the experimental inaccuracies which may be judged by the dispersion of the points about a smooth curve and especially of the uncertainties in present knowledge of the stopping power of air for these low energy rays, it is impossible to insist too strongly upon this interpretation. It is possible that coincidence counter flights to still higher elevations would be able to give a more conclusive answer to this question.

The writer wishes to acknowledge the financial assistance given this work by the Carnegie Institution of Washington, as well as the assistance of various individuals. Mr. John Marshall, Jr., cooperated in making the flights. The work in Minnesota was carried out with the help of the Minnesota Department of Conservation through the courtesy of G. M. Conzet. Mr. J. Patterson of the Canadian Meteorological Service helped in arranging the Churchill flights.

[6] T. H. Johnson, Rev. Sci. Inst. **9**, 218 (1938).

[7] G. Pfotzer, Zeits. f. Physik **102**, 23 (1936).

[8] W. F. G. Swann, J. Frank. Inst. **224**, 415 (1937).

[9] This conclusion is in agreement with the results presented at the Washington Meeting of the American Physical Society by Bowen, Millikan and Neher.

I. General Theory of the Earth's Shadow Effect of Cosmic Radiation

E. J. SCHREMP*
Massachusetts Institute of Technology, Cambridge, Massachusetts

(Received April 14, 1938)

An inquiry is made into the fundamental mode of origin of the allowed cone of cosmic radiation introduced by Lemaitre and Vallarta. Two kinds of allowed cone are distinguished. One of these, that discussed by Lemaitre and Vallarta, postulates the presence of an impenetrable earth; for it all forbidden directions are due to the earth's shadow effect. The second type of allowed cone, applicable in the first approximation to such problems as that of the sun's magnetic field, does not postulate the presence of an impenetrable earth; for it all forbidden directions are associated with bounded charged particle orbits. The general topological features of each of these kinds of allowed cone, and their relationship to one another, are described.

1

WE shall be concerned with the reduced motions of a charged particle in the meridian plane of a magnetic dipole.[1] These motions may be classified into three types: (1) completely bounded motions which never attain an infinite distance from the dipole; (2) semi-bounded motions which are bounded in the future but not in the past, or in the past but not in the future; and (3) completely unbounded motions which are bounded neither in the past nor in the future. In this classification it is assumed that an impenetrable earth is absent.

It is convenient to introduce the notion of an orbital section, by which we shall mean any segment of an orbit joining two consecutive points at which the function[2] $P(x, \lambda; \gamma_1)$ attains relative minima. Any orbital section at both ends of which the orbit returns toward the dipole will be termed reentrant. If an entire orbit contains n reentrant sections it will be called an n-reentrant orbit; if it contains no reentrant sections it will be called a nonreentrant orbit. All orbits for which n is finite or zero must be completely unbounded. Orbits for which n is infinite may be either bounded or unbounded.

Two periodic orbits, discovered by Störmer[3] and studied by Lemaitre and Vallarta,[4, 5] are intimately connected with the reentrant orbits defined above. Lemaitre and Vallarta[4] first estimated the range of simultaneous existence of these two periodic orbits to be the interval[2] $0.783 \leqq \gamma_1 \leqq 1$. Lemaitre[5] subsequently refined this interval to $0.78856 \leqq \gamma_1 \leqq 1$. We shall henceforth speak of them as the two principal periodic orbits.

2

In the interval $0.78856 \leqq \gamma_1 \leqq 1$ in which they simultaneously exist, the two principal periodic orbits form left- and right-hand limits (with respect to the coordinate[2] x) of the family of all reentrant sections normal to the equator, as may be seen from certain results of Störmer.[6] Since no orbital section normal to the equator and outside this interval of x may be reentrant, it follows *a fortiori* that no other section outside this interval may be reentrant. Moreover, through every equatorial point within this interval of x, and for a given γ_1 in the above-mentioned range, there passes a singly infinite pencil of reentrant sections, delimited on the left and right by two symmetrical self-reversing reentrant sections making angles[2] η and $-\eta$ with the equator. These facts lead to theorem 1: *For each γ_1 in the interval $0.78856 \leqq \gamma_1 \leqq 1$ the totality of reentrant orbits may be generated by moving the equatorial*

* At present at Washington University, St. Louis, Missouri.

[1] C. Störmer, Zeits. f. Astrophys. **1**, 237 (1930), has shown that the actual space trajectories may be reduced to motions in the meridian plane. It is the latter which are dealt with in the Lemaitre-Vallarta theory of the allowed cone. See for instance G. Lemaitre and M. S. Vallarta, Phys. Rev. **49**, 719 (1936).

[2] For the necessary definitions see G. Lemaitre and M. S. Vallarta, Phys. Rev. **49**, 719 (1936).

[3] C. Störmer, Zeits. f. Astrophys. **1**, 237 (1930).

[4] G. Lemaitre and M. S. Vallarta, Phys. Rev. **43**, 87 (1933).

[5] G. Lemaitre, Ann. de la Soc. Sci. de Bruxelles **A54**, 194 (1934). Recent work by O. Godart, Ann. de la Soc. Sci. de Bruxelles **A58**, 27 (1938), indicates that the value 0.78856 should be revised to 0.788541.

[6] See reference 3, Fig. 9.

point and its associated pencil of reentrant sections from the inner to the outer principal periodic orbit.

By the same reasoning one is led to theorem 2: *For each γ_1 in the interval $\gamma_1 > 1$ the totality of reentrant orbits may be generated by moving the equatorial point and its associated pencil of reentrant sections from the inner principal periodic orbit to the outer boundary curve $P(x, \lambda; \gamma_1) = 0$ of the bounded region of possible motions.* All such orbits are completely bounded, and of course n is infinite for them.

Together with Lemaitre's result[5] on the range of simultaneous existence of the two principal periodic orbits, theorem 1 leads to theorem 3: *In the interval $\gamma_1 < 0.78856$ no reentrant orbits, and hence no bounded orbits, exist.*

3

By theorem 3, for $\gamma_1 < 0.78856$ all orbits are completely unbounded. By theorem 2, for $\gamma_1 > 1$ all orbits are either completely bounded or completely unbounded according as they lie within the bounded or unbounded regions of possible motion. But by theorem 1, for $0.78856 \leqq \gamma_1 \leqq 1$ bounded and unbounded orbits may coexist.

The problem of ascertaining the relative distributions of bounded and unbounded orbits has been completely solved by theorems 2 and 3 for all values of γ_1 outside the interval $0.78856 \leqq \gamma_1 \leqq 1$. The resolution of this problem in the remaining interval requires an application of point set theory. Using such methods the writer has proved theorem 4: *In the interval $0.78856 \leqq \gamma_1 \leqq 1$ the set of all bounded orbits is nowhere dense on the whole manifold of motions.* After several attempts to extend these methods it has been further conjectured that this set is of zero measure.

By an extension of a theorem due to Poincaré[7] one is led to theorem 5: *All bounded orbits are stable in the sense of Poisson; i.e., they return infinitely often to the neighborhood of their initial state.* The proof of this theorem rests on theorems 1 and 2. We shall give a physical interpretation to this theorem in Section 5.

A detailed mathematical treatment of these matters will be published elsewhere.

[7] H. Poincaré, *Méthodes nouvelles de la mécanique céleste*, Vol. 3, chap. 26. See also G. D. Birkhoff, *Dynamical Systems*, American Mathematical Society Colloquium Publications Vol. IX, p. 189 ff.

4

Having thus determined the relative distributions of bounded and unbounded orbits for all values of γ_1 we find it now possible to give a rather complete description of the structure of the allowed cone in the absence of the earth's shadow effect. In this case the total allowed cone has three distinct parts: (1) the cone for $\gamma_1 < 0.78856$ in which all directions are allowed (all orbits are completely unbounded); (2) the spherical segment $0.78856 \leqq \gamma_1 \leqq 1$ in which all directions are allowed (all orbits are completely unbounded) except for a nondense set of forbidden loci (corresponding to the nondense set of bounded orbits); (3) the cone for $\gamma_1 > 1$ (the Störmer cone[8]) in which all directions are forbidden (all orbits are completely bounded).

These considerations, in which the property of boundedness and not the earth's shadow effect accounts for forbidden directions, may be applied to such problems as that of the allowed cone in the magnetic field of the sun, introduced by Janossy[9] and, independently, by Vallarta.[10] In this problem of the sun's allowed cone at the earth, the foregoing considerations evidently neglect the relatively small shadow effects arising from the presence of the earth and sun in the sun's own magnetic field. The inclusion of these small shadow effects would slightly augment the forbidden directions provided for above by the criterion of boundedness alone.

5

Lemaitre[11] has defined as orbits of the first kind all those orbits which are asymptotic (on the side toward the dipole) to the outer principal periodic orbit. By means of them Lemaitre and Vallarta have shown the existence of a main cone[4, 12] within which all directions are allowed, and of a region of penumbra[12] between the main cone and the Störmer cone within which some directions are allowed and others are forbidden.

Their result holds both for the case of the allowed cone in the absence of an impenetrable

[8] C. Störmer, Publ. Univ. Obs. Oslo, No. 11, p. 10 (1933).
[9] L. Janossy, Zeits. f. Physik **104**, 430 (1937).
[10] M. S. Vallarta, Nature **139**, 839 (1937).
[11] G. Lemaitre, Ann. de la Soc. Sci. de Bruxelles **A54**, 162 (1934).
[12] G. Lemaitre and M. S. Vallarta, Phys. Rev. **49**, 720 (1936).

earth and for the case of the allowed cone in the presence of an impenetrable earth, but with considerable differences in the character of the penumbra in the two cases. For in the first case the region of penumbra is densely filled with allowed directions, as we have seen in Section 4; while in the second case the region of penumbra is no longer densely filled with allowed directions but may include alternating allowed and forbidden regions ranging from infinitesimal to finite size, as we shall see in Section 7.

In the case where an impenetrable earth is absent, orbits of the first kind may be associated with at least a part of the nondense set of bounded orbits referred to above. For by an immediate corollary to theorem 1 every orbit of the first kind is a transition orbit between two orbital classes having distinct values of n. In any particular instance where one of these values of n is infinite the orbit of the first kind concerned may actually define one member of the above-mentioned nondense set of forbidden loci.

In the case where an impenetrable earth is present, orbits of the first kind may again be generators of the allowed cone. But here they acquire this property as a result of a discontinuous shadow effect. For any asymptotic half-orbit reaching a given point on the earth may be viewed as the limit of an infinite sequence of self-reversing reentrant half-orbits, the reversal points of which form an infinite sequence of points lying on the upper and lower branches of the boundary curve $P(x, \lambda; \gamma_1) = 0$, and approaching the two reversal points of the outer principal periodic orbit as limit points.[13] Since every such self-reversing orbit must have emanated from the earth in one sense before it reached the earth in the opposite sense, the direction of incidence for every such orbit must be forbidden in consequence of the earth's shadow effect. Since this argument applies to every orbit in this sequence, including the limiting asymptotic orbit, one is led to the following theorem 6: *If any half-orbit of the first kind, possessing an arbitrary number of reentrant sections, is a limit on one side of half-orbits coming from infinity unobstructed by the earth, then it must be a limit on the other side of self-reversing half-orbits which are blocked by the earth.* It is thus evident that immediately beyond every boundary formed by orbits of the first kind, whether it be a boundary of the main cone or of some allowed region of the penumbra, there must exist an enveloping forbidden region of at least infinitesimal size, associated with orbits emanating from, or in the shadow of, the earth.[14] It is further evident that the criterion for a discontinuous shadow effect, by which we have ascertained if any given orbit of the first kind may be a generator of the allowed cone, includes as a very special case the criterion of boundedness set forth in the preceding paragraph.

It is interesting to note that, while the condition of boundedness is essential for the existence of the forbidden directions discussed in Section 4, the criterion of boundedness may be dispensed with entirely in the present case where an impenetrable earth is postulated, without in any way affecting the resulting form of the allowed cone. For in the latter case theorem 5 leads to the result that every bounded orbit reaching a given point of the earth must have previously emanated from the earth. That is, wherever in the latter case the criterion of boundedness may be applied, the criterion of shadow also applies. However, since the assumption that all cosmic-ray particles originate at infinity is at present the commonly accepted one, we are retaining here the point of view that the Störmer cone and the nondense set of directional loci discussed in Section 4 are forbidden irrespectively of the earth's shadow effect; although there is the alternative possibility of assuming cosmic-ray particles to originate also at finite points, and therefore of abandoning the criterion of boundedness.

6

Lemaitre[11] has defined as orbits of the second kind another class of orbits which may be generators of the allowed cone. These orbits differ from orbits of the first kind in that they are associated with a continuous shadow effect. Their definition, which of course must require the presence of an

[13] G. Lemaitre, reference 11, p. 171, has in another connection shown that certain asymptotic orbits are limits of a sequence of periodic orbits.

[14] G. Lemaitre, reference 11, p. 165, has stated that an asymptotic orbit may separate orbits coming from infinity from other orbits coming from the earth, and may therefore be a generator of the allowed cone.

impenetrable earth, will be restated here. Consider any general half-orbit reaching a given point on the earth and having a finite number n of reentrant sections. Such an orbit will have at least n minima and maxima of x. If none of its minima lies within the earth, this half-orbit will have come unobstructed from infinity and its direction of incidence at the given point will be allowed. If any of its minima lies within the earth, the orbit will be in shadow and its direction of incidence at the given point will be forbidden. Between these two cases there may exist a continuous transition, marked by the presence of a half-orbit whose lowest minimum of x is tangent to the earth. All such orbits are termed orbits of the second kind.

We have stated above that an n-reentrant half-orbit reaching a given point of the earth will have at least n minima and maxima of x. The excess minima and maxima, when they exist, arise in much the same way for all half-orbits, independently of the number of reentrant sections possessed by them. One is thus led to distinguish a wide class of orbits of the second kind which are tangent to the earth at one of these excess minima. These orbits will be termed simple orbits of the second kind. Since they may have an arbitrary number of reentrant sections, they may be common generators of the main cone and of all allowed penumbral regions. The continuous locus of their directions of incidence at a given point will be called the simple shadow cone. In the following paper a complete analysis is made of this cone.

7

A few simple considerations of the topology of orbits having various numbers n of reentrant sections readily reveal the existence of distinct families of such orbits, the topological structure of which principally depends on the number n. These considerations further show that all such families having finite values of n form whole continua of similar orbits. The simplest example of this fact is the well-known family of non-reentrant half-orbits associated with the main cone. Such considerations led the writer three years ago to infer the existence, for suitable energies and at suitable points on the earth, of allowed directional regions in the penumbra ranging from infinitesimal to finite size.[15] The existence of the infinite sequence of self-reversing reentrant orbits described in Section 5 enables one in particular to infer the existence of a corresponding infinite sequence of alternating allowed and forbidden regions expanding outward from the main cone, and ranging from infinitesimal to finite size. Not only is it characteristic of the main cone to be bordered by such an infinite sequence of forbidden and allowed regions, but it is characteristic of each allowed member of this sequence, and in fact of any penumbral allowed region, to be similarly bordered. These qualitative inferences, particularly with regard to the existence of finite allowed penumbral regions, have recently been confirmed by Dr. R. Albagli, whose quantitative results on the structure of the penumbra will be published shortly.

It is possible to give a more definitive form to the necessary condition mentioned above for the existence of allowed directional regions in the penumbra. Clearly this necessary condition applies only in the presence of an impenetrable earth, and then it may be expressed in the statement that there must exist reentrant half-orbits coming to a given point unobstructed by the earth. We shall see that not all points (x, λ) in the meridian plane (and hence not all energies and points on the earth) admit this condition for a given value of γ_1. In fact it is possible to establish the following theorem 7: *For any given γ_1 in the range $0.78856 \leqq \gamma_1 \leqq 1$ there exists an upper limiting value x^0 beyond which no point (x, λ) may be reached by reentrant orbits coming from infinity unobstructed by the earth.* Moreover theorem 1 indicates a direct method[16] for ascertaining this x^0 for each γ_1, which has been quantitatively applied by Dr. R. Albagli and will be described in more detail in her forthcoming paper. We shall give one proof[17] of theorem 7 here. Consider any

[15] G. Lemaitre, reference 11, p. 171, speaks of an infinite number of penumbral bands with a point of accumulation, approaching zero size at this point. These bands are again referred to by Lemaitre and Vallarta in their subsequent papers, e.g., Phys. Rev. **47**, 435 (1935); Phys. Rev. **49**, 720 (1936).

[16] As will be seen in the following proof of theorem 7, the values of x^0 may be found from a knowledge of the asymptotic family. This family has been generated, as a limiting case, in the course of a general program of generating reentrant orbits in accordance with theorem 1, undertaken by Dr. Albagli.

[17] The writer's original proof was constructed before theorem 1 had been established, and was based on certain

equatorial point lying between the two principal periodic orbits, and the pencil of reentrant sections generated at that point in accordance with theorem 1. This pencil of reentrant sections may be continued until a locus of first minima of x is reached. Now this locus of first minima has the following properties. As the equatorial point is moved continuously from the inner to the outer principal periodic orbit, there arises a continuous sequence of loci of first minima, bounded on the left by the locus of first minima of the asymptotic family and on the right by the inner principal periodic orbit. Let us identify the above-mentioned limiting value x^0 with the greatest value of x on the locus of first minima of the asymptotic family, and let us further consider the orbit tangent to the earth through any point (x, λ') for which $x \geqq x^0$. By the above results every such orbit, if reentrant at all, must be reentrant on both sides of this tangent point (x, λ'). Hence no point (x, λ) for which $x \geqq x^0$ may be reached by reentrant orbits coming from infinity and having all their minima outside the earth. This completes the proof. By use of the above-mentioned relation between x^0 and γ_1 it has been possible to restate theorem 7 in the following equivalent form: *For every point* (x, λ) *such that* $e^x/2\gamma_1 = r \geqq 0.414$ *there exists an upper limiting* $\gamma_1^0 \leqq 1$ *beyond which no penumbral allowed directions exist.*[18] From the foregoing discussion it may be seen in particular that all points (x, λ) outside the limiting periodic orbit[5] for $\gamma_1 = 0.78856$ (i.e., for which $r \geqq 0.70389$) have no allowed penumbral directions whatsoever.

Theorem 7 indicates that with decreasing latitude and increasing energy the penumbral region tends toward a limiting condition of complete darkness. Together with a few simple considerations of the force function $P(x, \lambda; \gamma_1)$ it indicates, conversely, that with increasing latitude and decreasing energy the penumbral region tends toward a limiting condition of complete light. Lastly, it indicates that for intermediate latitudes and energies the penumbral region will exhibit its most significant phase, marked especially by the presence of alternating finite allowed and forbidden regions.

Interpreting these results physically, we may draw the following broad conclusions. For low latitudes and high energies the total allowed cone reduces essentially to the main cone of Lemaitre and Vallarta. For intermediate latitudes and energies it exhibits its most complex form, and, as early conjectured by the writer, may be expected to lead to a highly anomalous behavior in the directional distribution of cosmic-ray intensities.[19] For high latitudes and low energies it reduces essentially to the simple shadow cone, to be described in the following paper.

A few general remarks should finally be made concerning the foregoing theorems. Wherever they contain quantitative statements, it should be pointed out that the numerical expressions used are the results of numerical or mechanical integration. Except for one type of argument, on certain continuity properties of the integrals of motion, there is no further dependence upon such calculations. It is conceivable that the whole qualitative discussion of these theorems may be given independently of such calculations, and with complete mathematical rigor. Such a method of approach has been attempted, but has not been sufficiently developed for presentation here.

The author is grateful to Professor M. S. Vallarta for having introduced him into the field of theoretical research opened by this dynamical problem, and for his assistance in the preparation of this paper. A like debt of gratitude is due Dr. Albagli and Dr. Banos for frequent helpful discussions.

properties of the asymptotic family derived from the results of Lemaitre and Vallarta. See reference 2, p. 722, for a description of the asymptotic families and their envelopes.

[18] G. Lemaitre, reference 11, p. 173, has stated that the limit $\gamma_1 = 1$ is thus reached only for values of $r < 0.414$.

[19] E. J. Schremp, Phys. Rev. **53**, 915A (1938).

II. The Simple Shadow Cone of Cosmic Radiation

E. J. SCHREMP*
Massachusetts Institute of Technology, Cambridge, Massachusetts
(Received April 14, 1938)

The present paper is a brief summary of the results obtained from a study, by means of Bush's differential analyzer, of those trajectories of a charged particle in the field of a magnetic dipole which determine the simple shadow cone for all latitudes and energies.

1

AT every point of the earth there is a special type of shadow effect leading to a simple shadow cone outside of which all charged particles of a given energy are blocked by the earth. The simple shadow cone and the Störmer cone,[1] taken together, define an upper limit to the extent of the total allowed cone in the presence of an impenetrable earth.[2] The former is in general a common boundary of the main cone of Lemaitre and Vallarta[3] and of the penumbral allowed regions described in the preceding paper (I, Section 7); its generators are the simple orbits of the second kind there defined (I, Section 6). An example of such an orbit is shown in Fig. 1.

2

The problem of ascertaining the simple shadow cone for all latitudes[4] λ and energies r is essentially quite straightforward. It is only necessary to obtain for each λ and r the family of all orbits possessing sections OT like that of orbit B in Fig. 1. This is a one parameter family, the parameter[4] being γ_1. The angles[4] (η, θ) defined by this family provide the simple shadow cone for the observation point λ and energy r. The orbits in question have been obtained with the aid of Bush's differential analyzer.[5] The differential equations to be integrated are well known from Störmer's work.[6] Except for the entirely different type of initial conditions which we shall presently describe, the mechanical connections of the differential analyzer for this investigation were identical with those used by Lemaitre and Vallarta in their investigation of asymptotic orbits.[7] We shall therefore pass over these details which are outlined fully in their paper.

In choosing a systematic method of attack, and one involving the greatest simplicity in the initial conditions and the greatest efficiency of operation of the differential analyzer, advantage was taken of the fact (Fig. 1) that all simple orbits of the second kind may be generated by starting at suitable points T with vertical tangent, and continuing the orbit away from the equator and through the point O. The procedure was therefore to fix γ_1 and x_T (and therefore the particle energy referred to the earth's surface) and then to vary λ_T. The sequence of orbits

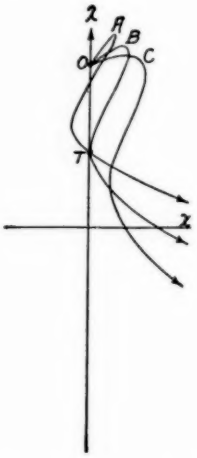

FIG. 1. Simple orbit of the second kind (orbit B). Vertical line represents the earth's surface. Orbit A is in shadow. Orbit C, if nonreentrant, gives an allowed direction at O corresponding to the interior of the main cone. If reentrant, orbit C may or may not be in shadow, according to the positions of its subsequent minima of x.

* At present at Washington University, St. Louis, Missouri.

[1] See preceding paper (hereinafter designated as I), reference 8.

[2] I, Sections 5 and 6.

[3] I, references 4 and 12.

[4] I, reference 2.

[5] V. Bush, J. Frank. Inst. **212**, 447 (1931).

[6] See Eq. (1), G. Lemaitre and M. S. Vallarta, Phys. Rev. **50**, 493 (1936).

[7] G. Lemaitre and M. S. Vallarta, Phys. Rev. **50**, 493 (1936).

obtained in this way has the appearance shown in Fig. 2. The lower limit $\lambda_T=\lambda_2$ is characterized by the fact that the orbit associated with it is a self-reversing orbit, and therefore a transition orbit between simple orbits of the second kind and other orbits of the second kind of more general type (cf. I, Section 6). The upper limit $\lambda_T=\lambda_1$ is characterized by the fact that the orbit associated with this point no longer possesses a minimum of x at T, but instead has an inflection

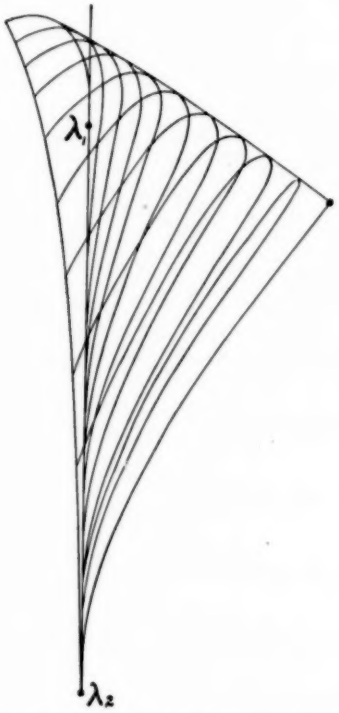

FIG. 2. Family of simple orbits of the second kind, $x=$const. Vertical line represents the earth's surface.

point at T and is therefore a transition orbit between simple orbits of the second kind and orbits having maxima at T and minima at points within the earth. All orbits of the latter class are clearly in shadow, and are therefore not generators of the simple shadow cone for the given energy.

Thus for each value of γ_1 there is a definite sub-region of the region of possible motions in the meridian plane (bounded by the lines[4] $P(x,\lambda;\gamma_1)=0$) in which all points are satisfactory starting points for simple orbits of the second kind. We can now proceed to outline how this sub-region may be mapped out. The upper

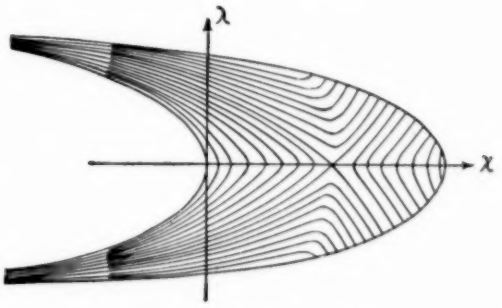

FIG. 3. Lines of zero acceleration.

boundary of this sub-region is given by the condition that $d^2x/d\sigma^2=0$, which may be expressed analytically from the corresponding equation of motion. The loci of $d^2x/d\sigma^2=0$ are shown schematically in Fig. 3. The acceleration $d^2\lambda/d\sigma^2$ is alternately positive and negative in the four quadrants bounded by the equator and the line $\theta=0$ (last line to the left in Fig. 3). These two lines are the loci $d^2\lambda/d\sigma^2=0$ and are independent of γ_1. The corresponding regions for $d^2x/d\sigma^2$ are separated by the other lines in the figure, which show a continuous progression for different values of γ_1. The locus which crosses the equator at a double point corresponds to $\gamma_1=2/(3^{3/4})$. This divides the plane into four quadrants in which the acceleration $d^2x/d\sigma^2$ for this value of γ_1 is alternately positive and negative. For $\gamma_1>2/(3^{3/4})$ the corresponding pairs of loci cross the equator; for $\gamma_1<2/(3^{3/4})$ they do not. These loci divide the plane in a similar way into regions where the sign of the acceleration $d^2x/d\sigma^2$ alternates from positive to negative and vice versa.

The lower boundary of the sub-region of the meridian plane within which simple orbits of the second kind may exist is given by the locus of first minima of x of all self-reversing orbits; i.e., of all orbits starting normally to the line $P(x,\lambda;\gamma_1)=0$. This locus (Fig. 4) is not given analytically but was readily obtained by integrating the family of all such self-reversing orbits for each γ_1 by means of the differential analyzer. The procedure was to start these orbits at their reversal points on the upper branch of the boundary line $P(x,\lambda;\gamma_1)=0$ and carry them to their first minima of x, at which point the machine was stopped. Those lines which are not closed in Fig. 4 terminate on the lower branch of the lines $d^2x/d\sigma^2=0$ for the corresponding γ_1.

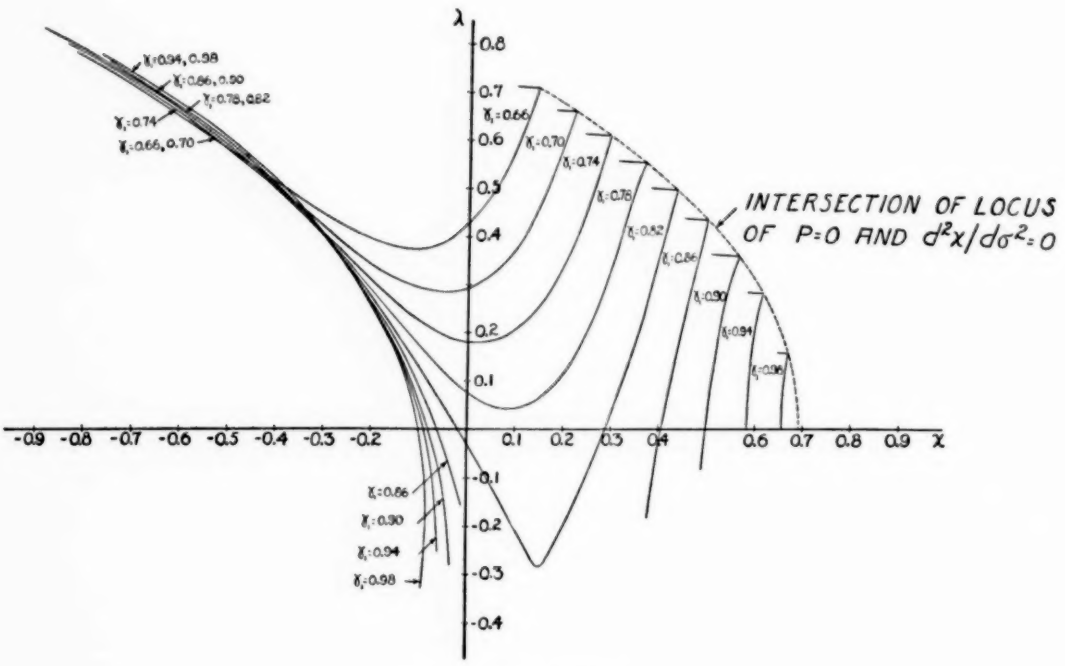

FIG. 4. The loci $dx/d\sigma=0$.

Such lines are not drawn in the figure but are indicated schematically in Fig. 3. A notable by-product of this investigation is that the intersection of the lines $dx/d\sigma=0$ with the equator gives with good accuracy the pair of principal periodic orbits (cf. I, Section 1), for the latter are precisely the self-reversing orbits intersecting the equator at right angles. Table I gives the intercepts of the pair of principal periodic orbits on the equator for the values of γ_1 shown in Fig. 4. These figures are in good agreement with the calculations of Störmer[8] for $\gamma_1=0.97$ and $\gamma_1=0.80$, which we obtain by interpolation from the above table. They are also in good agreement with the calculations of much higher precision of Lemaitre[9] for the pair of principal periodic orbits for $\gamma_1=0.80$. The maximum difference between the machine results and the calculated results is 5 units of the third decimal. A more severe judgment of the precision of these results may be obtained by referring to the high precision calculations of Lemaitre and Vallarta,[10] according to which the outer principal periodic orbit for $\gamma_1=0.929898$ is at $x_0=0.563906$ instead of at 0.562 according to the present results, and to those of Banos,[11] who obtained $x_0=0.3818258$ for $\gamma_1=0.8500008$ as compared with $x_0=0.380$.

[8] I, reference 1.
[9] I, reference 5.
[10] G. Lemaitre and M. S. Vallarta, Ann. de la Soc. Sci. de Bruxelles **A56**, 102 (1936).

3

Once the sub-region of admissible starting points for simple orbits of the second kind has been mapped out, as outlined in the preceding section, for each value of γ_1, the remaining program of integration is clearly defined, and consists in integrating for families of simple orbits of the second kind such as that shown in Fig. 2 for sets of values of x and γ_1 which cover the whole range of existence of such orbits. For this purpose we chose values of the energy from

TABLE I. *Intercepts of the pair of principal periodic orbits on the equator for various values of* γ_1.

γ_1	x_0 (outer orbit)	x_1 (inner orbit)
0.98	0.656	−0.098
0.94	0.583	−0.091
0.90	0.499	−0.082
0.86	0.405	−0.062
0.82	0.288	−0.016

[11] Ph. D. thesis, M.I.T., January, 1938, as yet unpublished.

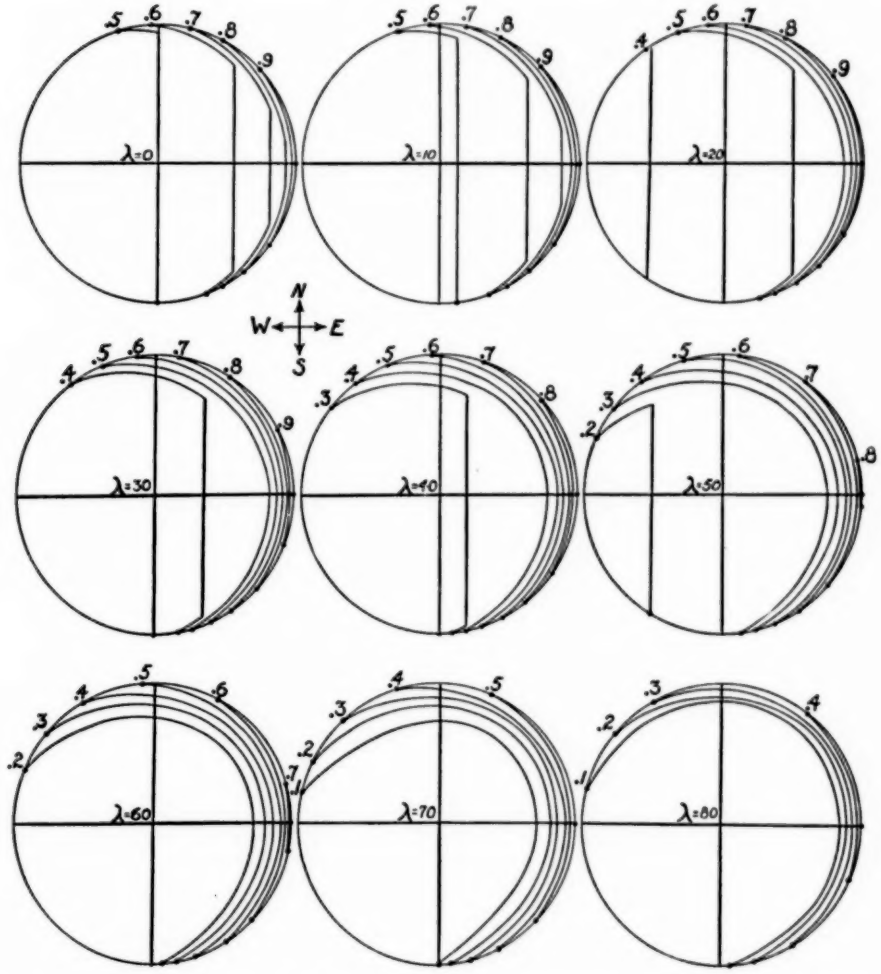

FIG. 5. Simple shadow cones. Positive particles, northern hemisphere. Energies in Störmers.

0.1 to 0.9 Störmer[12] by steps of 0.1, and of γ_1 from 0.62 to 0.98 by steps of 0.04. The procedure is as follows: first one fixes a value of the energy r and chooses a value of γ_1 (and therefore of x). Along the chosen line $x=$const. one determines then the intersections of the two lines $dx/d\sigma=0$ and $d^2x/d\sigma^2=0$. These two intersections determine the latitude range to be studied. Next a family of trajectories with minima in this interval of λ is generated by means of the differential analyzer. This is done by choosing a suitable interval of λ (from 2° to 5°) and following a simple orbit of the second kind from its x minimum (point T, Fig. 1) in a direction away from the equator until a maximum is reached and then the orbit returns to the earth at O (Fig. 1). At O the slope η is then determined. For each chosen value of γ_1, and each chosen value of x, one thus obtains a curve giving η as a function of λ, which ends at the two points $(-\pi/2, \lambda_1)$ and $(\pi/2, \lambda_2)$, which for a certain value of λ near λ_{max}, has $\eta=0$. (See Fig. 2.) This λ_{max} is reached at the point where the envelope of the system of simple orbits of the second kind intersects the given line $x=$const. From these curves, diagrams are then constructed giving λ as a function of γ_1 for different values of η. Similar diagrams are then prepared for all values of r which were studied.

Once these diagrams are obtained the simple shadow cone may be immediately plotted in the

[12] For a definition of the Störmer unit see I, reference 2, p. 720. For a table of equivalence between the energy in Störmers and the energy in electron volts see I, reference 4, Table VI.

usual representation adopted by Lemaitre and Vallarta; i.e., the horizontal projection of the unit sphere. The procedure is simply to fix the latitude λ and the energy r and read off the diagrams the angle η and the corresponding value of γ_1; the angle θ is then calculated from Störmer's formula.[13] The final results are presented in this way in Fig. 5, where each diagram refers to a fixed latitude λ and each curve in a given diagram refers to a fixed energy r (in Störmers) as shown. It will be observed that for certain latitudes and energies the simple shadow cone ends abruptly at a value of θ corresponding to $\gamma_1=1$. This merely signifies that further continuation of the simple shadow cone beyond this value of θ brings it into the Störmer cone, which marks a transition to forbidden directions arising from a different cause (cf. I, Section 5).

It will be further observed that the simple shadow cone of a given energy opens up gradually with increasing latitude and ultimately covers a complete hemisphere. The latitude at which this happens corresponds to the disappearance of families of simple orbits of the second kind, which takes place where the locus $d^2x/d\sigma^2=0$ meets the locus $dx/d\sigma=0$ at the boundary $P(x, \lambda; \gamma_1)=0$ (dotted line in Fig. 4). The first locus is given by

$$2\gamma_1 r-\cos^2\lambda=r^4 \tag{1}$$

and the line $P(x, \lambda; \gamma_1)=0$ by

$$2\gamma_1 r-\cos^2\lambda=r^2\cos\lambda, \tag{2}$$

which intersect for

$$\cos\lambda=r^2 \tag{3}$$

or

$$\gamma_1=r^3. \tag{4}$$

In this connection it is interesting to note that the original latitude effect curves given by Lemaitre and Vallarta[14] reach 100 percent intensity at that latitude, for each r (except 0.8 and 0.9), for which $\gamma_1=0.783$. When the simple shadow cone is taken into account, 100 percent intensity is not reached until the latitude given by (3) is attained. This introduces a maximum difference of about 6 degrees. A corresponding modification, to which they have already called attention, must be made in Lemaitre and Vallarta's Fig. 10.[15] Instead of this curve one should use the relation expressed by Eq. (3).

One will further observe a unique property possessed by the simple shadow cone. For $\gamma_1<0.78856$ no reentrant orbits, and therefore no orbits of the first kind, exist (I, theorem 3). Hence no boundary sheets of the main cone or penumbra may exist for $\gamma_1<0.78856$, except that boundary of the main cone provided by the simple shadow cone, which may extend below the limiting $\gamma_1=0.78856$, as Eq. (4) shows.

As pointed out in the preceding paper, (I, Section 7), for low latitudes and high energies the total allowed cone reduces essentially to the main cone of Lemaitre and Vallarta. In all such cases the simple shadow cone only slightly affects the form of the main cone. For intermediate latitudes and energies the simple shadow cone affects not only the form of the main cone but that of each discrete penumbral allowed region. For high latitudes and low energies the "probability" for allowed penumbral directions is nearly unity everywhere within the combined simple shadow cone and Störmer cone. Hence, in this last case, the total allowed cone may be viewed as given very nearly by the combined simple shadow cone and Störmer cone.

Acknowledgments

The author is especially grateful to Professor M. S. Vallarta for having introduced him into the fascinating field of theoretical research opened by this dynamical problem, and for his constant assistance in the preparation of this paper. A like debt of gratitude is due Professor Vallarta, Dr. R. Albagli, and Dr. Alfredo Banos, Jr., for their frequent helpful discussions in connection with this and the preceding research. For the extensive funds made available for the operation of the differential analyzer, by Dr. Vannevar Bush on one occasion and by Dr. Karl T. Compton on a second, and for the generous cooperation of Professor S. H. Caldwell, Mr. C. E. Shannon, and their assistants throughout the period of operation of the differential analyzer, the author wishes also to express his deep appreciation.

[13] I, reference 2, Eq. (1), p. 721.
[14] I, reference 4, Fig. 1.
[15] Reference 7, Fig. 10, p. 503.

Diffuse Scattering of X-Rays from Piezoelectrically Oscillating Quartz

G. E. M. Jauncey and W. A. Bruce
Wayman Crow Hall of Physics, Washington University, St. Louis, Missouri
(Received June 13, 1938)

Bertsch's investigation of the effect of the different modes and types of piezoelectric oscillations of quartz on the intensity of Laue spots and Bragg reflections necessitates a similar investigation of the effect of the different modes and types of vibration on diffuse scattering. Extending the result found by Jauncey and Deming we find that in all cases the piezoelectric oscillations have no effect on the intensity of the diffuse scattering. Since the diffuse scattering cannot be affected by secondary extinction, it is concluded that the change of intensity of the Laue spots is due to a decrease of secondary extinction in the body of the crystal.

Introduction

Fox and Carr[1] were the first to show that the intensity of the Laue spots from a thin quartz plate is increased when the plate is set into piezoelectric oscillation. The Laue spots produced by a nonoscillating quartz plate are double due to very little reflection from the interior of the crystal where the extinction coefficient is high. When the crystal is oscillating the space between the two parts of each Laue spot becomes black indicating that the interior of the crystal loses its high extinction coefficient. Further work by Barrett and Howe[2] shows that piezoelectric oscillations introduce a fine structure into the Laue spots. The effects of etching found by Colby and Harris[3] indicate that the increased intensity of the Laue spots is not due to increased reflection from the layers near the two surfaces of the crystal. This together with the fine structure found by Barrett and Howe supports the view that the increased intensity produced by the oscillations is due to increased reflection from the interior of the crystal. Barrett and Howe ascribe the increased reflection from the interior of the crystal to a reduction of primary extinction while Colby and Harris ascribe it to a reduction of secondary extinction. Bertsch[4] has found that the intensity of the Laue spots and Bragg reflections is variously affected by the different modes and types of vibrations. From his results it is concluded that increased reflection occurs from those parts of the crystal which are at a node of motion or antinode of stress.

Diffuse scattering of x-rays as measured by the transmission method[5] is a volume and not a surface phenomenon and so it seemed worth while to examine the effect of piezoelectric oscillations on the intensity of diffuse scattering. This was first done by Jauncey and Deming,[6] who found that the oscillations have no effect. However, Jauncey and Deming only used a Y cut crystal and one mode of oscillation. In view of the work of Bertsch it is necessary to study the effect of different types and modes of vibration upon the intensity of diffuse scattering.

Experimental Method

We did most of the work with a $15\times15\times0.823$ mm^3 X cut crystal and a $15\times15\times1.05$ mm^3 Y cut crystal. Both crystals were unetched and unpolished. A crystal under test was mounted in a holder consisting of two brass plates each with a 5 mm hole. Between each brass plate and the crystal was placed a 0.15 mm sheet of aluminum which covered the whole area of the crystal plate. The x-ray beam passed through the crystal and the two thicknesses of aluminum. The aluminum was kept pressed against the crystal with light brass springs which were adjusted so that the crystal was free to oscillate. Electric oscillations were produced by coupling to the tank circuit of an oscillator embodying one WE212D tube. This

[1] G. W. Fox and P. H. Carr, Phys. Rev. **37**, 1622 (1931).
[2] C. S. Barrett and C. E. Howe, Phys. Rev. **39**, 889 (1932).
[3] M. Y. Colby and S. Harris, Phys. Rev. **43**, 562 (1933).
[4] C. V. Bertsch, Phys. Rev. **49**, 128 (1936). For further information concerning the modes and types of oscillations of quartz, reference is made to H. Osterberg, Phys. Rev. **43**, 819 (1933), and R. S. I. **5**, 183 (1933).
[5] G. E. M. Jauncey and W. D. Claus, Phys. Rev. **46**, 941 (1934).
[6] G. E. M. Jauncey and J. H. Deming, Phys. Rev. **48**, 462 (1935).

delivered a peak voltage of 1500 v. Resonance was checked in two ways—first, by an electric light bulb in series with the crystal and pick-up coil and, second, by the increased intensity of the Laue spot as measured by the ionization chamber and electrometer. The usual diffuse scattering transmission method was used in these experiments.[5] A collimated beam of x-rays from a tungsten target tube operating at a peak voltage of 37 kv was allowed to fall upon the quartz plate. The ionization chamber was set up at an angle ϕ and the normal to the crystal plate at an angle θ with respect to the direction of the primary beam. In an X or Y cut crystal the plate is parallel to the optic axis. We have found it convenient to introduce α, which is the angle between the optic axis and the plane of scattering.

Results

A typical result is shown in Fig. 1, where it is seen that although the oscillations cause an increase in the intensity of the Laue spot they have no effect on the diffuse scattering. In order to show more certainly the zero effect of the vibrations a typical set of observations is shown in Table I. The average deflection time for the non-oscillating crystal was 62.88 sec., while that for the oscillating crystal was 62.87 sec. The average deflection time for the leak was 105 sec. We may

TABLE I. *Y cut crystal*, $\phi = 30°$, $\alpha = 0°$.

θ	Deflection Time			
	Not Oscillating sec.		Oscillating sec.	
10°	63.8 66.0	61.8 65.2	63.6 64.0	63.7 64.0
10.5°	66.0 63.9	60.2 63.2	64.9 63.5	63.5 61.6
11°	63.0 63.5	64.0 63.0	63.0 63.7	62.4 59.4
Laue Spot				
16.0	63.3 61.0	59.6 61.4	62.4 64.2	61.6 59.9
16.5	62.0 62.7	65.4 60.2	60.0 64.2	63.5 61.6
17.0	62.0 65.0	63.5 59.4	63.4 63.7	61.7 65.4

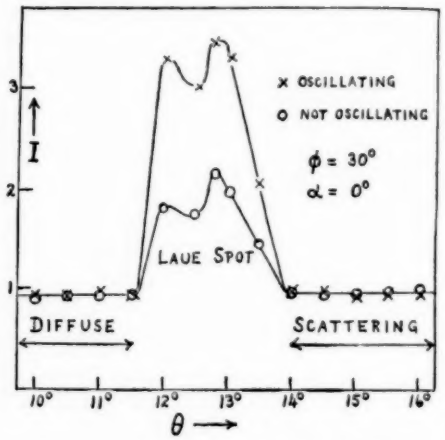

FIG. 1. Diffuse scattering from a Y cut quartz crystal.

conclude therefore that Table I confirms Jauncey and Deming's conclusion that the oscillations produce no change in the diffuse scattering. Similar results for various values of α and for the X cut crystal were obtained. Thickness vibrations up to the second harmonic and width vibrations to the third harmonic also had no effect on the diffuse scattering. We therefore conclude that the piezoelectric oscillations in no case affect the diffuse scattering from quartz.

Discussion

Since the effect of piezoelectric oscillations on the intensity of Laue spots is due to a reduction of extinction and since these oscillations have no effect on diffuse scattering we conclude that extinction has no effect on diffuse scattering. As between primary and secondary extinction we can see no reason why secondary extinction should affect diffuse scattering. It is possible that primary extinction would affect diffuse scattering. It is therefore our opinion that it is a reduction of secondary extinction which gives rise to the increase of intensity of the Laue spots when the crystal oscillates.

Fox and Frederick[7] have recently discussed the division of the total x-ray energy which enters the quartz plate. Since there is no reason to expect a change of the photoelectric absorption due to oscillations and since there is no change in the diffuse scattering, they feel that the only

[7] G. W. Fox and J. R. Frederick, Phys. Rev. **53**, 135 (1938).

place for the necessary complementary change is in the transmitted beam. However, both they and Jauncey and Jacques[8] were unable to find any noticeable change in the transmitted beam. We suggest that the conservation of energy merely requires that dL, the increase in intensity of all the Laue spots, equal $-dT$, the decrease of the intensity of the transmitted beam. The conservation of energy does not require that $dL/L=-dT/T$ since $L\neq T$. The transmitted intensity, T, is of the order of $1000L$ as is shown by the relative exposure times for producing equal photographic blackness in the Laue spots and the transmitted beam. Although the ratio $(L+dL)/L$ is measurably different from unity, the ratio $(T-dT)/T$ is not.

[8] G. E. M. Jauncey and A. T. Jacques, Phys. Rev. **50**, 672 (1936).

AUGUST 1, 1938 PHYSICAL REVIEW VOLUME 54

The Yield of Alpha-Particles from Beryllium Bombarded by Protons

GRAHAM T. HATCH
University of Chicago, Chicago, Illinois

(Received May 27, 1938)

Experiments to determine the excitation function of the reaction $_4Be^9(p,\alpha)_3Li^6$ for proton energies up to 400 kv are reported. It is shown that the yield is very large, *ca.* 4×10^{-6} alpha-particle per proton at 400 kv, but the derived thin target curve shows a marked flattening from the exponential form observed at lower voltages. The cross section is nearly constant above 300 kv, and has a value of about 2.3×10^{-25} cm^2.

INTRODUCTION

THE reactions

$$Be^9+H^1\rightarrow Li^6+He^4 \quad (1)$$

$$\rightarrow Be^8+H^2 \quad (2)$$

were first studied by Oliphant, Kempton, and Rutherford[1] who used electric counting methods. They were particularly interested in determining the end products and establishing the reactions. Allen[2] studied the yield of the two reactions at voltages below 125 kv and determined the ratio of the two yields. Williams, Haxby and Shepherd[3] continued the yield curve for the two reactions to 238 kv. Because of the very high efficiency of the process, it has been thought worth while to continue the study of the yield to still higher voltages. To this end, reaction (1) was particularly studied, while the ratio of the yields of reactions (1) and (2) was determined whenever conditions of measurement were sufficiently favorable.

[1] Oliphant, Kempton, and Rutherford, Proc. Roy. Soc. **150**, 241 (1935).
[2] J. S. Allen, Phys. Rev. **51**, 182 (1937).
[3] Williams, Haxby and Shepherd, Phys. Rev. **52**, 1031 (1937).

APPARATUS

Proton source

The proton source was a low voltage arc of the probeless type, similar to that described by Lamar, Samson, and Compton.[4] Ions from this were subjected to an initial small acceleration to collimate the beam, and introduced into the main acceleration tube. The acceleration took place in a horizontal tube in four gaps, across which the potential was distributed by means of variable corona points. The tube was evacuated by two 6″ oil diffusion pumps in parallel working into a two stage 3″ oil diffusion pump.

The accelerating voltage was supplied by a voltage quadrupling circuit of the Cockcroft and Walton type. This was operated from a 60-cycle transformer which could give a 165 kv wave above ground. Because of insulation difficulties this transformer was operated with the case and center of the primary connected to the center of the secondary. It was mounted on an insulating stand, and the primary fed through a 1 : 1 high voltage insulation transformer.

[4] Lamar, Samson and Compton, Phys. Rev. **48**, 886 (1935).

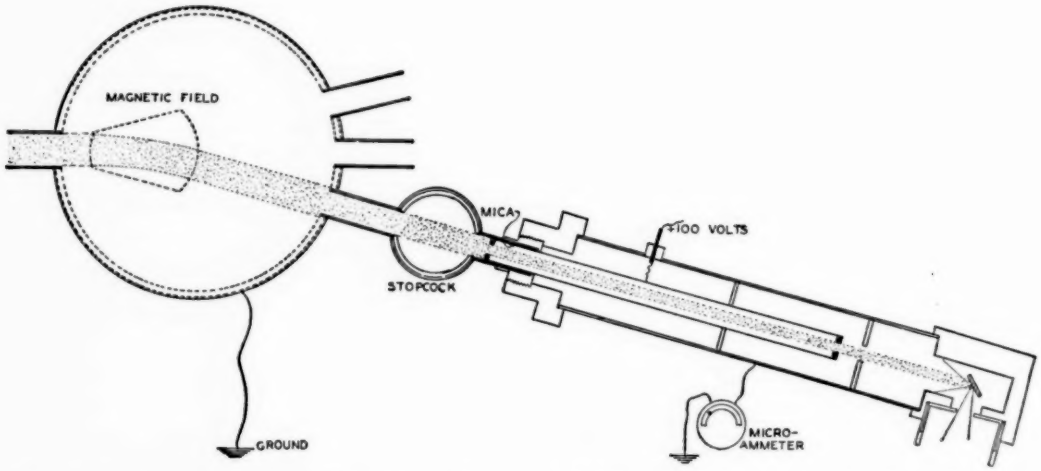

FIG. 1. The target assembly, showing the arrangement of diaphragms to control secondary electrons.

Voltmeter

The accelerating voltage was measured by means of a column of 750 selected 10 megohm metallized I.R.C. resistors rated at one watt or 1000 volts each. These were assembled in a fashion similar to that described by Hafstad, Heydenburg and Tuve.[5] Groups of 30 were inserted in pure gum rubber tubing. The tubing was then stretched and the ends tied off. When the tubing was allowed to contract, it brought the resistors in close electrical contact. These groups were wound spirally between corona shields, and the whole column inserted in a glass cylinder in an atmosphere of nitrogen. Tests showed no signs of corona to above 500 kv.

In measuring the resistance of this column, use was made of a 40 kv x-ray set previously developed in this laboratory by Allison, Stearns and Bowersox. This set consisted of a transformer rectifier set fed by a 220-volt 540-cycle generator. The generator was driven by a 60-cycle synchronous motor. The generator field current was supplied either by a separate exciter or by a bank of storage batteries. An automatic stabilizing circuit driven by the d.c. high voltage output and operating on the field circuit of the generator kept voltage fluctuation below one part in 10,000. Measurement of the voltage was accomplished by the use of a bank of Taylor wire-wound resistors and a potentiometer. A bridge circuit was arranged to measure the resistance of the resistors before and after each use of them. The maximum error in the mean voltage measurement was estimated at 0.1 percent.

The output from this set was applied to the column of 750 resistors to determine its resistance for low current values. Currents were measured with a potentiometer and standard resistor. A sample value taken was:

Voltage	$33{,}352 \pm 33$ volts
Current	$(4.236 \pm 0.002) \times 10^{-6}$ amp.
Resistance	$(7.878 \pm 0.016) \times 10^{9}$ ohms.

After the value of the resistance was determined for small currents, it was considered sufficient to establish the variation of resistance with current for a random selection of the resistors. For this purpose 29 resistors were chosen at random, and their resistance measured as a function of current. Voltages were supplied by the x-ray set, and currents measured as in the former case. The resulting relationship, shown in Fig. 3 was used to determine the resistance of the entire column, and a table giving voltage as a function of current through the resistors constructed.

Target assembly

After acceleration, the ion beam was analyzed magnetically and the proton component directed at the target. The arrangement is shown diagrammatically in Fig. 2. The beam after analysis

[5] Hafstad, Heydenburg and Tuve, Phys. Rev. **50**, 504 (1936).

passed through a vacuum stopcock and into a 28 cm aluminum collimating tube. In the ends of this tube were mounted diaphragms having circular openings 6 mm in diameter. These were the beam limiting apertures, and determined the size of the focal spot.

To prevent the escape of secondaries from the target to the tube, an auxiliary diaphragm connected to the target chamber was placed directly beyond the end of the aluminum tube. A hole in this 9 mm in diameter allowed the beam to pass through without touching, but subtended such a small solid angle at the target as to be negligible. To eliminate any effect due to the capture in the target chamber of secondary electrons from the beam limiting diaphragm, the aluminum tube was raised to a positive potential. A study of the measured beam current as a function of this voltage showed that the current increased about 100 percent as the voltage was varied from 0 to 30, and was very nearly constant from 30 to 150 volts which was the highest point taken. This was taken as indicating that above 30 volts all secondaries from the tube diaphragm were driven back to it and that up to 150 volts at least, the field did not penetrate far enough into the target chamber to attract the secondaries from the target. Consequently the voltage was fixed at 100 volts, and the measured current assumed to be the true proton current.

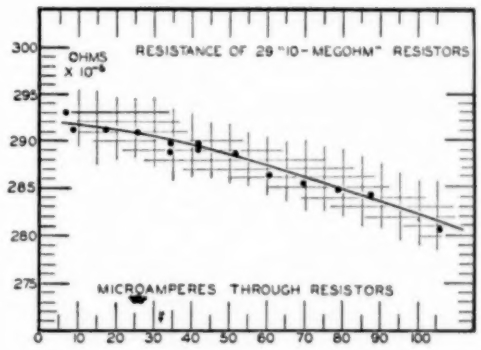

FIG. 3.

The target was a disk of beryllium metal 16 mm in diameter ground to smooth finish and mounted on a truncated steel cylinder at an angle of 45° to the beam. In the early stages of this work, the problem of carbon contamination of the target was studied. The advantages of using oil diffusion pumps are very often almost counter-balanced by the troublesome deposition

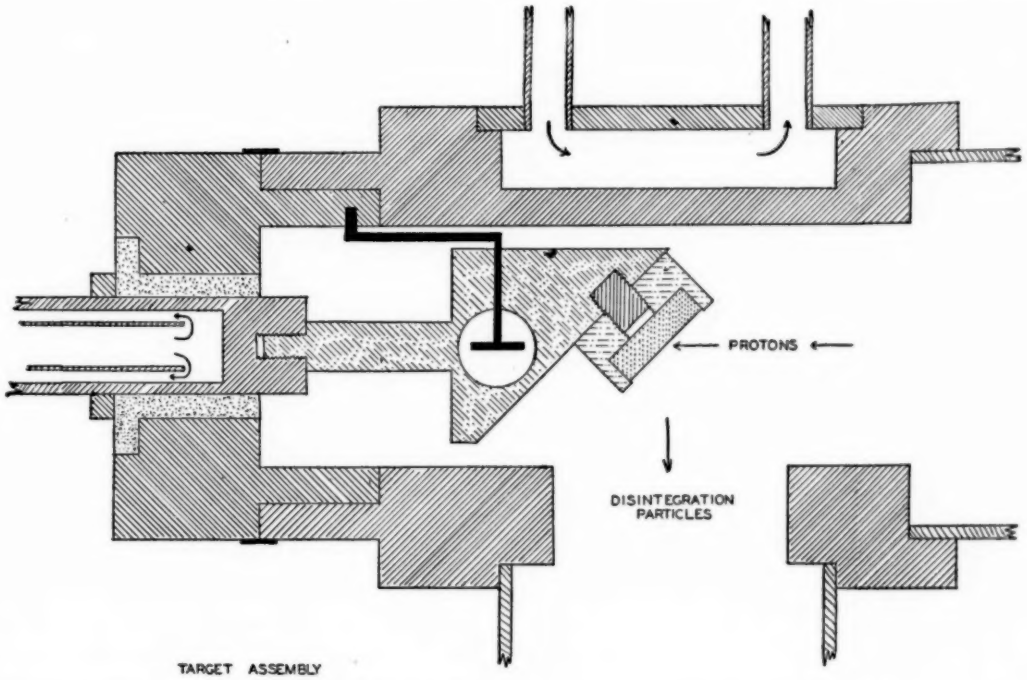

FIG. 2. Enlarged view of the target, showing the mounting of the heaters. The heavy black line represents the filament support.

of carbon on the targets by the bombarding beam. In many cases it has been necessary to change targets frequently to escape the ever present carbon films. This is particularly dangerous when, as in this case, the disintegration particles are of very short range. It is quite possible that many of them may be completely absorbed in the carbon layer. In this laboratory the difficulty was overcome very simply, as shown in Fig. 2. A pair of tungsten filaments was mounted in a hole drilled through the target holder. Current was supplied to these from a transformer, and the whole target preheated for ten to fifteen minutes before bombardment. The target was thus raised to a temperature sufficient to drive off any oil which had condensed on the target, and thus eliminated carbon formation. With this treatment, targets remained clean indefinitely.

Beam current measurement

Because of the very high yields found, the beam current was kept low. For most of the work it was of the order of 0.02 microamp. The current integrator which was then available had leakage currents of the same magnitude, so that it was decided to use a galvanometer for the current measurement. Readings were taken at 2 or 3 second intervals during bombardment and recorded and averaged on a calculating machine.

Recording system

Alpha-particles resulting from the disintegration were brought out of the target chamber through a collodion window of between 1 and 2 mm stopping power at right angles to the beam. The window was mounted over a single hole 0.0646 cm in diameter in a phosphor bronze disk 2.94 cm from the center of the target.

An ionization chamber was used to record the particles. This chamber was 3 mm deep and 1.5 cm in diameter. The ionization chamber was placed less than a millimeter from the collodion window leading to the target chamber, so that at all times, the window was the limiting aperture and defined the solid angle. The amplifier used was that constructed by Allen.[2] Its output was applied to a scale-of-sixteen counter using the circuit described by Stevenson and Getting,[6] and also through an additional stage of amplification, to a cathode-ray oscilloscope. The oscilloscope was used at all times to check the operation of the set and recording systems. Disturbances in the amplifier due to heavy corona bursts, gassy rectifiers, and improper shielding, are easily recognized by this means, whereas the counters record these disturbances as particles. Photographic records of the oscilloscope traces were made at several points. A Leica camera at f : 1.9 and Agfa ultra-speed panchromatic film were used. The duration of a pulse on the oscilloscope was about 0.0002 second but it was found that even with the ordinary green fluorescent screen enough intensity resulted to give clear sharp photographs. Exposures were limited to $\frac{1}{8}$ second because the general illumination of the tube tended to fog the film for longer exposures. As many as 70 exposures were made during a run, each representing about twenty pulses.

The scaling circuit was arranged to have a controlled variable bias applied to the grids of the input stage to regulate the recording threshold. It was determined that a linear relationship existed between the bias voltage and the size of the minimum pulse recorded. The output of the scaling circuit was applied to a Cenco impulse counter. Counting rates were kept at all times below twenty per second. The usual counting rate was 10 per second, and the beam current was adjusted to maintain rates of this magnitude at all voltages. According to the theory of losses of a scaling circuit as derived in this laboratory by Alaoglu and Smith,[7] the losses at this rate were approximately 0.4 percent and are due to the amplifier. The time constant of the amplifier was about 0.0004 second.

Measurements

Measurements were made by use of the bias recording method described by Allen.[2] Because of the large straggling found at the higher proton energies with thick targets, it was not possible to assume that a reading taken at a given bias represented recording of all the alpha-particles and none of the deuterons. Instead, it was necessary to record the entire bias curve. Such a

[6] Stevenson and Getting, Rev. Sci. Inst. **8**, 414 (1937).

[7] Alaoglu and Smith, Phys. Rev. **53**, 832 (1938).

curve did not show flat plateaus like those found at lower voltages. The wide straggling of the alpha-particles coming from different layers of the target caused a large spread in the amount of ionization produced in the chamber, and caused overlapping of the deuteron and alpha-particle groups. The earlier work of Oliphant, Kempton, and Rutherford[1] had indicated the danger of this overlapping when caused by too great path difference between the target and the ionization chamber. This difficulty was eliminated by the close placing of the chamber, but the thick target straggling is harder to offset. The work of Kirchner and Neuert[8] on the ionization produced by alpha-particles at the very end of their range indicated how far from the end of the range it was possible to distinguish alpha-particles from deuterons. By the use of their result, a method was devised for extrapolating the alpha-particle section of the curve through the discontinuity produced by the deuterons.

The use of this method will be illustrated by a sample analysis of the bias curve shown in Fig. 4. This curve becomes noticeably different from zero in the region of 16 volts bias. This corresponds, according to an adaptation of Kirchner and Neuert's curves, to alpha-particles whose range ends approximately 2.5 mm beyond the center of the ionization chamber. It was assumed that these alpha-particles come from the extreme outer layer of the target. It is also assumed that particles which are recorded at lower biases are those which come from deeper layers of the target. This neglects the straggling found in initially homogeneous particles, but a partial correction showed that this effect caused only a negligible error. At approximately 12 volts bias, just before the deuteron group appears, Kirchner and Neuert's ionization curve indicates that the particles received are 1.02 mm from the end of their range. This difference in the alpha-particle

TABLE I. *The ratio of deuterons to alpha-particles at several voltages.*

D/α	kv	D/α	kv
1.18	204	1.56	282
1.46	228	1.34	305
1.48	250	1.64	330
1.58	256	1.34	360

[8] Kirchner and Neuert, Physik. Zeits. **38**, 969 (1938).

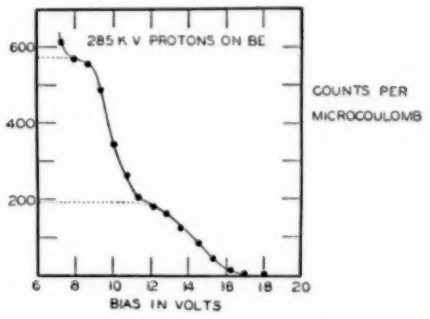

FIG. 4. A sample bias curve.

ranges is assumed to be due entirely to the thick target effect. From this difference, the depth in the target from which the alpha-particles have come may be calculated, and the loss in energy of the protons in penetrating to this depth estimated from range energy relationships. In this case, this loss amounted to 95 kv, so that the residual energy of the protons was 190 kv. It was then assumed that the yield of alpha-particles shown at 12 volts bias represented the yield due to protons from 190 kv to 285 kv. To get the true thick target yield, there would have to be added to this the yield due to protons below 190 kv. This is known from earlier work and from approximate solutions in this work. A large error in this term is not very important since the whole term represents a small fraction of the total yield. In this case, the yield at 12 volts was 180 alpha-particles, due to protons of energies between 190 kv and 285 kv, and 11 particles due to protons of energies below 190 kv. The sum of these, 191, is taken to be the true thick target yield at 285 kv. This method of extrapolation may be in considerable error, possibly as much as 20 percent and probably accounts for the scattering of points on the yield curve.

Above 400 kv straggling is so great that an appreciable number of alpha-particles do not penetrate the ionization chamber and thick target work is impractical. Moreover, the range of the scattered protons is large enough to interfere with the recording of the alpha-particles, necessitating the use of a different method for the higher voltage range.

Due to the shallowness of the ionization chamber used, it was very often difficult to record the deuteron group satisfactorily. Only

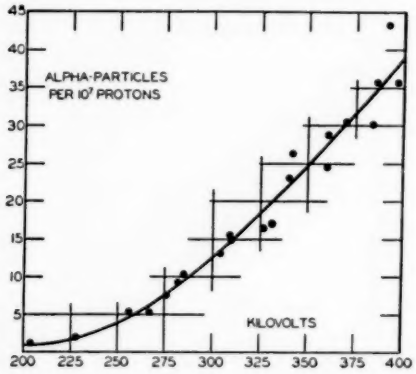

FIG. 5. The thick target yield curve.

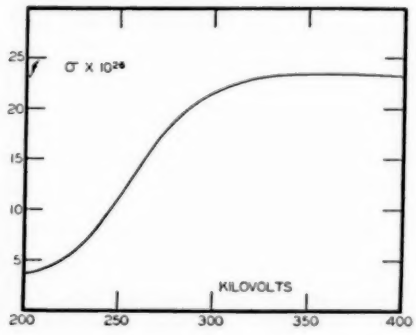

FIG. 6. The cross section for the reaction for thin targets.

occasionally, when the background noise in the amplifier was very low, could the total number of deuterons be estimated with any degree of accuracy. Consequently, only a few points were taken on the deuteron yield curve. Errors in these should be considerably larger than in the case of the alpha-particles.

RESULTS

Thick target yield

A sample bias curve is shown in Fig. 3. Curves of this type were taken at each proton energy used, and the number of alpha-particles represented was estimated. Assuming a spherical distribution of the ejected particles, the number of disintegrations was calculated. Calculation was made of the correction necessary due to the momentum of the incident proton. This was found to be 1.5 percent at 400 kv, and in view of the other much larger errors, was neglected. Uncertainties in the solid angle measurement introduce an error of not more than 10 percent in this result, and this error is of a systematic nature, so that the shape of the excitation curve is not affected by it.

The resulting thick target yield curve is shown in Fig. 5. The maximum over-all error in the measurement is estimated as less than 40 percent. Of this, about 15 percent is assigned to systematic errors which affect all points in the same direction, and 25 percent to random errors due principally to the difficulties inherent in the extrapolation of the bias curves. It seems probable that these would be large only in the direction of underestimation, particularly at the higher voltages. However, the points represent what is thought to be the most probable true value.

The curve was compared with that given by Williams, Haxby and Shepherd[8] to 238 kv which was as far as they carried the investigation. Their values were given for the total yield of alpha-particles and deuterons, and it was necessary to correct them for comparison with this work. The ratio $d/\alpha=1.4$ was assumed for this purpose, and with this correction, the results agree to within 20 percent. Since their estimated error was 50 percent, and the error of this work 40 percent, this is rather excellent agreement.

The ratio of d/α as determined at a few points is given in Table I. The values fluctuate rather widely, and little importance can be attached to them.

From the thick target excitation function, the yield curve for thin targets was obtained by taking differences. The interval chosen was 20 kv, and represents a target approximately 5×10^{-5} cm thick at 300 kv. From this in turn the cross section for the reaction for thin targets was calculated. This involved the use of the proton range-energy relationships as given by Livingston and Bethe,[9] and is subject to additional errors on that account. The cross section as a function of voltage is shown in Fig. 6. The curve shows a marked plateau above 300 kv.

If Bethe's estimate[10] of 1.5 Mev as the height of the potential barrier in beryllium is correct, we cannot assume the protons to be going over the top of it, and some sort of broad resonance is indicated. The cross section does not decrease

[9] Livingston and Bethe, Rev. Mod. Phys. **9**, 245 (1937).
[10] Bethe, Rev. Mod. Phys. **9**, 69 (1937).

on the high voltage side as fast as would be expected for an important resonance, but the estimated error of 25 percent exclusive of systematic errors might be large enough to conceal such a trend. However since it seems sure that any large errors in the cross section would be in the direction of underestimation, such an explanation does not seem probable.

On the other hand, the unusually high value found for the cross section introduces another question. On the assumption that the Coulomb radius of the beryllium nucleus is 5×10^{-13} the geometric cross section of the nucleus is approximately the same as the disintegration cross section. This suggests that protons having $L>0$ may be taking part in the reaction. Since protons of $L=1$ would not contribute to the yield at 90°, even higher order collisions would be called for. These would imply unsymmetrical distribution of the resulting α-particles, with probably a minimum distribution at 90°. No such unsymmetrical distribution has been reported, so that the interpretation is very questionable.

It is hoped that further work in this laboratory on the problem of angular distribution will clarify this matter.

ACKNOWLEDGMENTS

This work was carried out under the general direction of Professor S. K. Allison. Construction of the apparatus and the taking of the data were made possible only by the invaluable assistance of Professor Allison, Mr. L. S. Skaggs, and Mr. Nicholas M. Smith, Jr.

AUGUST 1, 1938 PHYSICAL REVIEW VOLUME 54

A Precise Measurement of the Energy Change in the Transmutation of Beryllium into Lithium by Proton Bombardment

SAMUEL K. ALLISON, LESTER S. SKAGGS AND NICHOLAS M. SMITH, JR.
University of Chicago, Chicago, Illinois

(Received May 27, 1938)

The very high yield of alpha-particles from the reaction $_4Be^9(p,\alpha)_3Li^6$ has made it possible to measure their energies by deviating a beam through 90° in an electrostatic field. A steady source of high voltage, which could be measured to 0.1 percent up to 40,000 volts, was used to deflect the alpha-particles. Two experiments are reported in which the beryllium was bombarded by 320 kv and 383 kv protons, respectively. The energy distribution curves of the alphas show a sharp high energy limit, and this limit increases with bombarding energy of the protons. The experiment shows that the energy balance of the reaction is 2.152 ± 0.04 Mev, corresponding to $2.310\pm0.04\times10^{-3}$ atomic weight unit. This establishes the difference in mass between Be^9 and Li^6 as 2.99804 ± 0.00009. If we assume that of the two, the mass of Li^6 is more accurately known, and adopt Livingston and Bethe's value of 6.01686 ±0.00020, the experiment shows that the mass of Be^9 is 9.01491 ± 0.00025.

THE nuclear transformations induced in beryllium by proton bombardment have been the subject of several investigations since the first extended report by Oliphant, Kempton, and Rutherford[1] appeared. In this report previous experiments and exploratory work by Cockcroft, Dee, Döpel, Kirchner, etc. are mentioned. More recently papers[2] by Döpel, Kirchner and Neuert, Zipprich, Allen, and Williams, Haxby, and Shepherd have appeared. G. T. Hatch, in this laboratory, has recently extended the yield curve of alpha-particles up to 400 kilovolts bombarding energy of protons.

It seems well established that two reactions occur simultaneously, one producing alpha-particles, the other, a singly charged particle which is probably a deuteron.

$$_4Be^9+{}_1H^1={}_3Li^6+{}_2He^4+Q, \quad (1)$$

$$_4Be^9+{}_1H^1={}_4Be^8+{}_1H^2+Q'. \quad (2)$$

The reported work previous to that of Hatch was

[1] Oliphant, Kempton, and Rutherford, Proc. Roy. Soc. Lond. **A150**, 241 (1935).

[2] R. Döpel, Zeits. f. Physik **91**, 796 (1934) and **104**, 666 (1937); B. Zipprich, Zeits. f. Physik **96**, 337 (1935); Kirchner and Neuert, Physik. Zeits. **36**, 54 (1935) and **38**, 969 (1937); J. S. Allen, Phys. Rev. **51**, 182 (1937); Williams, Haxby, and Shepherd, Phys. Rev. **52**, 1031 (1937); G. T. Hatch, Phys. Rev. **54**, 165 (1938).

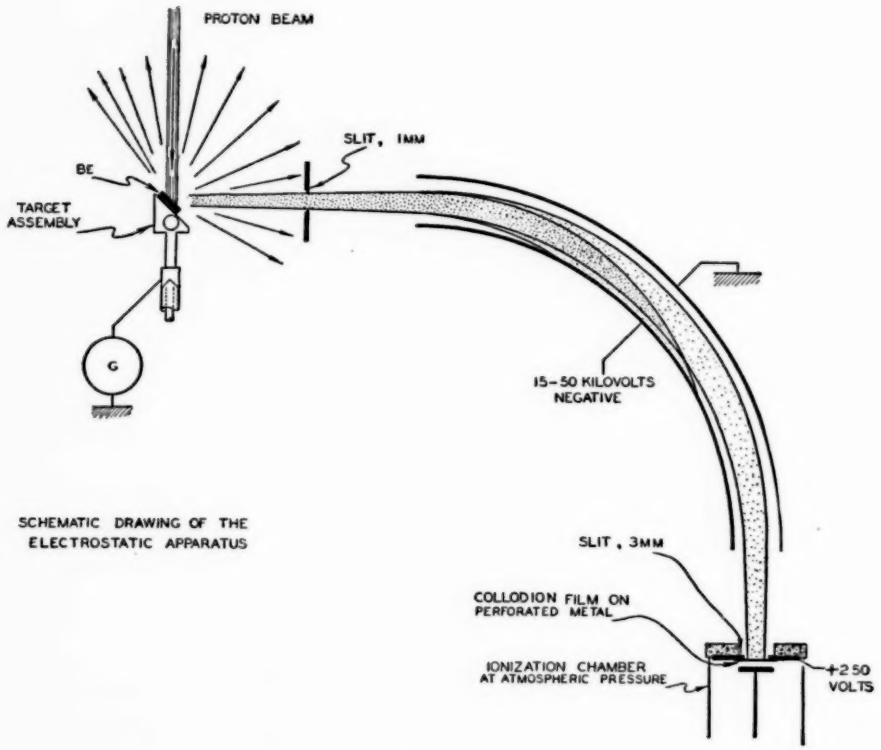

SCHEMATIC DRAWING OF THE ELECTROSTATIC APPARATUS

FIG. 1.

done at proton bombarding energies below 0.25 Mev. Under these conditions, the relative values of Q and Q' are such that the deuterons and alpha-particles have nearly the same range. The difficulty of their separate detection is thus increased. Table I shows the estimates of several observers concerning this range.

Because of the difficulty in showing that actually two different kinds of particles are present, Oliphant, Kempton, and Rutherford tried to separate the alpha's from the deuterons by passing the disintegration particles through an electric field between two parallel plates. The electric deflector was of low resolving power, and the particles showed no sign of separating into two groups. From this they concluded that $\frac{1}{2}Mv^2/ze$ (where ze is the charge of the particle) is the same for the alphas and deuterons. This would mean $E_\alpha = 2E_d$, where E is the energy of the particles. They assigned to E_α the value 1.1 Mev.

The measurement of the range of such low energy particles as these is an uncertain process, because of the necessity of introducing films, correcting for the depth of the ionization chamber, and straggling. At 7 mm range, an error of 1 mm represents roughly 200,000 volts, which is 15 percent of the total energy.

Hatch[2] has called attention to the remarkably large yield of alpha-particles from a solid target of beryllium under proton bombardment; at 400 kv a yield roughly 30 times that from a solid lithium target is obtained. Because of this high yield and low energy, it seemed to us worth while to try and increase the accuracy of the energy measurement by deflecting the particles in an electrostatic analyzer.

TABLE I. *Ranges of particles from beryllium under proton bombardment.*

OBSERVER	PROTON ENERGY (Mev)	ESTIMATED MEAN RANGE (cm)
Oliphant, Kempton, Rutherford	0.18	0.74
Döpel	0.12	continuous, out to 0.68
Kirchner and Neuert (1935)	0.16	discrete, 0.75
Kirchner and Neuert (1937)	0.14	α's 0.75; d's 0.8
Zipprich	0.05	0.66

We chose to construct an electrostatic deflection device instead of a magnetic analyzer largely because we had available in the laboratory a source of very constant high voltage which could be very accurately measured on a potentiometer-bridge circuit. The primary currrent for the high voltage is obtained from a 540-cycle generator, turned by a three phase synchronous motor mounted on the same shaft. The 540-cycle current is raised to a voltage up to 100,000 volts by a specially built transformer, rectified by kenetrons, and smoothed by a 0.1 microfarad condenser. The only appreciable current drain in our experiments was about 1 ma drawn through the Taylor wire-wound resistor of 2.8 megohms for measurement of the voltage. By means of a vacuum tube stabilizing circuit operating in the generator field, the output voltage of the system could be held constant to 2 volts in 30,000 over extended periods of time.[3]

The inner surfaces of the deflecting plates of the analyzer are sections of surfaces of two coaxial cylinders. The mean radius of the cylinders is 25.40 cm, and the space between them, 0.635 cm. The angle subtended by the deflecting plates at the axis is 90°. The plates are constructed of aluminum and are 8.26 cm high. They are held apart by two Bakelite insulators which pass through slots in the inner faces and are attached to the deflecting plates at their outsides. Thus the deflecting voltage is not supported over merely the 0.635 cm of insulator between the plates, and the contact between the plates and the separating insulator takes place in a relatively field-free region. After construction, a test of the spacing between the plates with a precision gauge showed a maximum variation of 0.005 cm from the mean. The plates were mounted in a vacuum chamber constructed of brass tubing.

The constants of such a deflector can be readily computed from the following equations, which are rather obvious approximations to the rigorous treatment:

$$r = Mv^2/Eze, \tag{3}$$

$$E = V/\{\tfrac{1}{2}(r_1+r_2)\log r_1/r_2\}, \quad r_2<r<r_1, \tag{4}$$

where r is the radius of curvature of the path of the particle through the analyzer,
r_1, r_2 are the radii of the analyzer plates,
V is the potential drop across the region between the analyzer plates.

For the beam of particles which travels along the average radius of the analyzer, we have $r=25.400$ cm, and r_1 and r_2 have the values 25.717 and 25.083 cm respectively. Using these values in the above equations, we find

$$E_2 = 20.00Vz \tag{5}$$

where E_2 is the energy of the particles in electron volts and V the deflecting potential in volts.

In a preliminary experiment, the analyzer was used on the beam of protons accelerated by our Cockcroft-Walton type circuit. The high voltage produced by the Cockcroft-Walton circuit could be accurately read by measuring the current through the high resistor whose calibration has been described by Hatch.[2] This voltage should be numerically equal to E_2, and in the region of 400 kv we found satisfactory agreement (2 to 3 percent) between the necessary analyzing voltage V and the E_2 measured with the 7.5×10^9 ohm resistor. More precise agreement could not be obtained due to the ripple in the output of the Cockcroft-Walton circuit.

Such an electrostatic deflector acts as a lens, whose focal points may be calculated by equations developed by Hughes and Rojansky, Herzog, and Dempster.[4] These equations are:

$$f^2=(l'-g)(l''-g),$$
$$f=\tfrac{1}{2}(r_1+r_2)/\{\sqrt{2}\sin 2^{\frac{1}{2}}\phi\},$$
$$g=\{\tfrac{1}{2}(r_1+r_2)/\sqrt{2}\}\cot 2^{\frac{1}{2}}\phi,$$

where l' is the distance from the entrance slit to the entrance of the analyzer, and l'' is the distance from the exit of the analyzer to the focal point. ϕ is the angle subtended by the analyzer plates at the axis. Particles of the same speed, but divergent in direction, which enter at the entrance slit, pursue different orbits through the analyzer, which, however, converge at the exit focus. With the numerical values of our analyzer, we find, as a special solution, $l'=l''=8.90$ cm.

[3] We are indebted to Mr. F. V. Stearns for the careful construction of the potentiometer-bridge circuit, and to Mr. R. B. Bowersox for the successful stabilizing circuit.

[4] A. L. Hughes and V. Rojansky, Phys. Rev. **34**, 284 (1929); R. Herzog, Zeits. f. Physik **89**, 447 (1934); A. J. Dempster, Phys. Rev. **51**, 67 (1936).

A slit 1 mm wide was placed at this distance from the entrance to the field, and a 3 mm slit was placed at the same distance from the exit. The entrance slit was 2.3 cm from the beryllium target. The 3 mm slit was a slot in the front cap of the ionization chamber in which the particles were counted. It was covered with screen and a thin foil and served as a wall of the vacuum chamber in which the analyzer operated. The height of this 3 mm slot was 2 cm.

The bursts of ionization due to the passage of charged particles through the detecting ionization chamber (3 mm deep) were amplified by a circuit of the Dunning[5] type, which was constructed by J. S. Allen.[2] The pulses were observed on the screen of an oscillograph. When the deflecting voltage of about 35,000 volts was put on the analyzer, the oscillograph showed disturbances of very high frequency, presumably connected with incipient discharges in the analyzer. Much experience in observing the oscillograph, however, made confusion of these disturbances with true particle pulses impossible. Two observers watched the oscillograph screen and counted independently the number of pulses due to particles in a given time. The two independent counts checked closely.

The resulting curves are shown in Fig. 2. The curve marked 320 kv corresponds to particles getting through the analyzer when 320 kv protons (magnetically selected) were directed at the beryllium target. Formation of carbon deposits on the target was prevented by the pre-heating method described by Hatch.[2] In taking the 320 kv curve, attention was concentrated on defining accurately the upper energy limit of the distribution, as the relatively large number of points along the upper limit indicates. Not much reliance can be placed on the shape of the 320 kv curve below the upper limit.

In taking the 383 kv curve, the observers selected visually pulses which were known to be of alpha-particle height. Deuteron pulses are only about 40 percent as intense as alpha-pulses at the maxima of specific ionization for both types, according to Kirchner and Neuert.[2] Thus it was established that the sharp upper limit found was due to alpha's. More confidence can

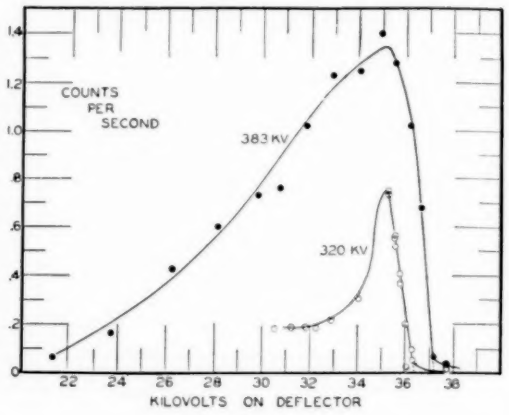

FIG. 2. The energy distribution of alpha-particles from $_4Be^9$ (p, α) $_3Li^6$ at proton energies of 320 and 383 kv. The energies of the alpha-particles may be obtained by multiplying the kilovolt values by 40.00.

be placed in the shape of the curve below the upper limit for this curve.

Although many kicks of deuteron size were seen, the noise level was too high to enable the observers to reach accurate conclusions. It seems certain, however, that there is no peak of comparable height for deuterons, and that they must be distributed over a wider energy range than the alphas. The energy spectrum of the deuterons is now under investigation.

The voltage at which the particles were describing exactly the average radius of the deflector was selected in the following manner. Let us consider a beam of particles, homogeneous in energy, admitted to the deflecting system through the 1 mm wide entrance slit. Due to the focusing action, this beam will again be one mm wide at the 3 mm slit, and changing the deflecting voltage will sweep this 1 mm beam across the 3 mm slit. When the center of the beam is displaced 2 mm from the center of the 3 mm slit, no particles will get through. From the equations of the analyzer,

$$r=\{\tfrac{1}{2}Mv^2(r_1+r_2)\log(r_1/r_2)\}/zeV,$$

whence $$dV/V=-dr/r.$$

Setting dr equal to 2 mm, the calculated correction dV is subtracted from the deflection voltage corresponding to the intersection of the extrapolated linear high energy edge with the kilovolt axis. The results are given in Table II.

A solution of the equations of conservation of

[5] J. R. Dunning, Rev. Sci. Inst. 5, 387 (1934).

energy and momentum for the special case of particles leaving at right angles to the proton beam gives

$$E_\alpha = \{E_p(1-M_p/M_{\mathrm{Li}})+Q\}/(1+M_\alpha/M_{\mathrm{Li}}),$$

where E_α is the energy of the alpha-particle,
E_p is the energy of the proton,
Q is the energy balance in the raction,
M_p, M_α, M_{Li} are the masses of the proton, alpha-particle and the lithium six isotope, respectively.

From this equation the values of Q in Table II were computed. It also follows that

$$dE_\alpha/dE_p = (1-M_p/M_{\mathrm{Li}})/(1+M_\alpha/M_{\mathrm{Li}}) = 0.500.$$

For the two curves shown in Fig. 2, dE_p is 0.063 Mev, from which the value of dE_α is computed to be 0.032 Mev. From Eq. (5) the corresponding dV is 0.794 kv. The difference in the intercepts on the axis of Fig. 2 is 0.92 kv, which is in agreement with the computed value within the limit of error. It is estimated that the experiment gives the energy of alpha-particles passing through the analyzer at a given deflecting voltage to about 2 percent.

The value of Q recommended by Livingston and Bethe,[6] is 2.28 Mev. The more precise value found in this work has a much higher internal consistency with other disintegration experiments. Consider the following cycle of reactions:

$$_4\mathrm{Be}^9 + {}_1\mathrm{H}^1 = {}_3\mathrm{Li}^6 + {}_2\mathrm{He}^4 + Q,$$
$$_4\mathrm{Be}^9 + {}_1\mathrm{H}^2 = {}_3\mathrm{Li}^7 + {}_2\mathrm{He}^4 + 7.19 \text{ Mev},$$
$${}_3\mathrm{Li}^6 + {}_1\mathrm{H}^2 = {}_3\mathrm{Li}^7 + {}_1\mathrm{H}^1 + 5.02 \text{ Mev}.$$

TABLE II. *Computations from curves of Fig. 2.*

Proton Energy (kv)	Maximum Deflecting Voltage (kv)	Corrected Deflecting Voltage (kv)	Alpha-Particle Energy (Mev)	Q (Mev)	Mass Equivalent of $Q\times10^3$
320	36.30	36.02	1.441	2.148	2.306
383	37.22	36.93	1.477	2.155	2.315

[6] Livingston and Bethe, Rev. Mod. Phys. **9**, 246 (1937).

The energy balances quoted above for the last two reactions are from Livingston and Bethe's report, and the ranges of the particles are long enough so that range determinations are quite reliable. The third of the above reactions subtracted from the second leaves the first. Thus the predicted Q for the first reaction is 2.17 Mev, which is in excellent agreement with the average of our two results, namely, 2.15 Mev.

The data from our experiment can be used to give a precise difference between the masses of Be^9 and Li^6, since the masses of the proton and alpha-particle are known with much higher accuracy than is the mass of either of the heavier atoms concerned. We have

$$M_{\mathrm{Be}} - M_{\mathrm{Li}} = M_\alpha + M_Q - M_p$$

where M_Q is the energy balance in mass units. We have used the factor 931 Mev equals 1 atomic weight unit to make this transformation. Using $M_\alpha = 4.00386 \pm 0.00006$,[7] $M_p = 1.00813 \pm 0.00002$[6] and taking an average value of the mass equivalent of Q as $2.316 \pm 0.04 \times 10^{-3}$, we obtain

$$M_{\mathrm{Be}} - M_{\mathrm{Li}} = 2.99804 \pm 0.00009.$$

Although neither the mass of Be^9 nor Li^6 is known with satisfactorily high accuracy, we may assume that of the two, Li^6 is the more accurate. Adopting Livingston and Bethe's value of 6.01686 ± 0.00020, we get

$$M_{\mathrm{Be}} = 9.01490 \pm 0.00025.$$

This is considerably lower than Livingston and Bethe's adjusted value of 9.01504 ± 0.00025, and is much lower than Jordan and Bainbridge's[8] mass-spectroscopic value of 9.01517 ± 0.00016.

We wish to thank Mr. G. T. Hatch and Mrs. E. R. Graves for assistance in performing the experiments.

[7] K. T. Bainbridge, Bull. Am. Phys. Soc. **13**, No. 2 (1938).
[8] E. B. Jordan and K. T. Bainbridge, Phys. Rev. **51**, 385 (1937).

The Preparation and Properties of Auroral Afterglows

JOSEPH KAPLAN
University of California at Los Angeles

(Received January 10, 1938)

The preparation of auroral afterglows in pure nitrogen is discussed in detail. A nomenclature is introduced for the five stages which are met most frequently in the preparation of these glows. In the normal order in which they occur they are the ozone, nitric oxide, cyanogen, Lewis-Rayleigh, and finally the auroral stage. Two plates, one showing the spectrum of the discharge in pure nitrogen, which is responsible for the production of the auroral glow, and one which shows the spectra of the nitric oxide, cyanogen and auroral stages, are reproduced.

I. INTRODUCTION

DURING the past year a considerable number of photographs have been made of nitrogen afterglow spectra with the purpose of showing the various stages in the preparation of auroral afterglows as practiced in the writer's laboratory. The inspiration for this work comes from the complete or partial failure of other observers to produce afterglows which have the spectra corresponding to that of the aurora. A discussion of these failures will be given. Laboratory studies of the earth's upper atmosphere have aided in the identification of upper atmosphere spectra obtained from auroral and night sky observations. A notable success in this field has been the identification of many night sky radiations as members of the Vegard-Kaplan bands of nitrogen. It has been possible to produce afterglows rich in the bands of this system and comparisons have been made with the bands present in the night sky spectra.[1]

II. DESCRIPTION OF TUBE AND ITS PREPARATION

The discharge tube consists of a central Pyrex or quartz bulb (100 cc to 5 liters) with side tubes of Pyrex which contain aluminum electrodes. Other side tubes may be added to introduce purifying reagents. Graded Pyrex seals are used. A tube may be filled with commercial tank nitrogen and sealed off. Streaming nitrogen cannot be used.

Various materials may be placed in the side tubes for purification and supplying nitrogen. $KMnO_4$ and P_2O_5 are employed for cleaning up hydrogen. By heating the $KMnO_4$ with a Bunsen flame it is possible to generate pure oxygen. This oxygen reacts with hydrogen in the discharge and water is formed. The P_2O_5 absorbs the water. This simple technique is found to be effective in cleaning up hydrogen. Experience in the preparation of auroral tubes has shown that strong auroral afterglows are produced only when hydrogen has been completely eliminated.[2]

$NaNO_2$ may be used as a safe and convenient source of nitrogen. On heating $NaNO_2$ in a horizontal tube it decomposes after melting and produces nitric oxide.[3] On operation of the tube the oxygen disappears and pure nitrogen remains. Nitrogen pressures vary from 10 mm to the lowest at which glow discharges are obtainable.

The tubes are operated on a 1 kw 15,000 to 25,000-volt sign transformer. An intermittent discharge is required in the preparation and later operation of the tube. This is produced by some device for making and breaking the primary current in the transformer.

III. STAGES IN THE PREPARATION OF THE GLOW TUBE

When carbon and oxygen are present as impurities five distinct stages can usually be observed in the preparation of a glow tube. These we shall name: (1) ozone stage, (2) nitric oxide stage, (3) cyanogen stage, (4) Lewis-Rayleigh afterglow, and (5) auroral stage. The first distinct afterglow stage shows a commonly observed green afterglow. It is ascribed to chemical reaction between NO_2 and O_3. Its spectrum appears

[1] Kaplan, Pub. Astr. Soc. Pac. **47**, 257 (1935).

[2] Kaplan, Nature **136**, 549 (1935).

[3] A horizontal tube is preferred to a vertical one since a vertical one usually cracks when the $NaNO_2$ is reheated.

to be continuous although banded structure has been reported by some observers. If a trace of carbon is present the red cyanogen bands may be superposed on the continuous background of the nitrogen oxygen glow and give the appearance of a banded structure. Ozone appears to be necessary for the glow. As the oxygen is cleaned up during the ozone stage the continuous afterglow becomes weak and finally disappears.

The nitric oxide stage next appears. The afterglow is blue in color and its spectrum is characterized by the presence of the β-bands of NO in the visible and ultraviolet and the γ-bands in the ultraviolet. This appears to be the first step in the production of the Lewis-Rayleigh afterglow which develops later.

If carbon is present the cyanogen stage follows. This is one of the most beautiful stages of the tube. The afterglow is a fairly long lived flash which takes on the same shape as that of the discharge. The luminosity of this glow is very high. In fact, it appears to be higher than that of any other nitrogen afterglow known to the writer. The spectrum of the afterglow easily observed through a direct vision spectroscope consists almost entirely of the two well-known band systems of the CN radical, the violet and the red systems. Particularly striking is the high intensity with which the cyanogen tail bands appear in the afterglow. The intensity is to the best of the writer's knowledge the best obtainable and makes this stage a valuable one for the study of these bands.[4]

The strong yellow glow follows the cleaning up of the carbon. This is called the Lewis-Rayleigh glow because of the work of Lewis and Rayleigh on the active nitrogen.

The relation of this glow to the nitric oxide glow is shown by the fact that the introduction of oxygen into the yellow glow produces the nitric oxide glow. Undoubtedly the mechanisms of the ozone stage and that in the Lewis-Rayleigh and NO stages are different. The presence of a dark stage in some tubes between the ozone and NO stages supports this conclusion.

It should be pointed out here that the sequence of distinct stages which has been described is not closely adhered to in all tubes. The duration of any stage depends of course on the amount of the particular impurity, oxygen or carbon, which is responsible for that stage. There have been tubes in which the straw-yellow Lewis-Rayleigh glow was practically missing and the auroral glow was followed by the cyanogen stage. On the other hand, tubes have been observed in which a distinct Lewis-Rayleigh glow has been present for a long time after the tube had passed through all the other stages. It appears as if the cyanogen stage may develop before a distinct Lewis-Rayleigh stage or it may develop just before the auroral stage.

The peculiar behavior of the cyanogen stage and certain extensive observations on interaction between pure oxygen and the auroral afterglows[5] has led us to believe that there are three afterglows distinct in a sense that there are three essentially different excitation mechanisms. These glows are the afterglow which is present in the ozone stage, the straw-yellow L-R glow, and the auroral glow.

While the three afterglow tubes have been presented for the purposes of classifying the afterglows we must not forget that after the tube has reached the auroral stage the afterglow is very definitely a function of pressure, current, and even of the duration of the exciting discharge.

Several interesting phenomena observed during the preparation of the auroral tubes will be described. When a tube which has not been used for some time is again operated it shows during the first few minutes of operation a spectrum in both discharge and afterglow which corresponds to a stage to which the tube is approaching. After operation for a few minutes it reverts to its proper stage and then on further operation continues to advance through later stages. This observation is interesting in that it gives one a preview of a stage toward which the tube is advancing.

Glows differing from those in the main portion of the tube occur in the narrow portion of the

[4] The close resemblance between the red CN bands and the first positive bands of N_2 makes it necessary to be careful in announcing results of band intensities in these glows. The strong band $\lambda 3883$ of the violet system persists with good relative intensity down to remarkably small carbon concentrations and one should always be on guard and not mistake these bands for N_2^+ bands since again the violet bands resemble the N_2^+ first negative bands very closely and lie in the same spectral range.

[5] Kaplan, Trans. Am. Geoph. Union (1936).

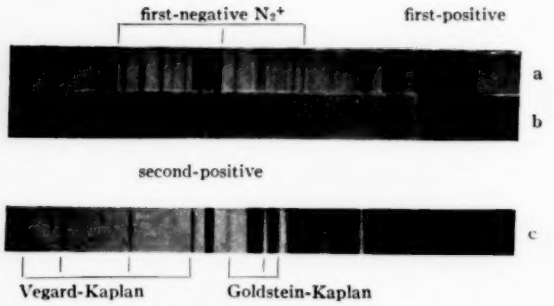

FIG. 1. *a*. Auroral discharge, visible; *b*. ordinary discharge, visible; *c*. auroral discharge, ultraviolet.

tube near the electrodes. These may be one stage in advance of the glows in the main section of the tube, that is, when the spherical section contains the auroral glow the smaller portion may be nearly dark, at least no visible light may be seen. There may be ultraviolet light as this phenomena has not been studied in quartz tubes. This observation leads us to suggest that there may be a "dark" stage later than the auroral stage.

There are three criteria which indicate that the tube is nearly or definitely in the auroral stage. The first is the violet and blue first negative bands of N_2^+. As the tube is almost through the cyanogen or L-R stages, depending on the sequence, these bands set in and as the tube progresses toward the auroral stage their intensity relative to the second-positive bands in the blue and violet increases so that finally the spectrum appears to be almost a pure ion spectrum in the blue and violet. The remarkable thing about the appearance of these bands at pressures as high as 10–20 mm is that they are emitted by the nitrogen molecule ion.

The second sign that the tube is on its way to a real auroral stage is the increasing relative intensity of the green sequence of the first-positive system of N_2. When one observes the first-positive bands through a direct-vision spectroscope there are four distinct sequences observable, red, yellow-orange, yellow-green and green. The green sequence consists of bands which arise on $v'=16-20$ and at the present time experi-

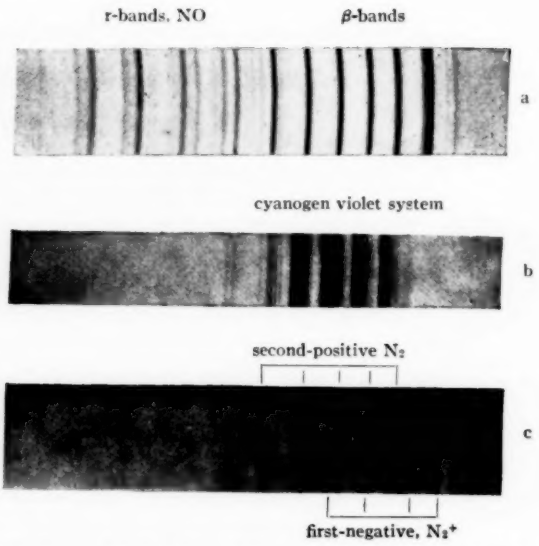

FIG. 2. *a*. Afterglow, nitric oxide stage; *b*. afterglow, cyanogen stage; *c*. afterglow, auroral stage.

ments are in progress in an attempt to obtain good plates of this characteristic enhancement of the green sequence.

Probably the most important criterion of the auroral stage is the presence of the Vegard-Kaplan bands, $A^3\Sigma \rightarrow X'\Sigma$. These bands also increase in intensity relative to the neighboring second-positive system as the tube progresses toward the auroral stage. In a sense they are the most interesting of the three criteria because it was in an auroral tube that they were first observed in gaseous nitrogen in the laboratory.

Finally, in closing, we wish to present two photographs. On Fig. 1 are spectra which illustrate a few typical discharge spectra which are obtained during the preparation of the tubes. On Fig. 2 is a sequence of afterglow spectra from the nitric oxide stage through to a very good auroral stage.

The writer wishes to acknowledge a grant-in-aid from the National Research Council and also the generous research funds which the University of California has granted to him during his work on this and other problems.

The Refractive Index of Air in the Visible and Photographic Infra-Red

DAVID BENDER
California Institute of Technology, Pasadena, California*
(Received April 13, 1938)

The refractive index of dry CO_2 free air has been measured from 5300A to 11177A by means of a Fabry-Perot interferometer with invar separating posts. The following dispersion curve was obtained for standard conditions (λ in microns):

$$(n_0-1)10^7=2885.59+15.77/\lambda^2+0.421/\lambda^4.$$

A comparison of the present results with those of other observers shows that this curve is higher by about 10 parts in 10^7, and that all curves are nearly parallel. This suggests that the discrepancies are due to systematic errors providing, as seems to be the case, that the constitution of air remains sufficiently constant. In the present experiments systematic errors due to phase change at reflection, methods of purification of the air, and bulk modulus of the invar posts were considered. A calculation concerning the oxygen absorption band at 7600A indicates that this band has no measurable effect on the dispersion of air.

FOR many purposes, in particular in astrophysical work, it is important to know the index of refraction of air to the limit of the photographic infra-red. In addition there exist discrepancies of the order of 10 to 15 parts in 10^7 among the results of various observers in the visible region. Such discrepancies might be attributed to variations in the composition of the air, but experiments carried out since 1850 indicate that the percentage of oxygen in normal, (0°C and 760 mm pressure) dry, CO_2 free air does not vary more than ± 0.2 percent.[1] This much change in the relative amount of oxygen and nitrogen would cause a change in the index of refraction of approximately 0.5 parts in 10^7, which is far too small to account for the discrepancies. For both of these reasons a precision study of this quantity seems justified.

In previous experiments the index of refraction has been measured out to approximately 9000A. The present experiments have pushed that limit more than 2000A farther into the red and show that, despite the inaccuracies accompanying measurements in these longer wave-length regions, the dispersion of air behaves normally. Because of this fact and the fact that the varying terms in the dispersion formula decrease toward the red, the curves of other observers can be extrapolated in this direction as much as two thousand angstroms with little loss in accuracy. In fact the consistency of this extrapolation as compared to observations throughout the regions considered, might well be a criterion for judging the validity of a given dispersion formula.

The method of obtaining the index of refraction used in the present experiment was to observe the change in the order of interference for each wave-length on a Fabry-Perot interferometer when it was placed in a vacuum and when it was placed in dry CO_2 free air. The temperature of the brass vacuum chamber was held constant by thermostat controls which kept the temperature of the air just outside the chamber within a range of ± 0.05°C. This temperature (taken as the temperature of the air in the vacuum chamber) was measured on a thermometer graduated in tenths of degrees and carefully checked against a similar one calibrated by the National Bureau of Standards. The pressure of the air was measured on a large closed tube manometer by means of a cathetometer, the glass scale of which had been previously calibrated by Campbell.[2]

The lines used were neon lines with only one exception, the mercury line at 10140A. For the lines out to 8800A the tube was operated under conditions which conformed to the requirements set by Jackson[3] for obtaining the neon secondary standards of wave-length. For lines farther out the current in the tube was increased from 25 milliamperes to 52 milliamperes in order to shorten the exposure. The lines out to 10000A could be obtained nearly as sharp as the shorter wave-lengths, but beyond that point the ex-

* Now at Louisiana State University.
[1] M. S. Blanchard and S. F. Pickering, Nat. Bur. Stand. Sci. Papers **21**, 167 (1926).
[2] Campbell and Houston, Phys. Rev. **39**, 601 (1932).
[3] C. V. Jackson, Proc. Roy Soc. **A143**, 124 (1933).

posures were so long (as much as twelve hours in some cases) and the lines so faint and broad that in this region the accuracy of the results is poor. The mercury line is inherently broader than most of the neon lines but it turned out that the neon lines at 11000A were of comparable broadness.

In order to obtain dry CO_2 free air several procedures were tried. Many of the runs were treated as follows: after first drying the air over calcium chloride and phosphorus pentoxide, it was passed through coils immersed in liquid air. This method will definitely remove the carbon dioxide and the water vapor, but it was thought that cooling the air might also remove a fraction of the oxygen. To investigate this, results were obtained when the carbon dioxide was removed by bubbling the air through a six normal solution of potassium hydroxide before it was dried over calcium chloride and phosphorus pentoxide. The results of the two methods were indistinguishable from one another. The final arrangement adopted was a combination of these two. After passing through the potassium hydroxide solution and over the calcium chloride and magnesium perchlorate, the air was passed through the cooled coils shielded with cylindrical copper jacket from direct contact with the liquid air. Never was there a trace of frozen dioxide or of frost that could be seen in the coil when the liquid air and the shield were quickly removed.

Each run consisted of at least three exposures alternately with vacuum and with air. In order to assure temperature equilibrium, the air was let in slowly and the exposure started after 30 to 50 minutes had elapsed. The vacuum was assured by pumping until the system would no longer take a discharge from the transformer used to excite the source.

Despite precautions to keep the temperature constant and to reduce vibration, the orders of interference on the two vacuum exposures failed to agree satisfactorily in almost 80 percent of the runs. These changes were random in direction and merely indicated that a selection of plates was necessary to reduce the accidental errors. A criterion for this selection was immediately available in the reproducibility of the orders of interference of the first and the last exposures. Only those plates on which the zero readings repeated to within 0.0030 fringes on the average were measured (except for wave-lengths beyond 10000A where the tolerance was increased to 0.015 fringes). A variation of 0.0030 fringes corresponds on the average to about one part in 10^7 in the index of refraction.

To find the fractional order of interference at the center of the plate a method of least squares was used on eight consecutive fringes. The method is essentially that developed by Rolt and Barrell.[4] With the observed fractional orders of interference the integral orders of interference were calculated in the usual manner and the index of refraction obtained as the ratio of the complete order of interference in air to the complete order in the vacuum.

The values of the index were obtained at some pressure between 700 mm and 740 mm of mercury and at some temperature between 25° and 31°C. To change the observed values of the index to standard conditions the formula $(n-1)/d = \text{constant}$ (d = density of air) was used. The ratio of the densities at the two conditions was assumed to be that of a perfect gas. Both Meggers and Peters[5] and Perard[6] have given values for the temperature coefficient of the index. Meggers and Peters find that it is slightly larger than the reciprocal of the absolute zero and that it decreases with increasing wave-length. Perard, on the other hand, states that the temperature coefficient is independent of wave-length and gives a value higher than that of the Bureau. At 7000A the error introduced by using the perfect gas coefficient over a temperature range of 30°C is according to the value of Meggers and Peters 0.9 part in 10^7, while according to the

TABLE I. *Distribution of weighting used in different wave-length regions.*

REGION	WEIGHTING
5300– 6500A	6.50
6500– 7600A	13.68
7600– 9000A	11.85
9000–10000A	2.61
10000–12000A	0.40
Total	35.04

[4] Rolt and Barrell, Proc. Roy. Soc. of London **122**, 122 (1929).

[5] Meggers and Peters, Nat. Bur. Stand. Bull. **14**, 697 (1918).

[6] Perard, J. de phys. et rad. **6**, 217 (1924).

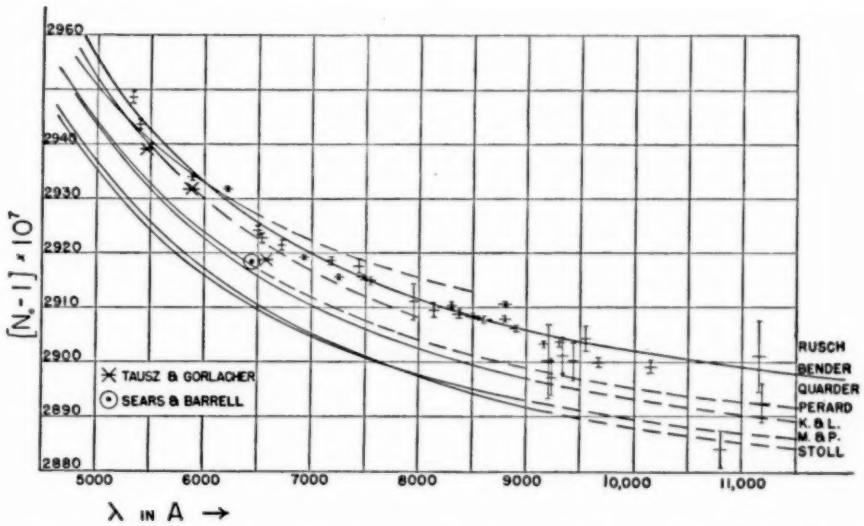

FIG. 1. Dispersion curves for normal air. The curves plotted are those obtained since 1918, except that the curve of Traub was omitted because of its proximity to that of Perard. The lengths of the lines give the estimated probable errors of the points used in the calculation of the author's curve.

value of Perard, it is 4 0 parts in 10^7. In view of these conflicting reports it seemed advisable simply to use the perfect gas coefficient.

In the estimation of probable error for each observation the following factors were taken into account: the error introduced because the zero readings did not repeat exactly, the error of measurement of the order of interference (of the same magnitude as the first) and the error due to the uncertainty in the pressure and temperature (always the smallest). At each wave-length used an average value was obtained from the observed values and weights calculated from the above errors. In order to calculate the weight of these averages (or probable errors as shown on the dispersion curves) several factors were considered. The total of the previous weights as well as the number of observations and the agreement among them entered into calculations. The final distribution of weighting among the wave-length regions used is given in Table I.

In order to make sure that the change of phase at reflection was a negligible factor, two separators were used in the interferometer: one of 14 mm, and one of 21 mm. No systematic difference in results was apparent between these two sets of measurements.

The posts in the separators were made of invar steel, which has a bulk modulus of about 12×10^{11} dynes/(sq. cm). This means that a pressure change of one atmosphere will cause a change in length of 2.8 parts in 10^7. Since the posts were free to expand against small springs, the value of the index will be in error by just this amount and must be increased. This correction was made.

The usual Cauchy dispersion formula was used to describe the results at standard conditions. (0°C and 760 mm of mercury.)

$$(n_0-1)\cdot10^7=A+(B/\lambda^2)+(C/\lambda^4).$$

The method of least squares applied to the observed averages at each wave-length and their probable errors gave for standard conditions (with λ in microns):

$$(n_0-1)\cdot10^7=2885.59+15.77/\lambda^2+0.421/\lambda^4 +[\pm2.16\pm2.19/\lambda^2\pm0.52/\lambda^4].^7$$

The dispersion curves show the observed values and the differences from calculated values. The lengths of the lines show the probable errors as obtained from the averaging of the separate measurements at each wave-length. In Table II there are compiled the constants in the dispersion formulae for the observers of the index of refraction of air, since 1918, several values calculated

[7] Obtained with the aid of equations, Whittaker and Robinson, *The Calculus of Observations*, second edition, p. 241.

from these constants, and the range over which measurements were taken. No extrapolations of greater than 2000 angstroms were made except in the case of Perard's curve. Not all data deal with CO_2 free air, but deal with dry air. The error introduced by the CO_2 in the air is quite negligible compared to the differences between observers. The values obtained by the various observers for n_0-1 are plotted in Fig. 1.

Since there exists at about 7600A, a strong oxygen absorption band, it becomes necessary to see theoretically whether or not this band and others near by could effect the dispersion enough to be measured. This band has been analyzed by Badger and Mecke,[8] who find it to extend over a range of nearly 70A and to have about forty lines. The f value for the band as a whole has been given by Childs and Mecke[9] as 0.4×10^{-9}. That is, there are Nf dispersing electrons per cu. cm where N is the number of molecules per cu. cm. From this we obtain the value of $(n-1)$ for these electrons at a point 50A away from the band center to be 0.42×10^{-10}. Since the band is broad and since it is composed of many lines, it is at once apparent that the effect of this band and any other fainter bands on the dispersion of air is negligible, as the results show.

It is apparent that the dispersion curves run in general parallel to one another. Consequently the present experiments, which cover a range of nearly 6000A, show, in comparison with other curves, that the dispersion of air can be adequately expressed throughout the whole visible and photographic infra-red by the Cauchy formula.

In order to explain the difference between observers of the index of refraction of air we must look for systematic errors. The most obvious possibility is that the composition of the air is not sufficiently constant from place to place and from time to time. As was mentioned above, experiments on the constitution of air seem to indicate that this deviation is not sufficient to cause the large differences that exist between observers. Perhaps insufficient care in the methods of sampling and purifying the air can explain the discrepancies. Simultaneous experiments measuring both the constitution and the index of refraction have not been carried out.

All experiments which measure the index of refraction of air use an air path which must not change in length when the path is evacuated. This ideal condition cannot actually be realized since all substances have definite bulk moduli, but in some experiments, especially those in which the Jamin type interferometer is used, this condition is less important than in others. It should not be inferred from this, however, that the Jamin type is much better, for the windows which are distorted by the change in pressure are in the interference path. For such experiments no correction needs be made, but for those which use a Fabry-Perot interferometer, it is necessary. Many observers, notably Meggers and Peters, have not made this correction, although it is not

TABLE II. *Dispersion formulae and values of the index.*

OBSERVER	REF.	A	B	C	5000A	7000A	9000A	11000A	RANGE A
Meggers and Peters (1918)	5	2875.66	13.412	0.378	2935.3	2904.6	2892.8	2887.0	2220–9000
Traub (1922)	10	2876.13*	16.397	0.127	2943.8	2910.1			1850–5460
Stoll (1922)	11	2871.87	16.170		2936.6	2904.9	2891.8	2885.2	4390–9220
Quarder (1924)	12	2879.87	18.04		2952.0	2916.7			2620–5780
Perard (1925)	6	2880.2	14.748	0.316	2944.2	2911.6	2898.9		4360–6440
Rusch (1927)	13	2893.19*	14.05	0.068	2950.5	2922.1			5460–6560 and 67,630
Tausz and Gorlacher (1931)	14	Only four measurements			2951.4	2915.0	(estimated)		
Sears and Barrell (1934)	15	Only one measurement (2918.4 at 6438A) = (2911.7 at 7000A)							
Kosters and Lampe (1934)	16	2877.10	15.84	0.194	2943.6	2910.2	2897.0	2890.3	2000–9000
Bender (1938)		2885.59	15.77	0.421	2955.4	2919.5	2905.7	2898.9	5300–11,780

* Formula not given in Cauchy form by author but changed to Cauchy form for better comparison in this table.

[8] Badger and Mecke, Zeits. f. Physik **60**, 59 (1930).
[9] Childs and Mecke, Zeits. f. Physik **68**, 344 (1931).
[10] Traub, Ann. d. Physik **61**, 533 (1920).
[11] Stoll, Ann. d. Physik **69**, 81 (1922).
[12] Quarder, Ann. d. Physik **74**, 255 (1924).
[13] Rusch, Ann. d. Physik **85**, 581 (1927).
[14] Tausz and Gorlacher, Zeits. f. tech. Physik **12**, 19 (1931).
[15] Sears and Barrell, Phil. Trans. Roy. Soc. **233**, 143 (1934).
[16] Kosters and Lampe, Physik. Zeits. **35**, 223 (1934).

nearly as large as the differences to be accounted for.

It is interesting to note that Tilton[17] claims some success in finding a correlation between the values for the index of refraction of air and the sunspot cycle.

It seems clear that no adequate explanation can be given of the various discrepancies, but that one can only attempt to eliminate systematic errors by careful attention to every detail.

In conclusion I wish to acknowledge the assistance and helpful guidance of Professor W. V. Houston and the many valuable suggestions of Professor I. S. Bowen in carrying out this research.

[17] Tilton, Nat. Bur. Stand. J. Research **13**, 11 (1934).

AUGUST 1, 1938 PHYSICAL REVIEW VOLUME 54

The Spectrum of Neutral Iridium, Ir I

WALTER ALBERTSON
George Eastman Research Laboratory of Physics, Massachusetts Institute of Technology, Cambridge, Massachusetts

(Received May 28, 1938)

A new description of the arc spectrum of iridium has been made. The present data include 3100 wave-lengths of which 1937 have been accounted for as combinations between 214 energy levels. The normal electron configuration of the Ir I is $5d^7 6s^2$ and the I.P. is approximately 9.2 volts. Tables of the most intense lines and of all of the energy levels are presented.

THE existing wave-length data for the arc spectrum of iridium have been improved and extended. Exposures from a 110-volt 2-ampere arc between rods of extremely pure iridium were taken in the first and second orders of the 35 foot, 30,000 line per inch grating at M.I.T., dispersion 0.4A/mm in the second order. Superimposed spectra from a standard iron arc permitted measurement of the iridium spectrum in terms of internationally adopted secondary standards.

New data are recorded from 4627A to 2159A, supplementing the excellent data of Meggers[1] (8426A to 4500A). Intensity estimates are on a scale of 100 to 1. The present list contains more than 3100 wave-lengths which have been assigned to Ir I by comparison with spark spectra. The earlier analysis[2] has been extended on the basis of new data until now 1937 lines are accounted for as combinations between 214 energy levels.

The complete list of classified lines is not published at this time since it is probable that most of the wave-lengths will be published elsewhere at a later date. A list of the most intense lines is presented in Table I. Column 1 gives the wave-length in international angstroms in air; column 2, estimated intensities (*r* signifies partial reversal); column 3, the term types of the two energy levels that give rise to the line.

All energy levels are presented in Table II. Column 1 gives the symbol which identifies the level; column 2, the term type; column 3, the energy value expressed in wave number units; column 4, the *J* value.

The electron configuration interactions are so great that the assignment of terms to definite configurations is nearly without meaning. However, the custom of assigning terms to the configuration which seems to play the most impor-

[1] Meggers, Sci. Papers Nat. Bur. Stand. **20**, 19 (1925).
[2] Albertson, Phys. Rev. **42**, 443 (1932).

TABLE I. *Most intense iridium arc lines.*

λ I.A.	Int.	Combination	λ I.A.	Int.	Combination
5449.50	80	$z^6G_{4\frac{1}{2}}^0 - e^6F_{4\frac{1}{2}}$	3212.121	60	$b^4F_{2\frac{1}{2}} - z^6G_{4\frac{1}{2}}^0$
4399.473	60	$z^6F_{3\frac{1}{2}}^0 - e^6F_{4\frac{1}{2}}$	3198.917	60	$b^4F_{2\frac{1}{2}} - z^6D_{2\frac{1}{2}}^0$
4268.096	80	$b^4F_{2\frac{1}{2}} - z^6D_{3\frac{1}{2}}^0$	3068.897	60	$b^4F_{4\frac{1}{2}} - z^6G_{3\frac{1}{2}}^0$
3992.114	80	$b^4F_{2\frac{1}{2}} - z^6F_{2\frac{1}{2}}^0$	2924.783	100*r*	$a^4F_{4\frac{1}{2}} - z^6G_{3\frac{1}{2}}^0$
3915.384	60	$b^4F_{2\frac{1}{2}} - z^6G_{2\frac{1}{2}}^0$	2916.357	60	$a^4F_{1\frac{1}{2}} - z^4D_{2\frac{1}{2}}^0$
3800.122	60*r*	$a^4F_{4\frac{1}{2}} - z^6D_{4\frac{1}{2}}^0$	2882.624	60	$b^4F_{4\frac{1}{2}} - z^4D_{3\frac{1}{2}}^0$
3513.638	80*r*	$a^4F_{4\frac{1}{2}} - z^6F_{5\frac{1}{2}}^0$	2849.724	80*r*	$a^4F_{4\frac{1}{2}} - z^6G_{4\frac{1}{2}}^0$
3448.967	60	$a^4F_{1\frac{1}{2}} - z^6D_{2\frac{1}{2}}^0$	2836.394	60	$a^4F_{1\frac{1}{2}} - z^6F_{2\frac{1}{2}}^0$
3437.006	60	$a^4F_{2\frac{1}{2}} - z^6G_{3\frac{1}{2}}^0$	2824.444	60*r*	$b^4F_{4\frac{1}{2}} - z^6G_{4\frac{1}{2}}^0$
3368.472	60	$b^4F_{4\frac{1}{2}} - z^6F_{4\frac{1}{2}}^0$	2664.783	50*r*	$a^4F_{4\frac{1}{2}} - z^4D_{3\frac{1}{2}}^0$
3266.446	60	$a^4F_{2\frac{1}{2}} - z^6F_{1\frac{1}{2}}^0$	2639.698	60*r*	$a^4F_{4\frac{1}{2}} - z^6F_{4\frac{1}{2}}^0$
3220.772	100*r*	$b^4F_{4\frac{1}{2}} - z^6F_{5\frac{1}{2}}^0$			

TABLE II. *Energy levels of* Ir I.

LEVEL	TERM TYPE	ENERGY	J VALUE	LEVEL	TERM TYPE	ENERGY	J VALUE
		Even Levels					
1	a^4F	0.00	4½	137	e^6F	52508.89	4½
2	b^4F	2834.96	4½	153		54892.63	4½
3	a^4F	4078.93	1½	158		55303.64	2½
4	a^4F	5784.58	2½	160		55382.00	3½
5	a^4F	6323.91	3½	165		55885.44	1½
6	b^4F	7106.57	3½	171		56416.08	4½
7	b^4F	9877.51	2½	174		56792.60	3½
8		10578.66	1½	181		57838.92	1½
9		11831.07	1½	189		59525.87	5½
10		12218.46	2½	191		59647.72	3½
11		12951.65	2½	193		59824.51	2½
12		13087.88	3½	194		59878.01	3½
13.		13939.79	4½	196		60012.24	4½
14		16103.33	2½	197		60062.44	2½
15		16565.35	1½	199		60663.13	1½
16		16681.19	½	200		61431.45	1½
17		17779.24	3½	201		61481.36	1½
18		18547.02	1½	202		62018.82	3½
19		19060.62	2½	203		62164.91	3½
20		19593.24	5½	204		62208.64	5½
21		20236.71	½	205		62220.91	3½–4½
22		22110.24	1½	206		62284.41	?
23		23310.36	2½	207		62377.74	3½
24		23505.91	4½	208		62475.80	½
25		26229.48	1½	209		62757.18	2½–3½
27		26365.16	3½	210		62835.40	4½
28		26404.17	2½	211		63391.27	1½
29		27913.84	4½	212		63469.72	4½
30		27970.05	1½	213		63976.18	3½
125	e^6F	51175.95	5½	214		64618.16	3½
		Odd Levels					
26	z^6D^0	26307.48	4½	52	z^4G^0	38568.05	3½
31	z^6F^0	28452.34	5½	53	z^4D^0	39289.29	½
32	z^6D^0	30529.66	3½	54	z^4F^0	39324.56	2½
33	z^6D^0	32463.57	1½	55	z^4G^0	39805.97	2½
34	z^6F^0	32513.42	4½	56	z^4G^0	39940.28	5½
35	z^6G^0	32830.78	6½	57		40291.19	3½
36	z^6D^0	33064.83	2½	58		40389.85	4½
37	z^6F^0	33874.43	3½	59	z^4F^0	40524.72	1½
38	z^6G^0	34180.48	5½	60		20710.78	3½
39	z^6F^0	34919.81	2½	61		41118.74	4½
40	z^6G^0	35080.71	4½	62		41210.33	½
41	z^6G^0	35410.61	3½	63		41522.22	2½
42	z^6D^0	35647.93	½	64		42014.44	½
43	z^6F^0	36390.15	1½	65		42029.14	1½
44	z^6G^0	37446.13	2½	66		42131.82	5½
45	z^4D^0	37515.34	3½	67		42267.86	2½
46	z^6G^0	37692.74	1½	68		42279.31	4½
47	z^4F^0	37871.72	4½	69		43071.77	2½
48	z^6F^0	38120.93	½	70		43176.15	3½
49	z^4F^0	38158.24	3½	71		43200.92	1½
50	z^4G^0	38229.75	4½	72		43592.23	3½
51	z^4D^0	38358.13	2½	73		44569.85	1½
		Odd Levels					
74		44596.77	2½	130		51983.90	½
75		44642.67	3½	131		52051.75	2½
76		44652.43	4½	132		52134.11	3½
77		44785.45	1½	133		52224.37	3½
78		45111.69	3½	134		52303.65	1½
79		45185.95	2½–3½	135		52327.33	2½
80		45259.14	1½	136		52388.36	½
81		45415.26	½	138		52605.16	2½
82		45503.15	½	139		52806.57	2½
83		45570.90	2½	140		53095.26	3½–4½
84		45895.83	3½	141		53552.90	2½
85		45957.33	5½	142		53642.06	4½
86		46093.84	2½	143		53686.98	3½
87		46220.33	4½	144		53771.90	3½
88		46371.64	4½	145		54061.30	5½
89		46471.84	1½	146		54119.23	2½
90		46618.13	1½	147		54140.85	3½
91		46655.94	2½	148		54319.92	1½
92		46978.02	3½	149		54566.06	3½
93		47011.09	2½	150		54639.29	2½
94		47165.12	3½	151		54667.53	4½
95		47203.81	½	152		54711.08	3½
96		47205.55	4½	154		54894.79	3½
97		47537.29	2½	155		54985.38	1½
98		47548.64	3½	156		55035.99	4½
99		47824.91	1½	157		55160.83	1½
100		47858.47	5½	159		55332.89	2½
101		48206.57	2½	161		55425.88	1½
102		48299.24	4½	162		55497.33	1½
103		48440.83	1½	163		55619.38	3½
104		48448.65	3½	164		55635.34	½
105		48629.22	3½	166		55913.57	2½
106		48801.91	?	167		56016.58	1½
107		49146.43	2½	168		56128.84	½
108		49158.60	4½	169		56264.76	2½
109		49342.51	1½	170		56371.05	3½
110		49446.21	1½	172		56538.45	1½
111		49621.32	2½	173		56788.21	1½
112		49719.17	5½	175		56838.78	1½–2½
113		49779.37	2½	176		57186.61	3½
114		49823.53	3½	177		57247.57	2½
115		50050.69	4½	178		57697.46	3½
116		50100.71	1½	179		57737.04	1½
117		50169.87	2½	180		57774.99	4½
118		50434.46	4½	182		58026.64	1½
119		50445.02	½	183		58042.02	2½
120		50564.12	1½	184		58383.13	1½
121		50580.39	3½	185		58570.58	4½
122		50606.36	5½	186		58625.08	3½
123		51107.94	3½	187		58754.35	2½–1½
124		51166.52	1½	188		59354.05	2½
126		51427.14	2½	190		59564.11	1½
127		51470.74	4½	192		59674.86	3½
128		51814.75	2½	195		59946.55	2½
129		51852.35	3½	198		60082.68	1½–2½

tant part in its origin will be followed here. Accordingly, the term a^4F is from $5d^76s^2$; b^4F from $5d^86s$; $z^6DFG°$ and $z^4DFG°$ from $5d^76s6p$; e^6F from $5d^77s$.

Since the departure from LS coupling is very big for all elements in the lower right corner of the period table, and also, since the interaction of terms having the same parity and J value quite large, the exact assignments of L and S values to the levels are meaningless. In the present case those values of L and S which seem to predominate are assigned to certain of the levels.

A simple series relationship is assumed to exist between $a^4F_{4\frac{1}{2}}$ and $e^6F_{5\frac{1}{2}}$, which yields an approximate value of 9.2 volts for the ionization potential of Ir I.

Secondary Emission of Beryllium

EDWIN G. SCHNEIDER*
Farnsworth Television Incorporated, Philadelphia, Pennsylvania
(Received March 28, 1938)

The secondary electron emission of beryllium films prepared by evaporation in a high vacuum has been studied. As the beryllium is deposited the secondary emission ratio (defined as the ratio of the number of electrons leaving the surface, to the number of primary electrons impinging on it) rises from that of the support metal to a value in the neighborhood of 2.5. The position of the maximum with respect to energy of primary electrons remains near that of the support metal. As the thickness of the layer is increased the ratio falls to less than unity and the voltage of the primary electrons necessary to reach the maximum drops to about 200 volts. Heating the thick beryllium layer to a bright red for a few minutes raises the emission to about 1.6 with the maximum at a primary energy of about 630 volts. Oxidation of the surface increases the emission to about 4.1. Explanations of these effects are discussed and arguments are presented favoring the acceptance of the value of 1.6 as the maximum secondary emission ratio to be expected for pure bulk beryllium.

MEASUREMENTS on the secondary emission of beryllium which had been exposed to air[1,2] indicate that the maximum ratio of secondary to primary electrons is 4.5 while data on beryllium films prepared under excellent vacuum conditions by evaporation[3] show that the ratio may be as low as 0.53. Although this discrepancy is readily explained by the assumption of a layer of oxide on the samples which had been exposed to air, the divergence of results is sufficient to invite further study.

For this purpose the electrode arrangement shown in Fig. 1 was used. G is a crude electron gun, S the secondary emitting surface, C the electrodes used to collect the secondary electrons, E a spiral filament wound around a small piece of beryllium, and B emission filaments so placed that all metal parts could be heated by electron bombardment.

By scattering powdered willemite over the elements of a tube of this design, it was possible to see the pattern made by the primary electrons striking the plate, S. With the focusing electrode of G at cathode potential or a volt or so negative the primary electron beam at the plate was less than a quarter of the distance between the collecting electrodes in width. Furthermore when the collector was at a potential sufficiently higher than that of the secondary emitting surface to make the space charge formed between S and C negligible, the measured secondary emission ratio was independent of the collector voltage. These observations are consistent with the view that all of the current from the electron gun strikes the surface, S, and that all of the secondary electrons are collected by C. If this assumption is true, the secondary emission ratio is obtained by dividing the current received by the collector by the current leaving the electron gun.

In all except two of the tubes used for measurement the metal parts were molybdenum, tantalum and tungsten. Because of the high melting points of these metals it was possible to reduce the residual gas to an extremely small quantity. There were no stopcocks or wax joints on the high vacuum side of the mercury pump and liquid nitrogen trap.

Pure tantalum wire was used for the evaporating filament because it showed less tendency to alloy with the beryllium than tungsten. A trial run without beryllium showed that heating the evaporating filament for two hours at a temperature about 200°C above that used for deposition of the beryllium did not change the secondary emission of a molybdenum plate. The beryllium films were always formed in less than thirty minutes.

The tubes were given a preliminary outgassing by heating the metal parts by high potential electron bombardment from the filaments, B, until no gas discharge was observed. An electric

* Now at Stevens Institute of Technology, Hoboken, N. J.

[1] P. L. Copeland, Phys. Rev. **46**, 167 (1934).
[2] B. Kurrelmeyer and L. J. Hayner, Phys. Rev. **52**, 952 (1937).
[3] H. Bruinning and J. H. de Boer, Physica **4**, 473 (1937); **5**, 17 (1938).

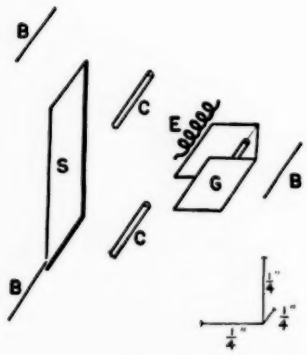

FIG. 1. Tube design. *G* is an electron gun; *S*, secondary emitting surface; *C*, collector; *E*, evaporating filament; *B*, bombarding filaments.

oven was then placed over the system and the glass was baked for two hours at 450° to 470°C. Following this treatment the metal parts were again heated until the gas pressure measured by a well-outgassed ionization gauge was less than 10^{-6} mm of Hg with the parts at a temperature of about 1800°C. For the two tubes with nickel plates the outgassing temperature was about 1200°C.

At the conclusion of this procedure a secondary emission curve was taken for the support metal of the plate. This served as a check on the adjustment of the apparatus and the effectiveness of the outgasing. In all cases the curves were in reasonable agreement with published curves for the metals used.

The beryllium was then slowly evaporated onto the plate by heating to a temperature just below the melting point of the beryllium.

Figure 2 shows a typical set of curves obtained with beryllium deposited on molybdenum. Curve I gives the secondary emission ratio for the molybdenum as a function of the primary electron voltage. Curve II shows the secondary emission when enough beryllium was evaporated to be barely visible on the glass nearest the evaporating filament. The plate was about four times this distance from the beryllium source. A heavy coat of beryllium, one which could be seen on the plate by the vanishing of small scratches, gave the result shown in curve III. Heating the plate to a bright red for a minute or two changed the emission to that of curve IV. By depositing more beryllium, followed by heating, the emission could be dropped to the low value and returned to about that of curve IV. The shift between these curves was continuous. Heating to a temperature above the melting point of the beryllium for a short time did not increase the emission much above that shown in curve IV, provided the deposit was not greatly reduced in thickness by evaporation of the beryllium.

This general behavior was observed in all of the tubes, but the values obtained varied considerably. Table I gives the values of the secondary emission ratio, R_m, for the maximum point of the curves and the primary electron voltage, V_p, necessary to reach the maximum.

The initial rise in secondary emission following the deposition of a very thin layer of beryllium may be caused (1) by impurities in the beryllium, (2) by the combination of the beryllium with residual gas either on the surface of the plate or in space, (3) by an unusually high secondary emission from a layer of beryllium so thin that it had properties radically different from the bulk metal, or (4) by a lowering of the work function of the surface without appreciable contribution of secondaries by the beryllium.

The large variation in the initial rise indicates that the controlling factor is quite sensitive to structure or material, but it hardly seems probable that the entire effect can be due to impurities which are more volatile than the beryllium because Bruining and de Boer[3] found that the alkali and alkaline earth metals all gave low secondary emission ratios when evaporated onto another metal. They did find, however, that all of these metals showed a large initial rise in

TABLE I. *Emission ratio R_m for the maximum point of the curves and the primary electron voltage V_p necessary to reach the maximum.*

Tube	Metal Used for Plate	Thin Layer, Maximum Rm		Thick Layer		Heat Treated Thick Layer	
		R_m	V_p	R_m	V_p	R_m	V_p
1	Mo	2.5	450	0.9	210	1.6	580
2	Mo	2.3	500	0.8	200	1.5	710
3	Mo	3.1	460	0.5	190	1.4	650
4	Ta	3.7	520	0.7	230	1.8	770
5	Ta	2.2	380	0.7	200	1.5	420
6	Ni	2.5	400	0.8	220	1.7	650
7	Ni	2.1	440	0.6	210	1.6	600
Average		2.6	450	0.7	210	1.6	630

secondary emission when present as a film a few microns thick or less.

This general tendency of the alkali and alkaline earth metals to raise the secondary emission of a high work function metal suggests that the effect is due to a lowering of the work function. This hypothesis is particularly plausible because the position of the maximum is very nearly that of the metal on which the thin layer is deposited. Further support for this hypothesis is given by some experiments on the stability of complex surfaces of high secondary emission such as the alkali oxides. The secondary emission of these surfaces fell to a low value after about ten hours when tungsten from a cathode was allowed to condense on the secondary emitter, while the more stable of these surfaces showed only a slight decrease in emission after several hundred hours of bombardment at the same current densities when the cathode was hidden behind deflecting plates. On the other hand, by allowing barium from an oxide coated cathode to condense on these surfaces a slight decrease in secondary emission could be observed after about fifty hours. Since the work function was much higher than that of the surfaces while that of barium was only slightly higher, it may be inferred, perhaps, that the change in emission was caused by a change in the work function.

The combination of the beryllium with residual gas may be responsible for the initial rise in secondary emission, but it is quite possible that the main contribution of an extremely thin layer of oxide might be a lowering of the work function.

The low value of secondary emission obtained for a thick layer of beryllium may be explained by one or more of the following assumptions:

1. Impurities in the layer.
2. This value represents the true secondary emission of pure beryllium.
3. A peculiar state of crystallization.
4. A very porous layer.

The first assumption can probably be neglected since the surface material represents the "middle fraction" of the distillate.

The second assumption is favored by Bruining and de Boer.[3] Although the low secondary emission represents a condition stable at room temperature, the author is inclined to believe that this secondary emission value is peculiar to

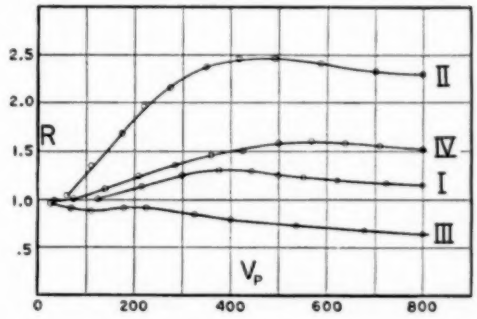

FIG. 2. Secondary emission ratio as a function of primary electron voltage. Curve I, Mo support plate; II, thin Be film; III, thick Be film; IV, thick heat treated Be film.

films prepared by evaporation and does not represent the correct value for bulk polycrystalline beryllium. Reasons for this view will be discussed later in the paper.

The third assumption could be tested by x-ray or electron diffraction experiments on surfaces of this type. Since no measurements of this nature on beryllium have come to the attention of the author, this assumption cannot be intelligently criticized. The data of Rao on polycrystalline nickel[4] and a single nickel crystal[5] show, however, that considerable difference in the secondary emission may result when the size and arrangement of the crystals in a metal are changed even though the fundamental crystal structure is unaltered.

The fourth assumption can be used to explain low secondary emission since primary electrons may be scattered along open channels in the metal to such depths that the secondaries are released in an electrostatically shielded region from which many do not escape. This assumption is supported by a number of rather crude observations. The heavy films had a matte surface, oxidized readily on exposure to air, and when very thick tended to peel in hair-like ribbons rather than flakes. Microscopic examination of the films was unsatisfactory because of the rapid oxidation on exposure to air. The surfaces of these oxidized specimens appeared rough even at high magnifications and no sign of crystal structure was visible. The layers which had been heated in vacuum showed slight evidence

[4] S. R. Rao, Proc. Roy. Soc. **128**, 41 (1930).
[5] S. R. Rao, Proc. Roy. Soc. **128**, 57 (1930).

of crystal structure and oxidized slightly less rapidly.

The rise in secondary emission when the thick beryllium films were heated to a bright red in vacuum may have been caused by the migration of impurities or by the reaction with residual gas. These processes should result in a change in work function of the surface. The author has been privileged to see some unpublished contact potential measurements on beryllium surfaces of this type by Dr. P. L. Copeland of the Armour Institute of Technology. His data show that the contact potential either does not change or increases by only a few tenths of a volt. This change is too small to permit appreciable surface contamination as an explanation of the effect.

If this rise in secondary emission caused by heat treatment is not due to impurities, it is probably the result of a recrystallization of the beryllium. The change in crystal structure may either alter the emission of the beryllium or close the pores in the original film.

One method of preparing pure gas free bulk beryllium is that of distillation in a vacuum followed by casting into the desired form, therefore these heat treated specimens should have the properties of polycrystalline beryllium. Since essentially the same emission was obtained by heating to a bright red for a few minutes as was obtained by actually melting the beryllium, the secondary emission value of 1.6 should be close to the proper value for the pure bulk metal. Traces of impurities or failure to obtain a sufficiently thick beryllium layer are the only evident factors which might prevent this value from approaching that of the bulk metal.

At the conclusion of the series of measurements, air was admitted to two of the tubes with beryllium coated plates. After these tubes were repumped, the secondary emission maximum was 3.9 at 730 volts in one case and 4.3 at 700 volts in the other. These values are comparable with the value of 4.5 reported in the literature.[1, 2] The discrepancy may be due to the heat treatment of the beryllium before exposure to air or to a difference in the outgasing of the oxidized surfaces.

Bruining and deBoer[3] have given a rather complete discussion of the factors causing an increase in secondary emission on oxidation, but may have underestimated the importance of the work function. Although there can be no doubt that the work function plays a smaller part in secondary than in thermionic emission, it is interesting to note that the highest values of secondary emission are obtained with materials of low work function, the alkali and alkaline earth oxides. Furthermore, cesium oxide with an excess of cesium has a higher secondary ratio than the other alkali oxides prepared by similar methods and has a lower work function. A comparison of a group of chemically related compounds such as the alkali oxides should give a better indication of the role of the work function in secondary emission than the comparison of two such different materials as barium and barium oxide.[3]

In conclusion the author wishes to thank Farnsworth Television Incorporated for permission to publish this material.

Atomic Electron Velocities in Hydrogen

A. L. HUGHES AND MERLE A. STARR
Wayman Crow Laboratory of Physics, Washington University, St. Louis, Missouri
(Received May 28, 1938)

When conditions are favorable to single scattering of fast electrons, those scattered through a suitable angle by gases of low atomic number fall into two distinct classes, (1) those scattered elastically by the nuclei and (2) those scattered inelastically by the atomic electrons. The inelastically scattered electrons have a distribution of energies about the most probable value, which is $V=V_0\cos^2\theta$, where V_0 and V are the energies of the incident electron before and after collision with an atomic electron, and θ is the angle of deflection. The distribution of energies among the inelastically scattered electrons is determined by the distribution of energies among the atomic electrons in such a way that the curve representing the *distribution of energies* among the scattered electrons, above or below the most probable value, is identical in shape with the *distribution of component velocities* among the atomic electrons. A beam of electrons with energies between 1737 and 4040 volts was directed into hydrogen at low pressure and the distribution of energies among those electrons which had been scattered at 34.2° measured. From this the distribution of component velocities among the atomic electrons follows immediately. The experimental curve is wider than the theoretical curve computed by Hicks by about 11 percent at the "half-width." In view of the exact agreement obtained previously with the same method in the case of helium, it is suggested that the assumptions underlying the theoretical calculation for the hydrogen molecule may have to be revised.

IN a previous paper[1] it was shown how, under certain conditions, measurements on the scattering of electrons by matter could be interpreted so as to give information on the distribution of velocities among the atomic electrons. The principle underlying the method is as follows. If a beam of sufficiently fast electrons passes through matter when the conditions are such that "single scattering" prevails, then an electron in the beam may be deflected *either* by a nucleus *or* by an atomic electron. (For electrons of sufficiently high speed, the probability of two or more scattering centers contributing deflections of the same order of magnitude to any one electron is negligibly small.) The electrons deflected by the nuclei suffer no loss of energy, while those deflected by atomic electrons lose an amount $V=V_0\cos^2\theta$, giving $V_1=V_0\sin^2\theta$ to the atomic electron. Here V_0 and V are the energies of the incident electron before and after scattering, V_1 the energy acquired by the atomic electron, and θ the angle of deflection of the incident electron. Thus we should expect to find that the electrons scattered through an appreciable angle by matter will be separated into two distinct groups, those scattered elastically by the nuclei and those scattered inelastically by the atomic electrons. Those scattered by the atomic electrons, however, will have a range of energies about a mean value, if the atomic electrons are in random motion instead of being at rest. The distribution of energies among the atomic electrons determines the distribution of energies among the scattered electrons, a relation which permits the former to be calculated from an experimental determination of the latter. This relation takes a particularly simple form if, in place of the energies of the atomic electrons, we consider their component velocities.[2] If $f(u)$ is the distribution of *component velocities* among the atomic electrons, $F(V'')$, the resulting distribution of *energies* among the electrons scattered at a suitably selected angle, has exactly the same shape as $f(u)$. V'' is the excess energy (positive or negative) which the scattered electron acquires as a result of a collision with an atomic electron having a component velocity u in a certain direction.[3] Thus an experimental study of electron scattering at a suitable angle, giving us $F(V'')$, the distribution of energies among the scattered electrons about the mean value, immediately tells us the shape of $f(u)$ for the component velocities of the atomic electrons.

[1] A. L. Hughes and Marvin M. Mann, Jr., Phys. Rev. **53**, 50 (1938).

[2] G. E. M. Jauncey, Phys. Rev. **50**, 326 (1936).

[3] The particular component of velocity which is significant in determining V'' is the one which the atomic electron had, before collision, in a direction at right angles to that of the scattered electron after collision. If the velocities of the atomic electrons are distributed isotropically in space then all the component velocities in any direction are on the average identical, and related in the same way to the resultant velocity.

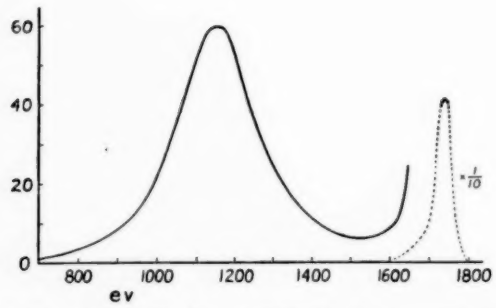

FIG. 1. Energy distribution of 1737-volt electrons scattered through 34.2° by hydrogen.

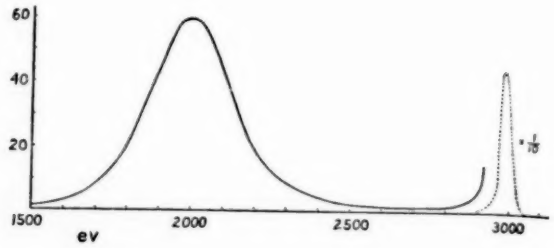

FIG. 2. Energy distribution of 2985-volt electrons scattered through 34.2° by hydrogen.

$f(\lambda'')$, the profile of the Compton modified band for x-ray scattering by the same atoms turns out to be identical in shape with $f(u)$. A full discussion of the relationship between $F(V'')$, $f(\lambda'')$, and $f(u)$ will be found in the first paper[1] on this topic.

This paper is concerned with the scattering of electrons by hydrogen and the conclusions which one can draw as to $f(u)$ for hydrogen. No description of the apparatus and of the method of taking and reducing observations will be given as they were identical with those described in the previous paper on helium [1] Hydrogen was obtained from a commercial cylinder and was said to be 99.9 percent pure. No further purification was attempted beyond passing it into the reservoir through two charcoal traps immersed in "dry-ice." The pressure of the hydrogen in the collision chamber was held at a constant value, about 0.004 mm during the experiments.

RESULTS

Measurements were made with electrons of energy 1737, 2985, 3588 and 4030 electron volts. The results are presented in the form of curves (Figs. 1, 2, 3, and 4) similar to those published for helium in the previous paper.[1] Each of the curves represents the mean of over 250 separate readings. The spread of the individual points about each curve is so small that, on the scale on which the drawings are reproduced, the dots representing the individual measurements would be so close to the curve that their separation from the curve would hardly be visible. It is evident that the higher the incident energy, the narrower, in relation to the value of the abscissa at which the maximum occurs, is the band representing the inelastically scattered electrons, and the more complete is the separation between it and the elastic peak.

The band representing the inelastically scattered 1737-volt electrons is not quite symmetrical with respect to the maximum. This is no doubt to be attributed to the fact that, as the energy of the incident electrons is reduced, the conditions for "single center scattering," as defined in the previous paper[1] are less and less strictly fulfilled. The separations, S_{exp}, between the elastic peak and the inelastic maximum are given in Table I. The theoretical separation is

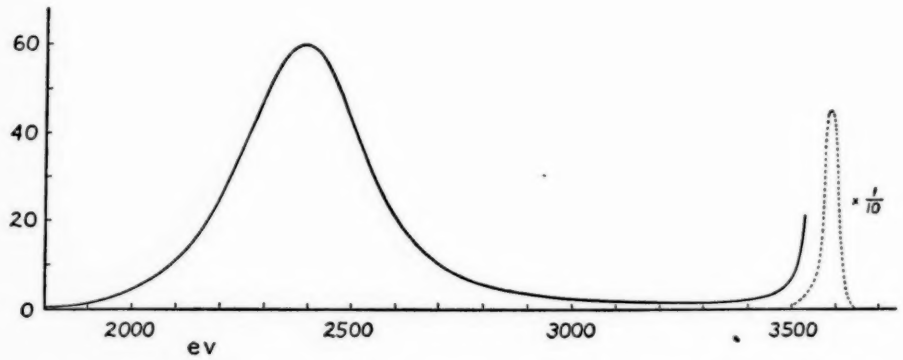

FIG. 3. Energy distribution of 3588-volt electrons scattered through 34.2° by hydrogen.

S_{theo} which is equal to $V_0 \sin^2 \theta$. In our apparatus, $\theta = 34.2°$.

It will be seen that the difference $S_{\text{exp}} - S_{\text{theo}}$ varies in such a way that no definite conclusions can be drawn. However, the value is always positive, which is the result that would follow from the very simple considerations presented in the previous paper on the assumption that the atomic electrons are not perfectly free. No quantitative conclusion can be drawn. It may be pointed out that the variations of the kind found in the last column of the table could be the result of an uncertainty in the exact value of the angle of scattering. The final adjustment of the electron beam to the middle of the apertures between the gun and the collision chamber was made by means of a small weak magnet near the anodes of the gun. This may alter θ by a few tenths of a degree. To obtain more precise information as to the meaning and reality of the difference, $S_{\text{exp}} - S_{\text{theo}}$, would require an apparatus in which the value of the angle could be set and held to within 0.1°.

The main purpose of this investigation is to determine the value of $f(u)$ for the atomic electrons in hydrogen. We shall use only the experimental results obtained with incident electron energies of 2985, 3588, and 4030 volts, since for these the distribution of energies among the inelastically scattered electrons is symmetrical about the middle. To obtain $f(u)$ for the atomic electrons we proceed as follows. In the notation of the earlier paper,[1] the abscissas both to the right and left of the maximum of the inelastic band may be labeled V''. Each experimental curve, as plotted in Figs. 2 to 4, therefore gives us two $F(V'')$ curves which may be averaged together. To get the $f(u)$ curves we merely change the abscissas in V'' into abscissas in u (or β) by the substitution

$$\beta(=u/c)\times 10^3 = V'' \div (0.5782\, V_0^{\frac{1}{2}}).$$

The $f(u)$ curves so obtained from Figs. 2 to 4 were almost exactly superposable. They were drawn on a large scale on accurate cross-section paper and the best possible mean curve constructed. This mean curve is made up from a total of 890 individual observations on the scattered electrons. From the way in which the individual points are scattered about the curve, the values of the points on the curve may be considered accurate to 2 percent over the range $\beta = 0$ to $\beta = 5\times 10^{-3}$ cm/sec. and to 5 percent over the range $\beta = 5\times 10^{-3}$ to $\beta = 9\times 10^{-3}$ cm/sec. The mean curve, adjusted to a maximum of 60.0, is plotted against β in Fig. 5, and the values of the ordinates, $f(u)$ are tabulated in the last column of Table II.

TABLE I. *Comparison of experimental and theoretical separations between the elastic and inelastic maxima for various electron energies.*

Incident Energy	S_{exp}	S_{theo}	$S_{\text{exp}} - S_{\text{theo}}$
1737 volts	587 volts	549 volts	38 volts
2985	988	943	45
3588	1200	1134	66
4030	1350	1274	76

Discussion

In order to compare our experimental results with theory we have tabulated in Table II, and plotted in Fig. 5, the values for $f(u)$ which have been obtained theoretically. The column and curve marked "K.R.R." are due to Kirkpatrick, Ross and Ritland[4] who computed $f(\lambda'')$, the profile of the modified band in the Compton effect for x-ray scattering by hydrogen atoms.

[4] P. Kirkpatrick, P. A. Ross, and H. O. Ritland, Phys. Rev. **50**, 928 (1936).

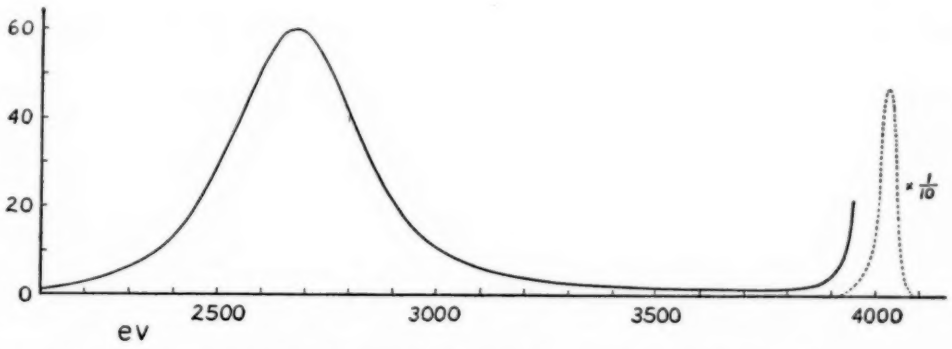

FIG. 4. Energy distribution of 4030-volt electrons scattered through 34.2° by hydrogen.

Since $f(\lambda'')$ and $f(u)$ have the same shape, the one automatically gives the other. The columns in Table II and the curves in Fig. 5 marked "2H" and "H_2" are due to Hicks.[5] The one marked "2H" is that computed for the hydrogen atom. It is puzzling that the theoretical values computed in these two papers for the hydrogen atom should differ as much as they do, in view of the fact that the wave mechanical picture of the hydrogen atom is presumably accurately known. One certainly cannot expect $f(u)$ for the hydrogen molecule to be the same as $f(u)$ for the atom; it is however instructive to have both of them available for comparison with our experimental $f(u)$ values. Various wave mechanical descriptions of the hydrogen molecule have been suggested. The one proposed by James and Coolidge[6] has given results in excellent accord with certain experimental data. But because of certain technical mathematical difficulties in adapting the James-Coolidge treatment of the hydrogen molecule to the problem of deriving a theoretical $f(u)$ curve, Hicks was unable to make use of their ideas. He therefore assumed another wave mechanical description of the hydrogen molecule, that due to Weinbaum. With this as a starting point he computed the values listed under "H_2" in Table II, and plotted as the curve marked "H_2" in Fig. 5. It will be seen that our experimental values for $f(u)$ differ appreciably from Hicks' "H_2" curve, and still more from the curves for atomic hydrogen. In view of our estimate of the degree of accuracy of our values, discussed earlier in the paper, it must be concluded that the difference is real. This is particularly significant in view of the fact that, for helium, the agreement with the "K.R.R." curve is very good, and with the Hicks "H-4" curve excellent. Since the experimental procedures for hydrogen and helium were identical, we must conclude that the experimental values for hydrogen are fully as accurate as those for helium. If one assumes that the agreement in the case of helium is not merely an accidental one, it follows that the theoretical calculations for hydrogen are probably in error.

There is one point which should be mentioned in that it may possibly have some bearing on the discrepancy. Helium is monatomic and hydrogen diatomic. The theory whereby $f(u)$ is shown to be identical in shape with the experimental $F(V'')$ is based on a strictly particle

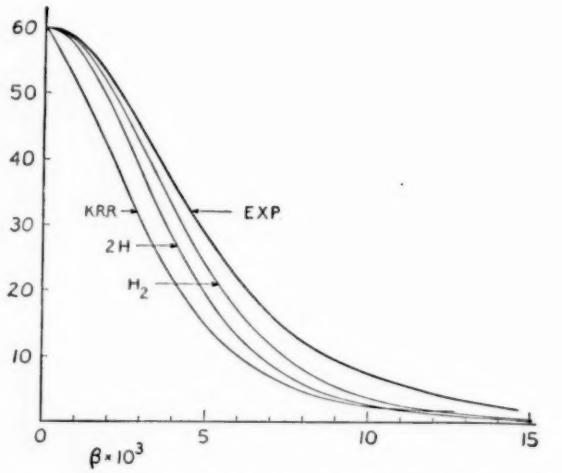

FIG. 5. Theoretical and experimental distributions of component velocities of atomic electrons in hydrogen, EXP., experimental values obtained in this investigation. K.R.R., theoretical value for the hydrogen atom due to Kirkpatrick, Ross and Ritland. 2H and H_2, theoretical curves due to Hicks for atomic and molecular hydrogen, respectively. Ordinates: values of $f(u)$. Abscissas: each unit $=\beta\times10^3=u/(3\times10^7)=\lambda''$ in X.U. (for $\lambda=695$ X.U. and $\theta=90°$).

TABLE II. *Theoretical and experimental velocity distributions for the atomic electrons in hydrogen, and the profile of the associated Compton modified band for* $\lambda=695$ *X.U. and* $\theta=90°$.

λ'' (X.U.)	u (CM/SEC.)	$f(u)$ (and $f(\lambda'')$) K.R.R.	HICKS (2H)	HICKS (H_2)	$f(u)$ EXPERIMENTAL
0	0×10^7	60.0	60.0	60.0	60.0
1	3	51.4	56.8	57.6	58.1
2	6	41.5	48.4	50.9	52.4
3	9	30.4	37.8	41.7	44.4
4	12	21.7	27.5	32.2	36.0
5	15	14.8	19.19	23.67	28.3
6	18	9.9	12.97	16.77	21.4
7	21	6.9	8.67	11.60	16.1
8	24	4.7	5.76	7.90	12.2
9	27	3.2	3.84	5.36	9.4
10	30	2.47	2.59	3.61	7.3
11	33		1.78	2.46	
12	36	1.73	1.21	1.67	4.4
13	39		.86	1.15	
14	42	.99	.60	.83	2.5
15	45		.43	.60	
20	60		.11	.16	

[5] B. Hicks, Phys. Rev. **52**, 436 (1937).
[6] H. M. James and A. S. Coolidge, J. Chem. Phys. **1**, 825 (1933).

point of view of the electrons and their interactions, and completely disregards their wave aspect. The agreement between theory and experiment may justify this in the case of helium. We have plenty of evidence, however, from electron diffraction effects that the elastic electron scattering does require us to use the wave aspect for a complete description of what happens. This raises the question as to whether or not it is necessary to modify the method of using the experimental data described in the earlier paper so as, in some way, to take account of the wave nature of the electrons in the inelastic electron scattering. We are inclined to think, however, that the simple particle view can be retained in the interpretation of this kind of experiment, and that the discrepancy will be removed by a more accurate method of handling the wave mechanical description of the hydrogen molecule.

We wish to thank Professor Kirkpatrick and Dr. Hicks for letting us have the numerical values from which their published curves were drawn.

AUGUST 1, 1938 PHYSICAL REVIEW VOLUME 54

A New Precision Method for the Determination of e/m for Electrons

A. E. SHAW
Ryerson Physical Laboratory, University of Chicago, Chicago, Illinois
(Received June 10, 1938)

The excellent focusing properties of crossed electric and magnetic fields have been utilized in the development of a new, precision method for the determination of e/m for electrons. This method differs from previous methods in that the final equation for e/m does not involve the velocity explicitly. Moreover, focusing criteria have been worked out which effectively eliminate any possible influence of electron energy upon the value of e/m. That this is a great source of error and uncertainty in other methods is shown by the great difference between the energy of the electrons before and after emergence from a slit. This effect is too great to arise from a contact potential difference but it can be attributed to direct electron bombardment of the slit and the subsequent formation of a surface charge on it. The magnitude of this charge is not constant but varies between 9 volts and 24 volts, depending upon the applied accelerating potential. The value of e/m obtained with the present apparatus is, $e/m_0=(1.7571\pm0.0013)\times10^7$ e.m.u., where 0.0013 is the probable error derived from a least squares solution of a set of observations for various electric and magnetic field intensities. Other sets differed from this by less than 1 : 5000. The mechanical accuracy of the present cylindrical condenser sets the limit on the precision attainable with the present apparatus. However, the error due to this cause is less than the probable error stated above. The limitations of the present condenser can be reduced considerably through the use of a new condenser designed in accordance with kinematic principles. The method presented here for the production of magnetic fields of great uniformity and a new, precise cylindrical condenser would permit a determination of e/m to be made with the method of crossed fields to within an accuracy of 1 : 3000.

I. INTRODUCTION

THE focusing properties of crossed electric and magnetic fields for electrons, in the case of circular orbits, were discussed in a recent[1] paper in this journal. It was found that this combination of fields is capable of extremely sharp focusing of electron beams that vary both in direction and in velocity.

This same field combination was investigated experimentally to determine its suitability for the accurate measurement of the specific charge of electrons. In practically all deflection measurements of e/m, the precision is limited by uncertainties in the velocity of the electrons. In the method of crossed fields, the final equation does not contain the velocity explicitly, hence uncertainties in the accelerating potential do not enter. Although the accelerating potential does not appear explicitly in the equation for e/m, provision must be made by focusing to adjust the velocity for any given ratio of intensities of the electric and magnetic fields.

[1] A. E. Shaw, Phys. Rev. **44**, 1006 (1933).

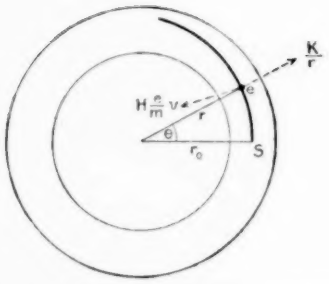

FIG. 1. Section through cylindrical condenser showing the accelerations of an electron in crossed electric and magnetic fields.

The aim of the present paper is: (1) to describe experimental focusing criteria which eliminate the velocity uncertainty from the method of crossed fields, and: (2) to present the details of the measurement of e/m by this new method.

II. THEORY OF METHOD

In Fig. 1 is shown a schematic representation of a cylindrical condenser in which a beam of charged particles is free to move under the action of a radial electric field and a magnetic field which is normal to the plane of the orbit.

A charged particle entering the field at S describes an orbit under the influence of a radial acceleration K/r due to the electric field, and of an acceleration $(He/m)v$, due to the magnetic field which acts at right angles to its direction of motion at every point of the orbit. If the direction of the two forces are as shown, the equations of motion in polar coordinates are,[2]

$$r''-r(\theta')^2=K/r-(He/m)r\theta', \tag{1}$$

$$(r^2\theta')'/r=(He/m)r', \tag{2}$$

where the primes indicate time derivatives. Eq. (2) can be written $(r^2\theta')'=\frac{1}{2}(He/m)\cdot(r^2)'$, which, integrated subject to the initial conditions that at $t=0$; $r=r_0$, $r'=r_0'$, $\theta=0$ and $\theta'=\theta_0'$ gives $\theta'=\frac{1}{2}(He/m)+A/r^2$, where $A=r_0^2[\theta_0'-\frac{1}{2}(He/m)]$ Substituting this value of θ' into Eq. (1), there results,

$$r''=A^2/r^3+K/r-r(\tfrac{1}{2}He/m)^2. \tag{3}$$

We are interested only in those orbits which are nearly circular, since only these may be described in the condenser under consideration. For the circular orbit $r=\rho$, a constant, the magnetic force is always directed along the radius vector, hence Eq. (3) becomes,

$$A^2/\rho^4=(\tfrac{1}{2}He/m)^2-K/\rho^2. \tag{4}$$

For orbits which differ by an amount x from a circle, $r=\rho$, let $r=\rho+x$, then Eq. (3) can be written,

$$x''=-x[(He/m)^2-2K/\rho^2]. \tag{5}$$

If the electric and magnetic fields and the initial angular velocity θ_0' are adjusted so that $A=0$, then from Eq. (4), $(He/m)^2=4K/\rho^2$ and Eq. (5) becomes,

$$x''=-\tfrac{1}{2}(He/m)^2x \tag{6}$$

and

$$\theta'=\tfrac{1}{2}(He/m). \tag{7}$$

The solution of Eq. (6) is

$$x=P\sin(He/m)t/\sqrt{2}. \tag{8}$$

The beam is focused when $x=0$; thus it is evident from Eq. (8) that a divergent bundle of rays is reunited after a time $t=\pi\sqrt{2}/(He/m)$. The angular distance traversed by the beam in this time t is obtained from the solution of Eq. (7). It is $\pi/\sqrt{2}$ radians, or 127° 17′.

If r be substituted for ρ in Eq. (1) and ρ be considered a function of θ', we find that ρ passes through a minimum for $\theta'=\frac{1}{2}He/m$. Therefore, when the adjustment of the electric and magnetic fields is such as to make $A=0$ and $(He/m)^2=4K/\rho^2$, we have particles with slightly different velocities describing approximately the same circular orbit.

To find the sharpness of focus, the orbits described by the particles having different directions and different velocities can be computed to a further approximation,[2] which gives a general equation for the radius vector of the path at the point of focus; *viz.*, $\theta=127°\ 17'$ as follows:

$$r=\rho(1-c_0+c_0^2/3+c_1^2/3+\delta^2+\pi c_1\delta/\sqrt{2}). \tag{9}$$

This equation contains the initial conditions associated with the entering slit, that is where $\theta=0$, we have for the point of entry, $r_0=\rho(1+c_0)$, and for the angle of entry, $(dr/\rho d\theta)_{\theta=0}=c_1$, and for the angular velocity at entry, $(d\theta/dt)_{\theta=0}=\frac{1}{2}H(1+\delta)e/m$.

[2] W. Bartky and A. J. Dempster, Phys. Rev. **33**, 1019 (1929). Cf. also J. Mattauch and R. Herzog, Zeits. f. Physik **89**, 786 (1934).

Since Eq. (9) is quadratic in δ it shows that there are in general two values of the velocity to give any r. For a beam of small angular divergence $c_1=0$ and these two values coincide at a minimum value for $\delta=0$. Thus at $\theta=\pi/\sqrt{2}$, $r=\rho(1-c_0+c_0^2/3)$, where ρ is expressed by the relation,

$$\rho^2=4K/(He/m)^2. \tag{10}$$

In the apparatus, c_0 was of the order of 0.00026, so that $\rho=\frac{1}{2}(r_0+r)$ to better than $1:10^6$.

In the event that c_1, the angle of entry at $\theta=0$, is not zero, the minimum value of the radius at $\theta=\pi/\sqrt{2}$, as δ is varied, is found from Eq. (9) to be $r=\rho(1-c_0+c_0^2/3-0.9c_1^2)$, so that $\frac{1}{2}(r_0+r)=\rho(1+c_0^2/6-0.45c_1^2)$ is the equation that connects ρ with the observed values of r_0 and r. The term $c_0^2/6$ is less than $1:10^6$ hence it can be neglected. In several preliminary tests sufficient gas was admitted to make the electron beam visible. It was then seen to be a sharp bundle down the center of the condenser with a maximum divergence of less than 1:50. Thus the term $0.45c_1^2$ is less than 1:6000 for the rays of maximum divergence and the change in ρ is less than 1:6000.

In the experimental realization of these conditions, either the electric field or the magnetic field is adjusted so that the beam is focused onto the collector at r, as a minimum value for variations of the velocity. Then from the value of ρ, e/m can be computed from $(e/m)^2=4K/H^2\rho^2$. The value of K may be deduced from the equation,

$$m\int_{r=r_1}^{r_2}\frac{K}{r}dr=eV, \tag{11}$$

where r_1 and r_2 represent respectively the radii of curvature of the inner and outer plates of the condenser and V is the potential difference across the condenser. The value of K from Eq. (11), when combined with Eq. (10) gives,

$$e/m=\frac{4V}{H^2\rho^2\log_e(r_2/r_1)}. \tag{12}$$

Thus we have an expression for e/m in terms of the electrostatic field intensity, the magnetic field intensity and the radius of curvature of the electron beam.

III. General Experimental Arrangement

The schematic diagram of the entire apparatus is shown in Fig. 2, where the cylindrical con-

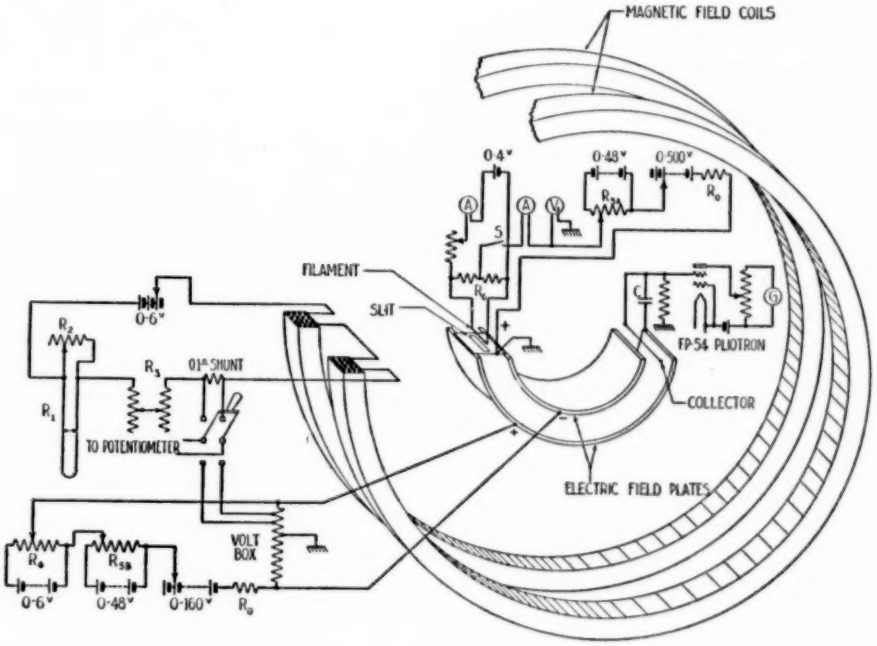

FIG. 2. Schematic diagram of the control circuits for the electric field, the magnetic field, the accelerating field and the electron collector.

denser and the magnetic field coils are represented in oblique projection.

(A) Source of electrons

The source of electrons was a coated cylindrical filament, 0.025 mm in diameter. The filament was mounted like a monochord string under the slight tension of a tungsten-molybdenum spring (T in Fig. 3) in order that its expansion when heated would not throw it out of the line of the slit. The tungsten-molybdenum spring was shunted by a flexible strip of pure silver which carried most of the heating current. The filament gave adequate emission when heated by currents of approximately 0.050 ampere. Although the filament support and its circuit were almost noninductive, the small heating currents served to minimize its magnetic field.

The activation of the filament required a heating current of 0.1 ampere and an accelerating potential of 350 volts. This process was carried out in a separate evacuated chamber outside of the main apparatus. When the filament was properly activated, it was mounted in its support and installed in the apparatus. In this way it was possible to retard the formation of partially insulating layers on the surface of the slit (S in Fig. 3) adjacent to the filament. It was found necessary to shield the filament on all sides in order to restrict the electrons to the slit.

(B) Slit

The photograph in Fig. 3 shows the slit, the collector and the inner plate of the cylindrical condenser. The slit S which collimated the electron beam, was 0.03 mm wide and 2.0 mm long. The plate in which the slit was formed was made of gold to avoid surface oxidation under electron bombardment. The slit was located symmetrically with respect to the two plates of the cylindrical condenser and its plane was radial. The radial position of the slit was set by means of a mechanical fixture which fitted over the inner plate of the cylindrical condenser. There was no electrostatic deflecting field in the region between the filament and the slit (see Figs. 2 and 4). It was necessary, therefore, to place the filament in such a position that the electrons, under the influence of the accelerating field and the magnetic field, entered the slit normally.

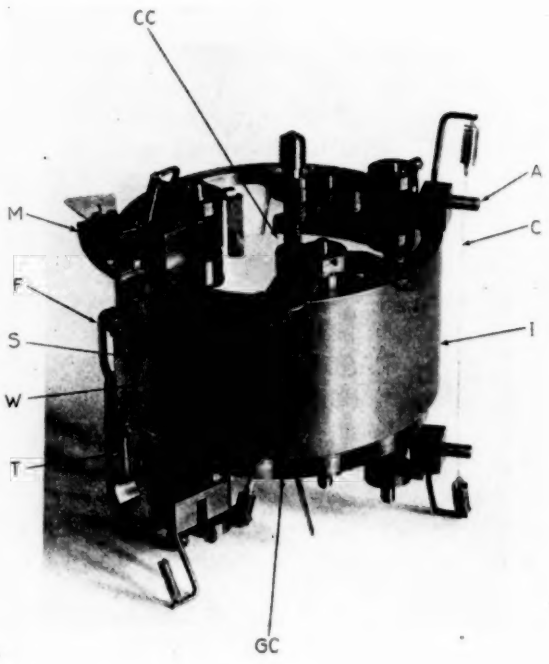

FIG. 3. Inner plate of cylindrical condenser, showing collector and slit system. C, gold wire collector, 0.045 mm diameter; A, 0.1 mm pitch adjusting screw; I, inner plate of cylindrical condenser; GC, accurate glass cylinder; CC, center of curvature of plates engraved on front face of GC; S, slit for beam, 0.03×2.0 mm; M, mechanism for adjusting slit; W, old wire slit, no longer used; F, filament support. Filament is directly in back of S; T, spring to compensate for expansion of filament.

The wire slit (W in Fig. 3), mentioned in an earlier paper,[1] served originally as the initial slit, the image of which was focused onto the collector. This wire slit has been abandoned because of difficulty with surface charges forming on it. The final readings presented in this paper were taken with the wire slit removed. The angle of refocus, namely 127° 17′, was measured between slit S and the collector, since the distortion of the radial field in the vicinity of the slit has a negligible effect on the position of focus.

(C) Accelerating field

The control circuit for the accelerating field is shown in Fig. 2. The accelerating potential was applied between the grounded slit and the midpoint of two 150,000 ohm resistances, R_6. The accelerating potential was read[3] on voltmeter V_A,

[3] The small drop due to the emission current was approximately 0.03 volt.

which was a precision instrument of one megohm. Resistance R_{5A} was a 2500 ohm slide-wire and R_0 was a 5000 ohm protective resistance. All potentials were supplied by storage cells to insure constancy.

Switch S provided an important control for the accelerating field. It was open while the electric and magnetic field circuits were being adjusted. Thus, in addition to minimizing the bombardment of the slit, the electrons from the filament were kept out of the cylindrical condenser until the electrostatic and the magnetic forces were adjusted approximately to bend them into a circular orbit. This same procedure was followed for each new set of values of the electric and magnetic fields.

(D) Collector

The electron beam was picked up by a cylindrical gold wire, 0.045 mm diameter (C in Fig. 3) which was connected to an FP 54 Pliotron,[4] as shown in Fig. 2. The current sensitivity of this circuit was of the order of 10^{-14} ampere and electron currents to the collector were of the order of 2×10^{-11} ampere.

The wire type of collector was chosen in order to avoid distortion of the radial electric field. One interesting feature of the use of a wire collector was the fact that the ratio of secondary electrons to primary electrons was greater than unity, thus giving the wire a net positive charge. This was verified by the use of a small Faraday chamber consisting of two coaxial tubes, the inner of which was joined to the Pliotron. With this arrangement, the secondary electrons were not able to escape and the collecting circuit showed a net negative charge. There appears to be no effective way of eliminating secondary emission under these circumstances, hence focusing was carried out in terms of a positive deflection. When operating at pressures of the order of 10^{-7} mm Hg, and small beam intensities, the deflections were very constant. It is also important to note that with the beam intensities used, no appreciable change, due to electron bombardment, took place on the surface of the collector, for long periods of time.

[4] L. A. DuBridge, Phys. Rev. **37**, 392 (1931).

Although the collector was located symmetrically with respect to the two plates of the cylindrical condenser, it was not electrostatically symmetrical because of its two supports. Thus when the potential across the electric field plates was varied, a charge was induced in the Pliotron circuit. Condenser C (Fig. 2) of air dielectric and capacity $2.48\mu\mu$f, established the electrostatic symmetry of the collector and eliminated the induced charge.

The adjustment of the collector with respect to angle and radius was carried out by means of the mechanism shown in Fig. 3. A was a 0.1 mm pitch screw of which there were two. These screws possessed one degree of freedom in rotation and their supports one degree of freedom in angle. This allowed the collector to be located at the proper angular distance from the slit and at the appropriate radius of curvature. The accuracy with which this angle may be set does not influence appreciably the ultimate precision of the determination. The method employed in the final measurement of the radius of curvature will be described in the section on the electric field.

(E) Electric field

(*a*) *Mechanical structure and physical measurement.*—The electric field was formed between two concentric cylindrical surfaces which were held concentric by means of an accurately turned glass cylinder (GC in Fig. 3). Upon the front face of this cylinder was engraved the center of curvature (CC in Fig. 3). The effective axial length of the electric field was about 3.0 cm whereas the axial width of the electron beam was only 0.2 cm.

The field plates were cast from a bronze whose magnetic susceptibility was checked by a sensitive method[5] and found to be negligibly small. After careful machining, each plate was coated electrolytically with a layer of 24-carat gold, in order to minimize the polarization described later.

The radii of curvature of the two cylindrical condenser plates were 3.4071 cm and 2.7901 cm. These dimensions were determined in the follow-

[5] E. B. Rosa, *et al.*, Bull. Nat. Bur. Stand. **8**, 285 (1912). Cf. also Jackson, Proc. Roy. Soc. **A104**, 672 (1923) for absolute method of calibration.

ing manner. First the diameter of the inner plate was measured in various azimuths by means of a Swedish Gage Company micrometer caliper. This micrometer, of grade *A*, was checked against its standard block at frequent intervals. The two cylindrical plates were assembled in their final position with respect to the glass cylinder and bolted together securely. This unit was then placed on the bed of a Geneva comparator in a fixture that permitted one degree of rotation about the axis of the glass cylinder which was perpendicular to the bed. An accurate steel sphere, coated with a thin layer of 24-carat gold, was attached to the end of a tool steel rod of diameter smaller than the sphere. The steel rod was arranged vertically so that the sphere, which was fastened to the lower end of the rod, lay between the two condenser plates. The support holding the sphere was independent of the bed of the comparator, and thus a translation of the bed of the comparator moved the condenser plates with respect to the sphere.[6] The sphere and the two plates were joined together in a simple electrical circuit in such a way that contact between the sphere and either of the plates was indicated on a galvanometer. In this manner, careful measurements were made of the radial separation of the condenser plates in the median plane of the electron beam in four different azimuths between the slit and the collector wire. This method of measuring the actual separation between two cylindrical surfaces is capable of precision and reproducibility.

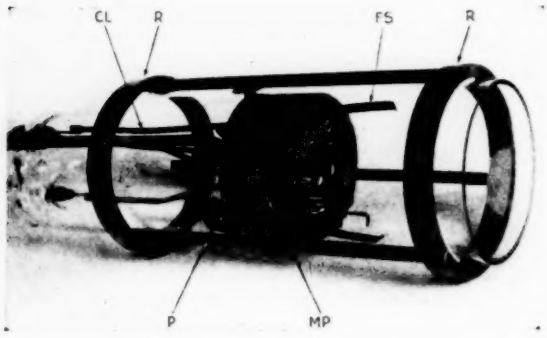

FIG. 4. Cylindrical condenser in glass tube. End plate removed. *CL*, spring connecting leads; *R*, ring supports; *MP*, median plane of electron beam; *P*, round glass pins that hold condenser in median plane under force of spring leads; *FS*, flat spring, of which there are six, to support condenser in glass tube.

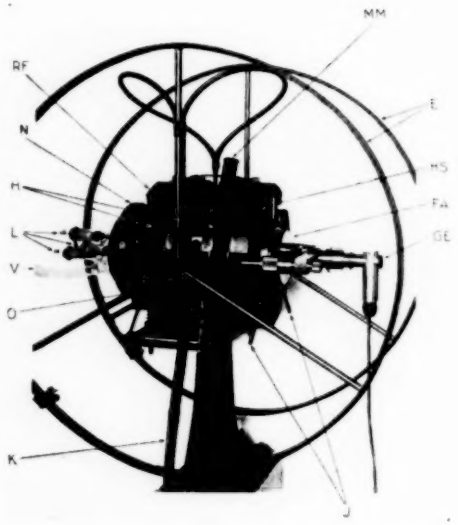

FIG. 5. Complete assembly of the entire apparatus with measuring microscopes in place. *FA*, glass tube containing cylindrical condenser; *E*, coils for investigating influence of earth's field; *GE*, combination Gauss eyepiece and telescope for locating cylindrical condenser; *J*, thumb screws to adjust position of cylindrical condenser—there are two in front and two in rear; *HS*, spring plunger which maintains glass tube (*FA*) in contact with thumb screws (*J*); *N*, nut to translate glass tube (*FA*) along axis of magnetic field; *MM*, median plane microscope to judge coincidence of median planes; *H*, magnetic field coils; *K*, noninductive connections to magnetic field coils; *RF* heat radiating fins; *L*, external leads for connections to cylindrical condenser, filament, etc.; *V*, vacuum pump connection; *O*, magnetometer mounted externally to indicate presence of stray fields.

In measuring the width of a slot by the motion of a sphere, no lost motion due to backlash in gears is permissible. This was avoided in the Geneva comparator through the use of an Ames dial gauge which was attached to the end of the comparator in contact with the bed. Thus the screw of the comparator served merely to translate the plates whose separation was desired. By choosing a measuring sphere of proper diameter, the displacement of the dial gauge was limited, thereby minimizing the slight periodic error due to the eccentricity of the pinion in the gauge. Finally, the dial gauge was calibrated against our

[6] It is assumed that the relative motion of the cylindrical plates and the sphere is along a diametral line. However, it can be shown that, even if the line of motion were not coincident with a diametral line by as much as 0.5 mm, the corresponding error in the measurement of the separation would not exceed 1 : 8000. This can be inferred from the equation,

$$Y=(r_2-r_1)[1+\tfrac{1}{2}(X^2/r_1r_2)+\cdots],$$

where Y is the separation of the two cylindrical surfaces of radii r_1 and r_2, measured along a line parallel to a diametral line but removed from it by a perpendicular distance X.

decimeter standard No. 56 which had recently[7] been checked by the National Bureau of Standards. The gold plated sphere was measured in a number of azimuths by means of an accurate micrometer caliper.

The precise location of the collector wire was determined by a slight modification of the foregoing method. The wire was connected electrically to the inner plate and thence through the galvanometer circuit to a gold plated sphere as before. In this way the wire was located with respect to the inner plate. However, one very important precaution is to be observed, that is, the wire must always contact the sphere at the end of that diameter of the sphere which lies along the line of the displacement. If the sphere were out of line on either side, the actual displacement would be greater, hence by rotating the condenser plates with respect to the sphere through a very small angle about their vertical axis, a minimum displacement of the sphere between the inner plate and the collector wire can be found. A number of such readings were taken first at a point below the median plane of the electron beam and then at a corresponding point above the median plane. This enabled the wire to be located parallel to an element of the inner cylindrical surface in the proper radial position.

The complete cylindrical condenser with filament, slit and collector installed and measured was mounted inside a glass tube, as shown in Fig. 4. This glass tube fits inside the magnetic field coils as indicated in Fig. 5. The two rings R (Fig. 4) were supported in the magnetic field coils on six points, four of which were rigid (J in Fig. 5) and two of which were flexible (HS in Fig. 5). The front flexible support, which consisted of a bronze helical spring was coupled to the ring R through a ball and socket, thus applying two degrees of constraint in translation. This method of mounting the glass tube inside the field coils provides three degrees of freedom in angle and one degree in translation. In addition, the nut N (Fig. 5) gives one degree in translation. This combined motion enabled the cylindrical condenser to be located symmetrically inside the magnetic field.

[7] L. V. Judson and B. L. Page, Nat. Bur. Stand. J. Research **13**, 757 (1934).

The actual location of the cylindrical condenser was accomplished by the use of a combination Gauss eyepiece and telescope (GE Fig. 5). The Gauss eyepiece was used to establish the plane of the trajectory normal to the magnetic field. After this, the telescopic objective was attached and the center of curvature of the cylindrical plates was located on the axis of the magnetic field. The reference plane for these adjustments was the polished front face of the glass cylinder (GC in Fig. 3). The microscope, MM in Fig. 5 was used to judge the coincidence of the median plane of the electron beam with the common median plane of the two magnetic field coils.

(*b*) *Electrical control circuits.*—The electric circuit which controls the electrostatic deflecting field is shown in Fig. 2. Rheostat R_4 consisted of a single layer of resistance wire wound in a helical groove on the surface of a cylinder. The cylinder was capable of rotation and a moving contact slid over every portion of the helical winding when the cylinder was turned about its axis. This provided a continuously variable potential for the fine adjustment of the electric field. The coarse adjustment was made by means of the slide wire R_{5B} and the switch attached to the 0–160 volt storage battery. The volt box[8] shown was used to measure the potentials applied to the electric field.

The slit and the wire collector were located practically midway between the two plates of the cylindrical condenser. In some of the preliminary experiments, the zero equipotential surface, containing the slit and the collector was also located midway by making $V_1 \neq V_2$. If we let r_1 and r_2 be respectively the radii of the inner and the outer plates of the cylindrical condenser, then;

$$eV_1 = m\int_{r=r_1}^{r_1+\frac{1}{2}(r_2-r_1)} \frac{K}{r}dr$$

and

$$eV_2 = m\int_{r_1+\frac{1}{2}(r_2-r_1)}^{r_2} \frac{K}{r}dr.$$

Experimentally, no observable difference was

[8] This was a Leeds and Northrup volt box that had been checked at the National Bureau of Standards and more recently had been rechecked along with the 0.1 ohm standard in the Standards Laboratory of the Commonwealth Edison Company, Chicago, through the courtesy of Mr. Stevens and Mr. Dondanville.

found between the adjustment for focus when these values of V were used and the adjustment when V_1 was made equal to V_2. The ground on the voltbox in Fig. 2 was the connection that established the zero surface.

(F) Magnetic field

(*a*) *Mechanical structure and electrical circuits.* —The magnetic field which was used to deflect the electron beam was produced by the two coils shown at H in Fig. 5. The coils were rectangular in cross section and each was composed of 119 turns of No. 12 Cotenamel wire, thoroughly shellacked. Each coil was wound on a bronze frame which slid without shake over an accurately turned cylinder of bronze. The coil frames were attached to the cylinder by three point screw supports in such a manner that the separation and the parallelism of the two coils could be adjusted with considerable accuracy. The coils were so arranged on their cylindrical support that when their individual median planes were parallel to each other, the magnetic axis of one coil was coincident with the magnetic axis of the other.

The determination of the constant of the magnetic field coils was made by means of the two standard coils shown in the schematic diagram of Fig. 6. Standard coil No. 1 consisted of two single layer coils of seven turns each of No. 12 enameled copper wire. The wire was wound in an 80° helical groove of pitch slightly greater than the diameter of the wire. These two coils were wound on the central portion of the cylinder, at the ends of which were located the two magnetic field coils. Standard coil No. 1 and the magnetic field coils were coaxial about axis A. For simplicity in representation, several turns have been omitted from the drawing of coil No. 1 in Fig. 6. The two coils of standard No. 1 were connected in series aiding and the two magnetic field coils were also series aiding.

The field of standard No. 1 was arranged to oppose the field of the magnetic field coils. The glass assembly shown in Fig. 4 was removed and a small oil-damped magnetometer, whose motion was magnified optically, was placed at a point which lay on the trajectory. This indicated when the two fields were equal. Equality was always judged for current reversals through both sets of

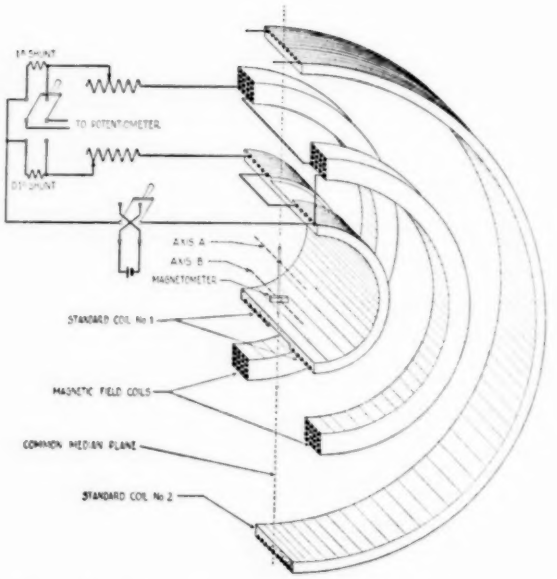

FIG. 6. Schematic diagram in section of the arrangement used for standardizing the magnetic field coils. The common median plane is parallel to plane of diagram.

coils, thus correcting for magnetic asymmetry, in the neighborhood of the coils. This null arrangement provided a simple, yet precise method for the determination of the constant of the magnetic field coils at the trajectory in terms of a standard coil. Since the plane of the trajectory was parallel to the plane of the magnetic meridian of the earth's field, as determined within the laboratory, it was unnecessary to compensate for the earth's field. From the spot finally formed on the collector after long bombardment, it may be concluded that the electrons were practically completely confined to the plane at right angles to the axis. Hence, with no component of motion normal to the plane of the orbit, the earth's field had no influence and spiralling was negligible.

The mathematical computation of the constant of standard No. 1 for points on the trajectory involved an infinite series. Although this series is rapidly convergent, it was nevertheless desirable to secure an additional experimental check of standard No. 1. This was accomplished by means of standard No. 2, also shown in Fig. 6. This standard, which could be attached to the assembly shown in Fig. 5, consisted of a single layer of 24 turns of No. 20 enameled copper wire. For simplicity, only a few turns are shown in the drawing. The wire was wound in an 80° helical

groove of pitch slightly greater than the diameter of the wire. The cylinder upon which this coil was wound was located so that the magnetic axis of the coil was coincident with axis B, which lay in the trajectory. That is to say, the radial distance between axes A and B was practically equal to the radius of the trajectory. Standard No. 2 could be utilized to compensate either standard No. 1, or the magnetic field coils. The procedure was identical in either case, and the magnetometer was used as before to indicate when the fields were equal.

The leads from the various coils were brought out in the plane which was normal to the common median plane (Fig. 6) in order to avoid the magnetic contributions of these short leads. The connecting wires to the control circuit were noninductive. In order further to eliminate stray fields, any material which affected the magnetometer was removed from the vicinity of the apparatus. It was found that anything which was too far off to disturb the magnetometer had no observable effect on the electron beam. The slight stray fields due to the slide wires in the accelerating field and in the electric field circuits were eliminated by allowing currents to flow to them through noninductive leads from the battery. The slide wires were then moved about until the magnetometer showed no deflection, even for current reversals. The slide wires were then fastened permanently in their respective positions. This procedure was followed in locating all of the control apparatus. After all the apparatus had been placed and the fields measured, the magnetometer was mounted permanently in position O shown in Fig. 5. Even though this was removed from the region of the trajectory, it was found that stray fields incapable of affecting the magnetometer in this position had no effect on the electron beam.

The control circuit for the magnetic field coils is shown in Fig. 2. Rheostat R_3 was for the coarse adjustment whereas R_1 shunted by R_2 provided the fine adjustment, which was used in the actual focusing of the electrons. Rheostats R_1 and R_3 were practically noninductive. R_1 consisted of a narrow loop of manganin wire shunted by a slider of the same material. This provided a continuously variable adjustment. R_3 consisted of two ribbon wound coils adjacent to each other with a common slider. The smallness of the current through R_2 and its remoteness from the main field made it unnecessary that it be noninductive.

The current for the magnetic field coils was supplied by large capacity lead storage cells and the absolute magnitude[8] of the current was read on the same potentiometer that was used to measure the potential of the electric field.

(*b*) *Evaluation of intensity constants for standard coils.*—Many coils have been devised for the production of homogeneous magnetic fields. These range all the way from various combinations of conical and cylindrical solenoids to finite groups of windings, of which the Helmholtz arrangement is perhaps the best known. The Helmholtz combination produces a field of uniform intensity in the neighborhood of the magnetic axis and in the common median plane. The author has found it possible to produce a field of uniform intensity in the median plane but at any desired point off the axis by reducing the usual separation implied by the Helmholtz arrangement.

The x component of the magnetic field intensity in oersteds of a single circular turn of wire carrying current i (e.m.u.) is given by[9]

$$H_x=\frac{2\pi i a^2}{r^3}\left\{1+\frac{3y^2}{2^2r^4}(a^2-4x^2)\right.$$
$$+\frac{45y^4}{2^2 4^2 r^8}(a^4-12a^2x^2+8x^4)$$
$$+\frac{45y^6}{2^2 4^2 6^2 r^{12}}(35a^6-840a^4x^2+1680a^2x^4-448x^6)$$
$$+\frac{15y^8}{2^2 4^2 6^2 8^2 r^{16}}(6615a^8-264{,}600a^6x^2$$
$$+1{,}058{,}400a^4x^4-84{,}672a^2x^6$$
$$\left.+120{,}960x^8)+\cdots\right\}. \quad (13)$$

Here x and y represent the coordinates of the point at which H_x is expressed, with the origin of

[9] A. Gray, *Absolute Measurements in Electricity and Magnetism*, second edition (1921), p. 212. The fifth term was derived by the author because of the insufficiently rapid convergence of the first four terms.

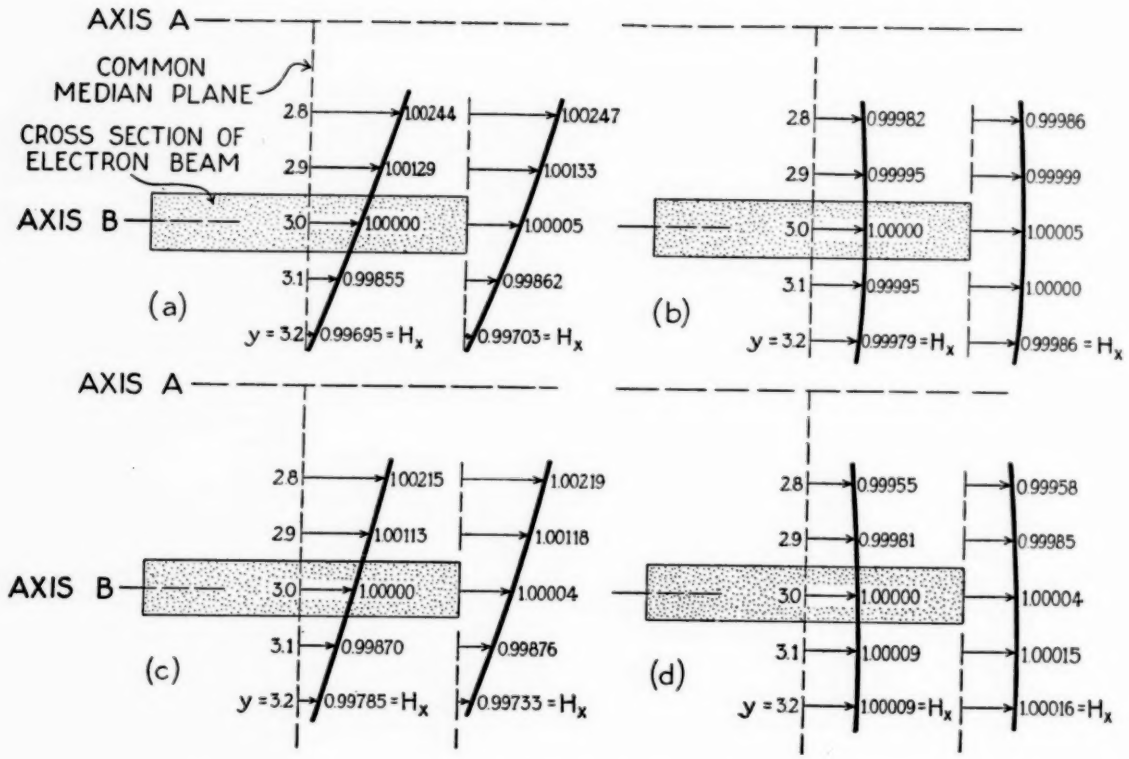

FIG. 7. Magnetic field intensity distribution diagrams, which show the intensity variation over the region in space traversed by the electron beam. The axes A and B refer to Fig. 6. Diagrams (a) and (b) illustrate respectively the case for two circular turns computed according to the Helmholtz separation ($x=4.0000$) and the improved separation ($x_4=3.4883$). (c) and (d) illustrate respectively the case for standard coil No. 1 computed according to the Helmholtz theory and according to the author's method. The values of H_x represent absolute field intensities for unit current, and y is in cm. The width of the cross section of the electron beam has been exaggerated to facilitate representation.

coordinates at the center of the coil of radius a, and $r^2=a^2+x^2$.

In the Helmholtz arrangement, $(\partial^2 H_x/\partial x^2)_{y=0}=0$ reveals the presence of a point at $x=a/2$, where $\partial H_x/\partial x$ is constant. Thus by combining two circular turns so that each contributes to the field at $x=a/2$, great uniformity is obtained along the axis at a point midway between the two turns.

In order to secure uniformity off the axis but in the common median plane of the two circular turns, the condition, $(\partial H_x/\partial y)=0$, was examined for a new separation. To a first approximation only the first three terms of Eq. (13) were used. This gave

$$\partial H_x/\partial y\,|_{y=\rho}=x^6+Ax^4+Bx^2-N=0,$$

where A and B are constant coefficients and N is the constant term. If ψ is substituted for x^2, this reduces to

$$f(\psi)=\psi^3+A\psi^2+B\psi-N=0$$

and as a first approximation $x=3.58148$ cm for field constancy at a point off the axis, $y=\rho=3.0$, the approximate radius of curvature of the beam. The convergence of the infinite series was not sufficiently rapid for three terms, hence it was necessary to compute the value of x to a higher degree of approximation. For this purpose, five terms were used, with the result that

$$\partial H_x/\partial y\,|_{y=\rho}=x_1^{14}+A_1x_1^{12}+B_1x_1^{10}+C_1x_1^8+D_1x_1^6+E_1x_1^4+F_1x_1^2-N_1=0,$$

where $A_1, B_1, \cdots, F_1$ represent the new constant coefficients, N_1 is the new constant term and x_1 is the new value of the separation. As before, the determination of x_1 can be simplified by sub-

stituting $\psi_1 = x_1^2$, with the result that

$$f(\psi_1) = \psi_1^7 + A_1\psi_1^6 + B_1\psi_1^5 + C_1\psi_1^4 + D_1\psi_1^3 + E_1\psi_1^2 + F_1\psi_1 - N_1 = 0.$$

Since the value of x obtained from the three term series represents an approximation to the root of the five term series, the evaluation of ψ_1 was carried out by the method of Newton.[10] When the first approximate root $x = x_1$ was taken to be 3.58148, succeeding values were obtained as follows: $x_2 = 3.49204$; $x_3 = 3.48887$; $x_4 = 3.48830$. The fourth approximation satisfies the original equation with a residue of 1 part in 1.5×10^6. When applied to a coil consisting of two circular turns, this value of x is the distance at which each of the turns must be located with respect to the common median plane in order to secure uniform intensity at a distance $y = \rho$ off the axis of the coils. The corresponding x for the Helmholtz pair would be 4.0000. In Fig. 7(a) and (b) are shown the field intensities computed[11] for these two separations, as applied to two single circular turns. The intensity in the region $y = \rho = 3.0$, is referred to unit value by proper choice of current ratios. The variation of intensity along the median plane with the new separation is of the order of 1 : 5000, for a variation in y of ± 2 mm, whereas in the Helmholtz case the variation is 12 times as much. The field at the edge of the electron beam, ± 1 mm from the common median plane, is also very constant. Fig. 7(c) and (d) illustrate the case of standard coil No. 1. Even in this case, where the cross section is finite, it is apparent that the improved separation produces a more uniform field along the median plane and over the section of the beam than the corresponding Helmholtz arrangement.

(*c*) *Intensity constant for standard No. 1.*—In order to compute the constant for standard No. 1, we shall regard it as made up of a pair of coils, each composed of a set of seven coaxial circular turns of equal radii. The contribution of each of the seven pairs of turns, which are symmetrical about the common median plane, was computed for $y = \rho$ by means of five terms of the infinite series (Eq. 13) and the separation used. The summation of these gave

$$H_{x(1)}\big|_{y=\rho} = 0.841651 \text{ oersted/ampere.} \quad (14)$$

An independent computation of the field was carried out by a new method of successive approximation[12] which confirms the sufficiency of the five terms previously used. This powerful, new method allows the absolute value of the field to be rapidly determined to any desired approximation.

The expression for field intensity at the point $y = \rho$ due to a single pair of circular turns of radius a and symmetrical about the common median plane at the improved separation used is

$$H_x\big|_{y=\rho} = 0.4\pi a i \bar{L}/\bar{A}^2$$

or for the seven symmetrical pairs,

$$H_x\big|_{y=\rho} = 0.4\pi a i \sum_{k=1}^{7} \frac{\bar{L}_k}{\bar{A}_k^2},$$

where $\bar{A} = \lim A_j = \lim B_j$;

$\bar{L} = \lim L_j = \lim M_j$;

$$A_{j+1} = \frac{A_j + B_j}{2}; \quad B_{j+1} = (A_j B_j)^{\frac{1}{2}};$$

$$L_{j+1} = \frac{L_j + M_j}{2}; \quad M_{j+1} = \frac{B_j L_j + A_j M_j}{2B_{j+1}};$$

and $A^2 = (LA)^2 + x^2$; $B^2 = (MB)^2 + x^2$,

where $LA = a + \rho$ and $MB = a - \rho$.

In this way the contributions of each of the seven symmetrical pairs were computed to an approximation better than $1 : 10^6$, with the result that the constant for standard No. 1 by this method is

$$H_{x(1)}\big|_{y=\rho} = 0.841591 \text{ oersted/ampere.} \quad (15)$$

The agreement between this value of H_x and that obtained by straightforward summation (Eq. 14) of the five term infinite series is about 1 : 14,000. Thus, terms beyond the fifth may be disregarded. When four terms of the series are used, the difference is 1 : 5000.

[10] Scarborough, *Numerical Mathematical Analysis* (Johns-Hopkins Press, 1930), p. 178.

[11] I take this opportunity to express my great appreciation of the valuable aid rendered by Dr. P. G. Saper throughout the entire work of computing the magnetic field.

[12] This method is due to Dr. W. Bartky to whom I express my gratitude.

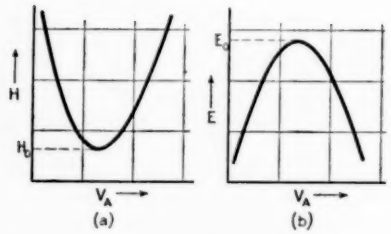

FIG. 8. Theoretical curves which show the variation, (a) in the magnetic field and, (b) in the electric field that is required in order to focus when the electron velocity is varied.

(*d*) *Intensity constant for standard No.* 2.—Thus far, no mention has been made of the helical nature of the current flowing in the various coils. The computations were based on the assumption that each turn of standard No. 1 was a circular turn.

In order to determine the effect of a helical current the constant of standard No. 2 was evaluated in terms of the line integral of the magnetic intensity taken around the helix which constituted this standard. The element of intensity for a point in the axis but off the common median plane is

$$dH_{x(2)}=a^2id\theta/[a^2+(\chi-p\theta)^2]^{\frac{3}{2}}, \qquad (16)$$

where a is the radius of the coil, $2\pi p$ the pitch, χ the distance from the reference plane to the point at which the field is expressed and $d\theta$ is the angle subtended on the axis by the normal component of the current element. The limits of integration are derived from the pitch and the number of turns on the coil. For the present computation, the limits were referred to the common median plane. Under these conditions, Eq. (16) reduces to

$$H_{x(2)}=\frac{4.8\pi i}{[a^2+(24p\pi)^2]^{\frac{3}{2}}}. \qquad (17)$$

Upon substituting numerical values,[13] the constant for standard No. 2 in its axis becomes

$$H_{x(2)}=0.843923 \text{ oersted/ampere}.$$

When standard No. 1 was compensated by standard No. 2

$$H_{x(1)}\,|_{y=p}=0.841480 \text{ oersted/ampere}. \qquad (18)$$

(*e*) *Intensity constant for magnetic field coils.*—Of the three values obtained for $H_{x(1)}$, as revealed by Eqs. (14), (15) and (18), the value from Eq. (15) supersedes that given by Eq. (14) since it is a closer approximation than the evaluation of the five terms of the infinite series. Furthermore, with the present arrangement of apparatus, it was more desirable to determine the constant of the magnetic field coils by the use of standard No. 1. Hence, for present purposes, standard No. 2 served merely as an experimental check on standard No. 1 with a resultant agreement of approximately 1 : 8000. For this reason, the constant of the magnetic field coils was computed in terms of Eq. (15) with the result that

$$H_{x(m)}=10.6291 \text{ oersted/ampere}.$$

In connection with the above method of compensation[14] for the determination of the constant of the magnetic field coils, it is important to recall that the intensity distribution diagrams shown in Fig. 7 were arrived at by computation. However, when standard No. 1 was used to determine the constant of the magnetic field coils, compensation occurred in the region of space occupied by the magnetometer. Since the cross section of the magnetometer was comparable with the cross section of the electron beam, it has been assumed that the constant of the magnetic field coils, as so determined, represented the field over this region. This is a reasonable assumption because an equally homogeneous intensity distribution would be expected for the magnetic field coils. As a matter of fact, Lyle[15] has shown that, as far as its external field is concerned, a circular coil of finite section can be replaced by one or more equivalent circular turns. Thus the theory, exemplified by Fig. 7(b), can be applied very simply to the equivalent pair of circular turns of a double coil of finite section in order to improve the uniformity for points off the axis.

[13] It is noteworthy that when $p=0$, Eq. (17) reduces to the standard form where the winding is assumed concentrated into a group of plane circular filaments. The field intensity computed from this arrangement exceeds by 14 : 10,000 the intensity determined from Eq. (17).

[14] In order to anticipate the thermal expansion of the coils and their supports due to the heating effect of the field current, compensation was carried out by means of appropriate current intensities after the normal current required to excite the field coils had produced thermal equilibrium. No effect due to this could be detected.

[15] Lyle, Phil. Mag. **3**, 310 (1902). Cf. also Barnett. Research Dept. Terr. Mag., Carnegie Inst. **4**, 382 (1921).

IV. Experimental Results

(A) Focusing criteria

Although Eq. (12) does not require that the electron velocity be determined in order to find e/m, only electrons of a certain voltage equivalent will reach the collector with given values of electric and magnetic fields. Let us consider the case of the dependence of the path upon the velocity only, and suppose the beam to have no divergence, that is $c_1=0$ in Eq. (9). Suppose further that the slit and collector are adjusted to the same distance from the center ($c_0=0$). Then at the collector, $r=\rho(1+\delta^2)$, where the velocity of the rays is defined in terms of δ by $v=\rho\theta_0'=\frac{1}{2}H\rho(1+\delta)e/m$. Thus the beam reaches the collector at the minimum distance ρ when $\delta=0$, or $v=\frac{1}{2}H\rho e/m$. Introducing the accelerating potential V_A in place of the velocity v, and substituting for $H\rho$ in Eq. (12), we find

$$V=2V_A\log_e(r_2/r_1). \tag{19}$$

This value of V_A gives a minimum value to r so that a slight variation in V_A moves the beam outward a very small amount.

In order to determine experimentally the electron velocity which must be employed with given electric and magnetic fields, we combine the two equations, $mv^2/\rho=Hev-Ee$ and $\frac{1}{2}mv^2=eV_A$, and solve for H with the result that

$$H=\frac{2V_A+\rho E}{\rho(2V_Ae/m)^{\frac{1}{2}}},$$

where E is the electric field intensity, H is the magnetic field intensity, ρ is the radius of curvature and V_A is the accelerating potential applied between the filament and the slit. This potential

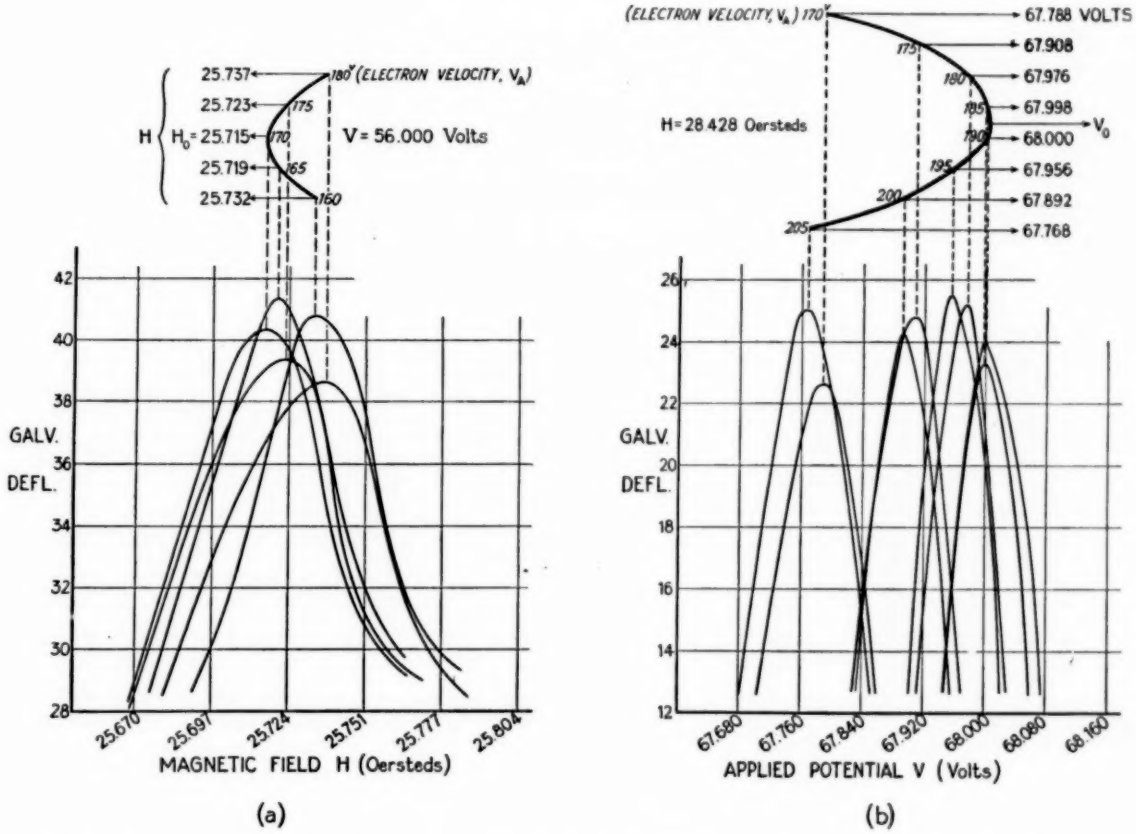

FIG. 9. Curves which show experimental results of test of focusing criteria. The sharpness of the focus increases slightly toward H_0 and V_0 and the focusing curve of maximum sharpness occurs in the magnetic case at H_0 and in the electric case at V_0. The width of the curve of maximum sharpness in both cases is slightly less than the theoretical width computed from the dimensions of the slit and the collector.

is measured externally by means of a precision megohm voltmeter (V_A in Fig. 2).

The curve shown in Fig. 8(a) represents the general form of the variation of H with V_A. This curve is the locus of the maxima of the individual focusing curves, each of which corresponds to a particular electron velocity and each is obtained by variations of H while that particular velocity is kept constant. It is to be understood, in obtaining the focusing curves, that E is constant when H is varied through the turning point in the curve which corresponds to the particular velocity.

In a similar manner, we get

$$E=[H\rho(2V_Ae/m)^{\frac{1}{2}}-2V_A]/\rho.$$

Fig. 8(b) shows the general form of the variation of E with V_A. In this case, the focusing curves are secured by varying the electric field intensity for a particular electron velocity at a constant magnetic field intensity.

Each of the curves shown in Fig. 8 reveals a unique value of the velocity V_A corresponding to particular values of electric or magnetic field intensity, namely H_0 and E_0. From $(\partial H/\partial V_A)=0$, we get, $V_A=\rho E/2$, at $H=H_0$; and from $(\partial E/\partial V_A)=0$, $V_A=(H^2\rho^2e/m)/8$, at $E=E_0$. When these values of V_A are substituted into their respective equation for H or E, the equation for e/m, in either case, becomes, $e/m=4E/H^2\rho$. The radial electric field intensity E is now expressed in terms of the applied potential V, and e/m reduces to

$$e/m=\frac{4V}{H^2\rho^2\log_e(r_2/r_1)}.$$

This equation for e/m corresponds to the unique velocity V_A associated with the turning points where $E=E_0$, when H is constant, or where $H=H_0$, when E is constant. Thus e/m is expressed in terms of a magnetic field intensity and an electric field intensity for a unique electron velocity V_A. Hence we see that in order to bring a beam of electrons to focus under the action of given electric and magnetic forces, the electrons must possess a unique velocity V_A, as defined by the foregoing criterion, even though this velocity does not enter the equation for e/m.

In Fig. 9 are shown typical results of the experimental test of the focusing criteria. The group of curves plotted in Fig. 9(a) with galvanometer deflection against magnetic field intensity H are the actual focusing curves. Each of the focusing curves was taken at the particular velocity indicated on the single curve shown above them in the figure. This single curve is the locus of the maxima of the focusing curves. Thus we have at the point corresponding with $H=H_0$ a magnetic field intensity of 25.715 oersted, a constant potential V of 56.000 volts across the electric field plates and an electron velocity of 170 volts, as applied and measured externally by V_A in Fig. 2. The group of curves shown in Fig. 9(b) illustrates the situation for a variation of the electric field. In this case, the focusing curves were secured by varying the potential V across the electric field plates for a constant magnetic field $H=28.428$ oersteds, with a particular electron velocity corresponding to each focusing curve. For this family of curves, $V_0=67.999$ volts.

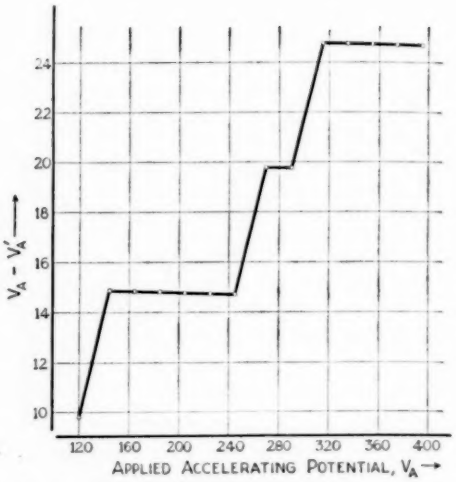

FIG. 10. Curve showing differences between the energy of the electrons before and after emergence from the slit (S in Fig. 3). The differences increase in approximately 5 volt steps.

It is evident from Fig. 9 that quite an appreciable uncertainty can exist in the evaluation of the electron velocity associated with the points $H=H_0$ or $E=E_0$, without affecting the determination of H_0 or E_0. For example, if the electron velocity were uncertain to the extent of ± 2 volts, at the point $H=H_0$, the maximum uncertainty in the magnetic field would not exceed 1:6000. *However, the velocity associated with the*

point $H=H_0$, or $E=E_0$, is merely incidental as far as the computation of e/m is concerned. The ultimate precision of the determination of e/m is related to the accuracy with which H_0 or E_0 can be ascertained from the so-called locus curves and is independent of the corresponding velocities. *In other words, the focusing criteria developed above serve merely as an experimental device for selecting particular electron velocities which can be focused with given electric and magnetic field intensities.*

(B) Magnitude and origin of the differences between experimental and theoretical values of V_A

The actual determination of e/m was carried out for a wide range of electric and magnetic field intensities, where the corresponding velocities varied from 120 to 400 volts. It is important to observe that the values of V_A that were required to give the adjustment for minimum $r=\rho$, did not agree with the values computed from Eq. (19). To illustrate the differences noted, it was found experimentally, for example, that for a given value of V and H, the value of V_A was 120 volts, as measured by the megohm voltmeter (V_A in Fig. 2), whereas from Eq. (19), V_A should have been 110 volts. Likewise for a higher value, V_A was 245 volts by measurement and only 230 volts by computation. Throughout the entire range of readings there was a difference between the value of accelerating potential measured experimentally and the value obtained by theoretical computation. This difference depended upon the magnitude of the applied accelerating potential, and was greater for the higher accelerating potentials. Curiously enough, the increase in this difference for increasing values of accelerating potential took place in approximately five volt steps. In order to distinguish these two potentials, we shall let V_A be the applied accelerating potential, as measured experimentally, and V_A' be the effective value obtained with the actual focusing data by theoretical computation from Eq. (19).

Figure 10 illustrates the variation in this difference as a function of the applied accelerating potential V_A. In Fig. 10, the axis of abscissas represents the applied accelerating potential, as measured externally by the megohm volt meter, and the ordinates are the differences between the applied accelerating potential and the effective accelerating potential, as defined by Eq. (19). We might think of the effective accelerating potential as the equivalent electron velocity associated with the electrons after they have emerged from the slit into the region of the deflecting fields. The applied accelerating potential, on the other hand, is the actual potential applied between the filament and the slit. Theoretically, these two velocities should be identical. However, it appears as if there existed in the neighborhood of the slit a retarding field which slowed down the electrons before they emerged from the slit. As a result of this retardation, the emergent electrons possessed the critical velocity required for focusing by the particular electric and magnetic forces operating. The velocity of the emergent electrons is expressed by Eq. (19) and the difference between this potential and the applied potential is a measure of the retarding field present. This retarding field may arise from an electronic charge which accumulates on the surface of the slit adjacent to the filament. That direct electron bombardment may modify a metal surface sufficiently to sustain a floating charge was pointed out in an earlier paper.[1]

From the foregoing, we infer the significant fact that in the method of crossed electric and magnetic fields the focusing is carried out with electrons whose effective velocity after emergence from the slit is known precisely from the electric and magnetic forces operating. *Therefore, any retardation experienced in the region of the slit does not constitute an uncertainty in this method of measuring e/m.* Since practically all other experimental methods that are used for the determination of e/m by electron deflection depend in one way or another upon a knowledge of the velocity of the electrons, the existence of this effect presents a serious difficulty in the use of these other methods.

(C) Attempts of Kirchner and Dunnington to correct for velocity uncertainties

Apparently the only correction which Kirchner[16] attempted to make for a possible velocity uncertainty was the correction for the contact

[16] F. Kirchner, Ann. d. Physik **12**, 503 (1932).

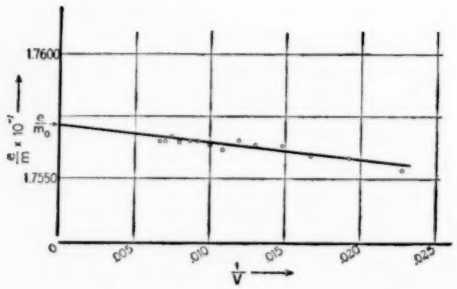

FIG. 11. Curve showing variation of the calculated value of e/m with the potential applied across the plates of the cylindrical condenser. $e/m_0 = kV'$; $e/m = kV$ and $e/m = e/m_0(1+\xi/V)$, where $k = 4\times10^7/H^2\rho^2 \log_e (r_2/r_1)$. $V = V' + \xi$ = applied potential; V' = actual deflecting potential and ξ = surface polarization layer, in volts. The data shown were taken under the following conditions; 24-carat gold surfaces on cylindrical condenser; $p = 5\times10^{-7}$ mm Hg. i (collector) $= 1.8\times10^{-10}$ amp.; $\rho = 3.0971$ cm; $\log_e (r_2/r_1) = 0.199787$; $\xi = 0.069$ volt.

potential difference between the hot cathode and the slit in his apparatus. Measurements were made of the electron emission at various temperatures over a potential range from 0 to 10 volts, between the hot cathode and the center of the brass anode. On the assumption of the validity of the $V^{\frac{1}{2}}$ law at these low voltages, a plot was made of I against V. The result was a curve which possessed a negative intercept on the voltage axis. This intercept was of the order of 1.5 volts and was interpreted by Kirchner as due to the contact P.D. between the hot cathode and the slit. This whole procedure depends upon the questionable assumption of the validity of the three-halves power law at low voltages. Volta potentials have been measured[17] by a scheme similar to this, but under circumstances which more closely approximated the assumptions of the theory. Furthermore, this method of correction does not take into account the presence of the space charge or polarization layer discussed under (**B**). Since the magnitude of the polarization layer depends upon the accelerating potential, it should be rather appreciable in Kirchner's experiment, where the accelerating potentials ranged from 1000 to 2000 volts.

The final equation employed by Dunnington[18] for the computation of e/m by his method appears to be independent of the velocity of the electrons. However, his elaborate experiments revealed that if the gold surfaces of the deflecting chamber and the slit system had suffered electron bombardment for fifteen hours or so, the subsequent values of e/m were appreciably altered. This difference was attributed to the formation of a polarization layer under direct electron bombardment. In order to correct for these polarization layers or surface charges, Dunnington assumed they were constant (constant emission current and small lapse of time). Hence extrapolation to infinite electron energy gave a corrected value of e/m.

In previous experiments,[1] the polarization layer which formed on the plates of the electrostatic field was found to be constant for a matter of hours, *provided no direct electron bombardment of the plates occurred. In the present paper it is shown that the layers formed under direct electron bombardment were not constant, but depended upon the velocity.* Furthermore, they appeared to be formed almost instantaneously and preliminary tests revealed the interesting fact that they were reversible. The accelerating potential in Dunnington's experiment is derived from the high frequency field, therefore, one would not expect the surface layers to be constant under these circumstances. There is also considerable possibility of such layers occurring on all the slits in Dunnington's apparatus with a consequent uncertainty in the electron energy and a distortion of the orbit.

(D) Determination of e/m

It was found most convenient to focus by varying the magnetic field for a constant electric field, since it was much easier to maintain the electric field constant than to maintain the magnetic field constant. The group of magnetic focusing curves shown in Fig. 9(a) constitutes one set of data for the calculation of e/m. In this case e/m would be expressed in terms of $H_0 = 25.715$ oersted, $V = 56.000$ volts, the average radial position of the slit and the collector, and the radii of the two condenser plates. However, the curves in Fig. 9 are merely typical, experimental curves which were taken during the investigation of the focusing theory. After the preliminary work on the focusing theory had been completed, the apparatus was very carefully gold plated again and then measured physically, after which several final sets of data were taken over a wide

[17] W. Schottky, Ann. d. Physik **44**, 1011 (1914).
[18] F. Dunnington, Phys. Rev. **52**, 475 (1937).

range of electric and magnetic field intensities. In the actual evaluation of e/m from these data, the peak values of the focusing curves could be ascertained without the necessity of plotting the focusing curves themselves. From the simple locus of these peak values, the values of H_0 were determined with considerable accuracy, as can be judged from the curves in Fig. 9. It is interesting to observe that in the process of collecting the final data, it was possible to repeat readings of the peak values of the focusing curves to better than 1 : 10,000.

The computation of e/m for the entire range of field intensities investigated revealed the dependence of the computed value upon the potential applied across the plates of the cylindrical condenser, as pointed out in an earlier paper.[1] The graph in Fig. 11 shows the variation of e/m with this potential. It is very important to recall that the surface polarization layer formed on the electric field plates is constant for: (1) a given intensity of electron beam; (2) constant gas pressure; and (3) clean metal surfaces, *provided no direct electron bombardment of these plates is allowed to occur during the process of focusing the beam*. In order to accomplish this, a shift to a new pair of electric and magnetic intensities was made only after the applied accelerating potential had been reduced to zero (see switch S in Fig. 2). In this way the electrons were kept out of the region between the electric field plates until the new set of field values had been adjusted approximately to bend the electrons into a circular orbit. After this preliminary adjustment, the focusing process was carried out with the beam deviating very little from the central circular orbit.

The final value of the specific charge was evaluated[19] from the data of Fig. 11, by the method of least squares, with the result that

$$e/m_0 = (1.7571 \pm 0.0013) \times 10^7 \text{ e.m.u.},$$

where the probable error is identified with the least squares solution.

Because of the physical limitations of the present cylindrical condenser, no attempt was made to push this determination to the extreme limits of accuracy attainable with this new method. However, the very slight eccentricity of the electric field plates does not invalidate the probable error stated.[20]

In view of the work completed up to the present time, it is of interest to make a conservative estimate of the ultimate precision that should be attainable with this new method. From the self-consistency obtained in both the theoretical and the experimental evaluation of the magnetic field intensity, 1 : 6000 is a conservative estimate of the accuracy with which the magnetic field intensity can be determined. The present limitation of the cylindrical condenser is mainly physical. This uncertainty will be reduced considerably with a new condenser designed along kinematic lines. The radius of curvature of the beam must be measured to 0.005 mm in order to be known to within 1 : 3000. Previous measurements suggest that this should present no difficulty. The constants of the standard cells, standard resistances and the volt box are well within the projected limit of 1 : 3000. It is, therefore, the confident and conservative hope of the author that with the new cylindrical condenser a determination of e/m will be possible to within a probable error of 1 : 3000.

It is a great pleasure to express my appreciation to Dr. A. J. Dempster for his very generous interest during the course of this work.

[19] I wish here to express my appreciation to Mrs. Ardis T. Monk for checking independently the final results of the computation of e/m.

[20] I am very grateful to Dr. Carl Eckart for an interesting discussion of this point.

The Pressure Coefficient of Thermal Conductivity of Metals

CHAUNCEY STARR*
Harvard University, Cambridge, Massachusetts
(Received June 13, 1938)

The pressure coefficients of thermal conductivity of copper, silver, and gold were determined by means of an improved longitudinal heat flow method. The results indicate that the ratio of the thermal to the electrical conductivity (the Wiedemann-Franz ratio) for these metals, over a pressure range of 12,000 kg/cm², has a small positive coefficient of approximately 1 percent in 10,000 kg/cm². These results are at variance with those of Bridgman who used a similar method but found that the pressure coefficient of the Wiedemann-Franz ratio may be either negative or positive and is more often negative. Experiments are reported which prove that the negative coefficients found by Bridgman were due to a systematic convection error undiscovered in his longitudinal heat flow method. It is reasonable to suppose that the positive pressure coefficient of the Wiedemann-Franz ratio is due to the nonelectronic part of the thermal conductivity, and this assumption is further supported by the correlation between these positive coefficients and the volume compressibilities of the metals.

INTRODUCTION

THE theory of electrical and thermal conductivity of metals based on quantum mechanics has given a qualitative understanding of most experimental results. One of the most important results explained has been the Wiedemann-Franz law, which states that the ratio of the thermal to the electrical conductivity is equal to LT, where T is the absolute temperature and L is a constant known as the Lorenz number which is the same for all metals. The quantum theory and the previous electron theories of conduction have based their quantitative deduction of this law upon the assumption that the conduction of heat in metals is due to the motion of "free" electrons. The results of these deductions were in fair agreement with experiment for a large number of metals. The quantum-mechanical derivation of the Wiedemann-Franz law, based on the electron motion assumption, is theoretically valid for most metals. Because of the approximations made in the theory, the results do not hold exactly for the transition metals or bismuth, or for temperatures much less than the Debye characteristic temperature. The theory neglects the contribution to the thermal conductivity made by the lattice vibrations and therefore should give too low a value for poor conductors. Aside from these exceptions, the fact that the theoretical result agrees well with experiment would indicate that the major phenomena involved in thermal conduction in metals had been accounted for.

The experimental investigation of the Wiedmann-Franz law as a function of pressure has been undertaken by Lussana[1] and Bridgman,[2] with widely divergent results. To the first order, the theory indicates that the ratio of thermal and electrical conduction should be independent of pressure. Since a pressure of 10,000 kg/cm² (1 atmosphere = 1.0332 kg/cm²) affects the electrical conductivity by only a few percent, the effect of pressure on the thermal conductivity should also be only a few percent—an amount difficult to determine precisely experimentally. Lussana, working up to 3000 kg/cm², had measured the effect of pressure on twelve metals. He found that the Wiedemann-Franz ratio remained nearly constant. However, the method he used was extremely unreliable in that the corrections for heat loss were more than ten times the effect investigated, and Lussana made the correction very inaccurately. A critical analysis of Lussana's results appears in Bridgman's paper. Bridgman used two methods for measuring the change of thermal conductivity with pressure. The first was a radial flow method and had the advantage of requiring very few corrections. The specimen was in the form of a cylinder that almost filled the bore of the pressure chamber. A heater wire was placed along the axis

* This work was done at the physics laboratory of Harvard University during the year 1936–37, while the author was a Charles A. Coffin Fellow and a Research Fellow in physics.

[1] S. Lussana, Nuovo Cimento **15**, 130 (1918) and **25**, 115 (1923).
[2] P. W. Bridgman, Proc. Am. Acad. Sci. **57**, 77 (1922).

of the specimen to produce radial heat flow and the temperature difference between two points at different radial distances from the axis was measured. The difficulties involved in preparing a homogeneous specimen with accurately placed thermocouple and heater wires limited the use of this method to poor conductors, Pb, Sn, and Cd. For good conductors, Bridgman used a longitudinal flow method. A source of heat was placed at one end of a rod, a sink at the other, and the temperature drop along the rod measured by a differential thermocouple. The heat loss from the specimen to the pressure cylinder was an important correction, of the order of magnitude of the effect being investigated. Using the longitudinal flow method Bridgman measured the pressure effect on Zn, Fe, Pt, Ag, Cu, Ni, Sb, and Bi.

Bridgman's results showed that the pressure coefficient of the Wiedemann-Franz ratio could be either positive or negative, and in many cases was so large as to indicate that an appreciable part of the thermal conductivity was nonelectronic in nature. For example, in the case of Ni, a pressure of 12,000 kg/cm² decreased the measured thermal conductivity by 14.5 percent and increased the electrical conductivity by 1.8 percent. The pressure could, at most, wipe out completely the nonelectronic part of the thermal conduction. Thus, the above result would place a lower limit of 16 percent upon the magnitude of the nonelectronic part of the total thermal conductivity. (Bridgman erroneously interpreted this limit as an upper limit.) If the nonelectronic part is not completely wiped out, but has a pressure coefficient similar to that of insulators, the fraction of the total thermal conductivity due to the nonelectronic part may be very much larger. The theoretical value for the Lorenz number due to electronic conduction alone is 2.45×10^{-8} (volt/degree)², and the best values for Ni give an experimental Lorenz number of 2.28. Not only is this difference too small to agree with the above analysis, but it is also of the wrong sign. In addition, the pressure coefficients of thermal conductivity of insulators, as found by Bridgman,[3] are all positive, as would be expected. It would therefore seem reasonable that if the nonelectronic part of the thermal conductivity of metals is due to lattice vibrations, this part should have a positive pressure coefficient, rather than the negative coefficient observed in most of the metals Bridgman investigated. Apparently, if Bridgman's experimental results were all correct, some fundamental phenomenon must have been overlooked in the theories of conduction in metals. Alternately, if the theories were fundamentally sound, the experimental results must have been vitiated by some unknown systematic error. Credence was lent this latter possibility by the fact that the metals investigated by the radial flow method, Pb and Sn, showed positive pressure coefficients, whereas all those investigated by the longitudinal flow method showed the anomalous negative coefficients. In an attempt to settle this question, the research reported in this paper was undertaken. Measurements were made on Cu, Ag, and Au by means of an improved longitudinal flow method. The results found showed that the Wiedemann-Franz ratio for these three metals, over a pressure range of 12,000 kg/cm², has a very small positive coefficient, and that the anomalous negative coefficients found by Bridgman were due to a systematic convection error undiscovered in his work.

Method and Apparatus

The difficulties involved in all thermal conductivity measurements are greatly enhanced in high pressure measurements due to the necessity of making the specimen small enough to fit into the pressure chamber, and because of the increased heat losses caused by the liquid used to transmit the hydrostatic pressure. The change of electrical conductivity in 12,000 kg/cm² pressure change is about 5 percent or less for most good conductors, and the corresponding change in thermal conductivity of the liquid used, petroleum ether, is about 125 percent. It is therefore essential, for precise measurements, that the fraction of the total heat input to the specimen that is lost through the liquid be made as small as possible. Any small heat loss not a function of pressure does not contribute to the experimental error since only the relative change in thermal conductivity is of interest.

[3] P. W. Bridgman, *The Physics of High Pressure* (Macmillan, 1931).

The known methods for measuring the thermal conductivity of metals fall into two general groups, dynamic and static. The dynamic methods have the valuable advantage of eliminating the necessity for determining heat losses, but unfortunately they cannot be used when the specimen is surrounded by a dense medium such as a liquid.[4] In the static methods, the variable heat losses may be determined as a function of pressure or minimized to such an extent that they do not affect the precision of the measurement. The radial method used by Bridgman utilized this latter principle, but as has been mentioned, had a limited applicability. In the longitudinal method, Bridgman determined the variable heat losses by theoretical analysis of the geometry of the apparatus. These losses, except for the best conductors, were generally of the same order of magnitude as the effect sought. It is apparent that the best method would be one that was of general applicability and utilized the principle of minimizing the heat losses. For this purpose a guard cylinder method was developed for use in this research. The specimen in the form of a long rod was mounted in the center of the pressure cylinder, one end in a large copper block and the other containing a heating coil as in the longitudinal flow method. Midway between the specimen and the pressure cylinder was placed a copper guard cylinder. The specimen and guard cylinder had a common cold sink, and the hot end of the guard cylinder completely enveloped the hot end of the specimen. By suitable adjustment of the current in the guard cylinder heating coil, the hot end of the guard cylinder could be brought to the same temperature as that of the specimen. This resulted in an approximately similar temperature distribution along the guard cylinder and the specimen, and the heat loss from the specimen was therefore very small and calculable. With this apparatus a number of tests were made upon a copper specimen, but the method was finally discarded because of the mechanical difficulties involved in precisely aligning the small sized apparatus, the trouble encountered with the six electrical leads into the pressure cylinder, and the length of time required to reach the thermal balance. However, if the experimental results warrant the work involved in an extremely high precision investigation, this method could be used. Finally an improved longitudinal flow apparatus, similar to the original apparatus of Bridgman, was developed. The results reported in this paper were found with this apparatus.

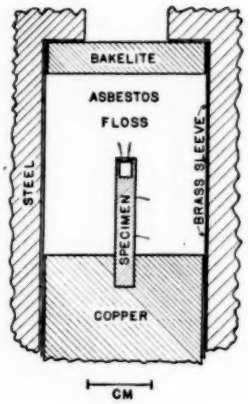

FIG. 1. Specimen mounted in pressure cylinder.

The specimen used in this longitudinal flow method was about 2 cm long and about 3 mm in diameter. The specimen was mounted concentric in the pressure cylinder, as shown in Fig. 1, and one end was soldered into a massive copper block which formed the cold sink. The heat source at the other end of the specimen consisted of a diminutive coil made of No. 36 D.C.C. Nichrome V wire embedded in a square bottomed hole 3 mm deep and made with a No. 44 drill. The coil contained enough wire to have a resistance greater than 10 ohms. A silicate (dental) cement was used to hold the coil in place since it was found that any movement of the coil, when the pressure was changed, altered the distribution of the heat flow and gave unreproducible results. A snug fitting copper disk was used to close the hole. The heating coil was thus completely surrounded by metal and therefore most of the heat developed entered the specimen. The Nichrome wire was soldered to No. 36 copper leads at a small distance from the specimen.

The thermocouples used for the three metals investigated, Cu, Ag, Au, were all made of No. 36 Advance wire. Since the difference in temperature of two points along the specimen was desired, the two couples were connected differentially with the specimen itself as the common

[4] C. Starr, Rev. Sci. Inst. 8, 61 (1937).

lead. This permitted the soldering of the Advance wire to the specimen. Bridgman used copper-constantan couples differentially connected and loosely held in holes in the specimen. This resulted in a movement of the thermocouples when pressure was changed and caused scattered readings. The method of direct soldering completely obviates this difficulty. The thermocouples were placed far enough from the ends of the specimen to be in a region of uniform heat flow and far enough apart to produce a satisfactory e.m.f.

The massive copper block fitted snugly into a thin brass sleeve (14 mil wall) which, in turn, fitted snugly into the pressure cylinder. The top of this sleeve was closed off by a Bakelite plug as shown in Fig. 1. The space between the specimen and this sleeve was completely filled with tightly packed asbestos floss. This asbestos floss served the very essential purpose of preventing convection currents in the surrounding liquid.

The dimensions of the apparatus and specimen were the result of a compromise between the ideal conditions and experimental convenience. The longer the specimen the smaller is the heat input required to produce a precisely measurable temperature difference and the less critical is the thermocouple placement. However, in order to reduce the fraction of the heat input lost laterally by the specimen to the pressure cylinder walls, it is desirable that the specimen be as short as possible and have a large cross section area. A simple calculation shows that the optimum diameter for the specimen is approximately one-half that of the pressure cylinder, but this would cause complications due to nonuniform heat flow. The maximum size of the pressure chamber was determined by the limitations of the hydrostatic pressure apparatus. A larger volume than that used would not have permitted reaching such high pressures. While a large inner bore is desirable in order to reduce lateral heat loss, an inner diameter greater than that used, about 1 inch, would require too heavy a cylinder for easy handling. The heating coil and the thermocouple leads were large enough in diameter (5 mils) for handling, but a simple calculation showed that they were not large enough to cause an appreciable heat loss along the leads. As only the change in this heat loss with pressure affects the final result, and this is very small, it can be neglected.

The necessary electrical measurements were the current through and the resistance of the heating coil, and the thermal e.m.f. produced by the temperature drop. The heating coil resistance was measured on a resistance bridge. The heating current, about 0.2 ampere, was supplied by a large capacity storage battery source and was measured by means of a standard 1 ohm resistance in series with the heating coil. The voltage drop across this standard resistance was determined with a potentiometer. The thermal e.m.f. was measured by an auxiliary potentiometer system. A variable dry-cell voltage source was connected in series with a 10,000 ohm and a 10 ohm manganin resistance. The voltage across the 10 ohm resistance was used to balance the thermal e.m.f. with a galvanometer as a null instrument. The voltage across the 10,000 ohm resistance was measured by the potentiometer. This system had a maximum voltage sensitivity better than 10^{-8} volt.

A reversing switch in the heating current circuit permitted the elimination of the effect of leakage currents. Although the heating circuit was well insulated from the thermocouple circuit, the latter was so sensitive that only a slight leakage was sufficient to affect the readings. The pressure transmitting liquid, petroleum ether, was an excellent insulator, but some leakage occurred in the four-terminal plug that carried the leads into the pressure cylinder, probably due to moisture in the insulation. A reversing switch was also used to eliminate parasitic e.m.f.'s in the galvanometer circuit. This switch was enclosed in a thermally insulated copper chamber so as not to become a source of thermal e.m.f.'s. Parasitic e.m.f.'s in the remainder of the thermocouple circuit could not be thus eliminated, so they were determined by measuring the residual e.m.f.'s before and after each set of readings with no heat input to the specimen. The parasitic e.m.f.'s were made as small as possible by placing the electrical connections and pressure cylinder in a constant temperature bath.

The production of the high pressures and the technique of high pressure measurements has been completely described by Bridgman.[3]

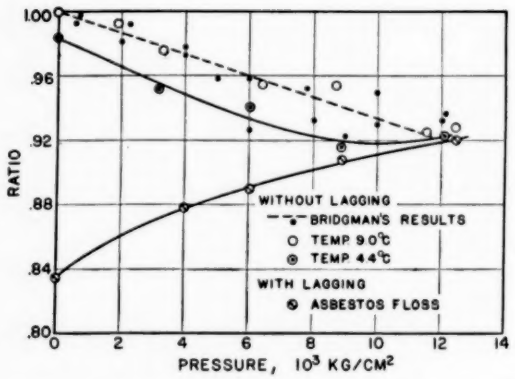

FIG. 2. Ratio of heat input to temperature drop (W/θ), in relative units, as a function of pressure for a copper specimen. The effect of temperature and lagging upon convection losses is illustrated. Bridgman's results are plotted for comparison.

EXPERIMENTAL PROCEDURE

The procedure for making the measurements was the same for all the specimens and for each value of the pressure. The apparatus was completely surrounded by a well-stirred ice bath and allowed to come to temperature equilibrium. With no input to the heating coil, the residual parasitic e.m.f. was recorded. The resistance of the heating coil was measured on a bridge, and the heating current switched on. In about fifteen minutes thermal equilibrium was reached and measurement of the thermal e.m.f. was made as previously described, for both positions of the galvanometer reversing switch, and for both positions of the heating current reversing switch. This gave four readings of the thermal e.m.f. Heating current was determined before and after each set of measurements. The input to the heating coil was then switched off, and after temperature equilibrium had been reached the residual parasitic e.m.f.'s were again determined. The pressure was then changed to the next desired value and after temperature equilibrium had been reached the parasitic e.m.f.'s were determined for the next set of measurements.

The true thermal e.m.f. for any given set of measurements was determined by subtracting the average parasitic e.m.f. from the average thermal e.m.f. The ratio of the heating coil watts to the true thermal e.m.f. was thus determined for each value of the pressure. Before and after each set of pressure measurements on a specimen, this ratio was determined at atmospheric pressure and with air in the pressure cylinder instead of petroleum ether. The apparatus was not disturbed for this purpose, the pressure cylinder being filled and emptied by means of a vacuum pump.

The thermal conductivity of the specimen is determined by the equation

$$K_s=(W/\theta)(d/a)/(1-m)(1-n)(1+p),$$

where W is the heat input to the specimen; θ is the temperature drop between the two thermojunctions, calculated from the thermoelectric power at atmospheric pressure; d is the distance between thermojunctions at atmospheric pressure; a is the cross section area of specimen at atmospheric pressure; m is the temperature correction due to the pressure variation of thermoelectric power; n is the dimensional correction due to linear compressibility; p is the heat loss correction due to the pressure variation of the thermal conductivity of the pressure transmitting liquid (petroleum ether). The data necessary for these corrections have all been determined by Bridgman.[3]

The solution of the heat flow equations for the conditions of the specimen indicates that the magnitude of the heat loss correction may be determined by the first-order approximation $p=CK_e/K_s$, where K_e is the thermal conductivity of the liquid, and K_s is that of the specimen. Bridgman[2] estimated the magnitude of the heat loss constant C from the geometry of the apparatus, but unfortunately the unavoidable approximations required caused a large probable error in the result. In this research C was determined from experimental data at atmospheric pressure by means of the equation

$$C/K_s=(r-1)/(K_e-rK_a),$$

TABLE I. *Measurements on copper specimen, at 1 kg/cm² and 0°C.*

SURROUNDING MEDIUM	LAGGING	TEMP. OF HOT END, °C	RATIO W/θ
Petroleum ether	None	9.0	1.000
		4.4	0.982
Glycerin	None	9.0	0.872
Petroleum ether	MgO	9.0	0.849
	Asbestos floss	9.0	0.834
Air	None	9.0	0.800

where r is the value of the ratio of $(W/\theta)_{\text{liquid}}$ to $(W/\theta)_{\text{air}}$; K_e is the thermal conductivity of the petroleum ether; K_a is the thermal conductivity of air. The (W/θ) ratio was determined with petroleum ether in the apparatus, and also with air, as described above. This experimental method appreciably reduced the probable error of the heat loss correction.

Convection Error

Preliminary experiments to determine the value of the heat loss constant C, as described above, indicated an extremely large correction was necessary. Since the required correction was an order of magnitude greater than that calculated from the geometrical considerations, loss of heat by convection was suspected.

The quantity determined directly from the experimental measurements is the ratio of the watts input to the specimen to the thermal e.m.f. produced by the temperature drop along the specimen. This ratio is given by the equation (discussed above)

$$(W/\theta)=K_s(a/d)(1-m)(1-n)(1+CK_e/K_s).$$

Since convection currents increase the heat loss from the specimen, their effect is similar to that of increased thermal conductivity of the surrounding liquid, i.e., they decrease the temperature drop for the same heat input and thus increase the ratio W/θ. In order to verify the presence of convection effects the ratio W/θ was determined at atmospheric pressure and 0°C with the space between specimen and cylinder filled with air, petroleum ether, and glycerine, and with this space also packed tightly with heat insulating material in order to hinder the motion of the liquid. The results of these measurements are tabulated in Table I. Fig. 2 shows the pressure measurements on a copper specimen with petroleum ether, with and without asbestos floss lagging. As the pressure increases, any convection effects tend to decrease due to the increased viscosity of the liquid. For this reason, all the experimental points at the high pressures tend to coincide. All the above data is consistent throughout with the behavior of convection effects. Bridgman's experimental points for copper are also plotted in Fig. 2. These would indicate that the error due to convection in Bridgman's measurements is about the same as that found with the present apparatus.

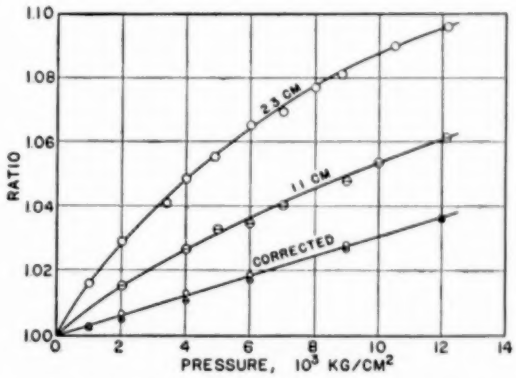

Fig. 3. Ratio of heat input to temperature drop (W/θ), in relative units, as a function of pressure for copper specimens of different lengths.

The theory of natural convection[5] gives the relation $h/\theta=\text{constant}\cdot\theta^b$, where h is the heat loss per second from cylinder specimen; θ is the temperature excess; b is a constant ranging from about 1/10 to 1/6. Bridgman tested his apparatus for presence of convection effects by changing his heat input and thus the temperature differences by a factor of 2. He assumed that h/θ was proportional to θ, so that any loss due to convection should also change by a factor of 2. His measurements indicated no change in the results, and he therefore assumed that his apparatus was free from convection. However, from the convection relations, with b assumed equal to 1/6, the change in convection loss due to halving the temperature is only 12 percent. As indicated in Table I, the total difference in heat loss, when convection is hindered by the presence of asbestos floss lagging about the specimen and when no lagging is present, is 16.6 percent. Under the assumption that this heat loss is completely due to convection, halving the temperature difference would reduce this by 12 percent or a total heat loss reduction of 2 percent. Since the precision of Bridgman's measurements was not very high, such a small change may have passed unnoticed. That such a change does occur is indicated by the experimental results shown in Table I and Fig. 2.

[5] J. K. Roberts, *Heat and Thermodynamics*, p. 234 (Blackie & Son, 1928).

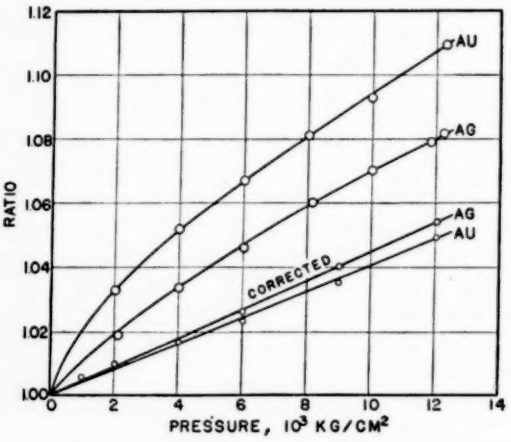

FIG. 4. Ratio of heat input to temperature drop (W/θ), in relative units, as a function of pressure for silver and gold specimens.

As a final test that the analysis of the convection effect was correct, measurements of the pressure coefficient of thermal conductivity were made on two copper specimens, one 2.3 cm long and the other 1.1 cm long. The specimens were surrounded by asbestos floss lagging in each case. Since some of the heat losses and corrections vary approximately as the square of the length, and some approximately as the length, the relationship between the various losses and corrections, and the heat input is different for two specimens. Any error or omission in the analysis of the correction to be applied to the measurements would thus be shown by a discrepancy in the results. The results of the measurements are shown in Fig. 3. After applying all the corrections discussed under experimental procedure, the pressure coefficient determined for the two specimens was the same, within the experimental error. This result conclusively indicates that the asbestos floss lagging has removed the convection error.

The effect on the results of the pressure coefficients of thermal conductivity of the asbestos floss lagging can be shown to be less than the experimental error of the results. As determined by direct measurement, the asbestos floss forms about 7 percent of the total volume of the specimen; petroleum ether the remainder. Assuming that the thermal conductivity pressure coefficient of the asbestos minerals is of the same order of magnitude as that of silica, the total effect of the asbestos is equivalent to less than 2 percent of the pressure coefficient of the liquid, or to about 0.1 percent in the final result. The results shown in Fig. 3 substantiate this also.

TABLE II. *Summary of results. Pressure coefficients* $\times 10^6$.

METAL	COEFFICIENT OF THERMAL CONDUCTIVITY	COEFFICIENT OF ELECTRICAL CONDUCTIVITY	COEFFICIENT OF WIEDEMANN-FRANZ RATIO	AVERAGE VOLUME COMPRESSIBILITY
Copper	3.0±0.3	1.86	1.1±0.3	0.69
Silver	4.5±0.3	3.44	1.1±0.3	0.94
Gold	4.0±0.4	2.98	1.0±0.4	0.55
Radial Method (Bridgman):				
Tin	13.2±0.7	10.13	2.8±0.6	1.79
Lead	17.3±0.4	13.79	3.1±0.3	2.20

RESULTS

The experimental determinations for copper, silver, and gold are shown in Figs. 3 and 4. The copper used was doubly deposited electrolytic copper with a spectrographically indicated purity of better than 99.999 percent. The silver and gold specimens were made from commercially pure materials, the silver 99.95 percent pure, and the gold 99.97 percent pure.

The results are summarized in Table II. Bridgman's radial flow determinations are also included, since these are not open to the convection error criticism and therefore are reliable.

These results indicate that the Wiedemann-Franz ratio for the metals and the pressure range investigated has a very small positive pressure coefficient. It is reasonable to suppose that this positive coefficient is due to the nonelectronic part of the thermal conductivity, and this assumption is further supported by the correlation between the positive coefficient and the compressibilities.

The writer is indebted to Professor P. W. Bridgman for his support of this research and to Harvard University for the use of their physics laboratories.

Change of Thermal Energy with Adiabatic Change of Magnetization in Iron, Nickel and Carbon Steel*

T. C. HARDY AND S. L. QUIMBY
Columbia University, New York, N. Y.

(Received June 6, 1938)

Previous methods for measuring the change in thermal energy which occurs when the magnetization of a ferromagnetic material is altered adiabatically have been so improved as to permit a precise study of this phenomenon in magnetically soft materials. The materials here dealt with are carbon steel, and annealed and unannealed Armco iron and nickel. The change in thermal energy of each of these substances is traced through a complete half-cycle of magnetization which starts with the maximum value of the intensity of magnetization. The external work done by the specimen at each stage of the process is likewise evaluated. The decrease in thermal energy on demagnetization is less than the external work done by the specimen in iron and steel, while in unannealed nickel it is greater. In annealed nickel the decrease in thermal energy is greater than the external work when the magnetization process is continuous and less when it is discontinuous.

THE problem dealt with in this research can best be understood by considering, initially, the interplay of energy between the parts of a system composed of an electric current generator connected to a solenoid, and a slender bar of ferromagnetic material lying axially within the solenoid. It can readily be shown[1] that the work done by the generator on the ferromagnetic specimen in producing a change of amount δJ in the magnetization is, per unit of volume, equal to $H_0\delta J$, where H_0 is the magnetic field strength of the current in the solenoid. Accordingly the work done on unit volume of the material in carrying the magnetization from J_1 to J_2 is given by the integral

$$\int_{J_1}^{J_2} H_0 dJ. \qquad (1)$$

If the process is performed adiabatically this quantity evaluates the change in the self-energy of the substance. The object of the present research is to ascertain experimentally what part of this energy change is of thermal character.

A portion of the self-energy represented by the integral (1) is definitely not of thermal origin, and, furthermore, depends in magnitude upon the shape of the specimen. This portion is equal to $(N/2)(J_2^2-J_1^2)$, where N is the "demagnetization factor" of the specimen. This is the mutual potential energy of the molecular magnets in their own magnetic field, or, as was pointed out long ago by Lord Rayleigh,[2] when integrated over the volume of the magnet it is the work which might be obtained, were the specimen flexible, by allowing its ends to approach each other under their mutual attraction. If this be subtracted from the total there remains, as a measure of the true change in *internal* energy per unit volume of the specimen, the integral

$$\int_{J_1}^{J_2} H dJ, \qquad (2)$$

in which $H=H_0-NJ$, and is the actual magnetic field intensity in the specimen.

If the substance is in a cyclic state of magnetization of amplitude J, and $J_1=-J_2=J$, then the initial and final states are magnetically identical and the entire change in internal energy is thermal. The integral (2) then evaluates the so-called "hysteresis loss" per half-cycle of magnetization. Over a portion of the half-cycle, however, the thermal contribution to the internal energy change can only be discovered by calorimetric measurement.[3]

EXPERIMENTAL METHOD

The experimental method is, briefly, the following: The change in temperature which accompanies a given adiabatic change in magnetization of the specimen is indicated by the deflection of

* Publication assisted by the Ernest Kempton Adams Fund for Physical Research of Columbia University.

[1] See for example, Bitter, *Introduction to Ferromagnetism*, p. 19.

[2] Rayleigh, Phil. Mag. **22**, 175 (1886); Scientific Papers, **2**, p. 546.

[3] Larmor, Proc. Roy. Soc. **71**, 239 (1903).

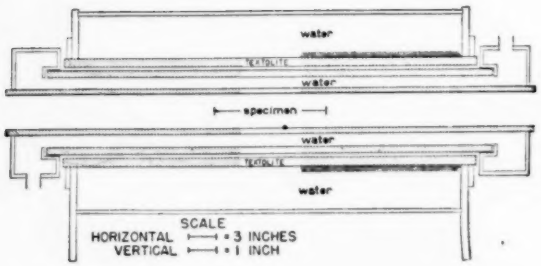

FIG. 1. Longitudinal section of the solenoid calorimeter.

a galvanometer connected to an array of thermocouples in thermal contact with the specimen. This temperature change is duplicated by sending a known current through the specimen for a measured time interval. It is then assumed that the original change in thermal energy per unit volume of the specimen is equal to $\rho i^2 t$, where ρ is the specific resistance, i the current density, and t the time.[4] The change in magnetization is effected in such manner that the heat associated with the eddy currents induced in the specimen is negligible. The experimental arrangements are such as to permit the detection of a change in thermal energy as small as 200 ergs per cm^3, and this corresponds to a change in temperature of about 5×10^{-6} degree centigrade.

The solenoid calorimeter

The specimen, in the form of a bar 1 mm in diameter and 30 cm long, is placed at the center of the solenoid calorimeter diagrammed in Fig. 1.

The two-layer solenoid winding is 40 inches long and 4 inches in diameter. The tubes which are cross hatched in the figure are textolite and the enveloping tube is brass. The temperature of the specimen and its environment is stabilized with the aid of two separate water baths, each circulated continuously by a centrifugal pump. The temperature of the inner bath, about 41.3°C, is held constant to better than 0.01°C by thermostatically controlling the temperature of the water in a reservoir placed in the circuit. The control is effected by a mercury in glass thermostat in connection with a 750 watt Mazda lamp operating at 170 watts. The operational procedure requires an almost continuous dissipation of heat in the solenoid. This heat is removed by the outer circulation of water, the temperature of which is held constant to 0.1°C at about 36°C by a thermostatically controlled electric fan directed against an automobile radiator placed in the circuit.

The thermocouple-galvanometer system

The thermocouples are constructed from 57 strips each of copper and constantan ribbon 0.001 inch thick and 8 mm long rolled from No. 40 copper and No. 35 constantan wire. These strips are soldered together at the ends in the relative configuration of the constituent lines of the letter "W." The "cold" junctions are soldered to a row of 57 copper pegs set 3.8 mm apart in a Bakelite strip. The "hot" junctions are affixed to the specimen with an adhesive prepared by dissolving clear glyptal cement in acetone. The cement is electrically nonconducting, and no junction is in electrical contact with the specimen. The specimen rests on a Bakelite strip, or, occasionally, hangs freely suspended by the attached thermocouples.

The thermocouple system is connected to a L and N type HS galvanometer which has 12 ohms critical damping resistance, 10 second period, and sensitivity of 17 mm per microvolt at 1 meter scale distance. A turn of variable orientation is placed in the circuit to permit the compensation of accidental magnetic flux linkage. The galvanometer deflections, which are almost ballistic in character, are amplified by the apparatus shown diagrammatically in Fig. 2.

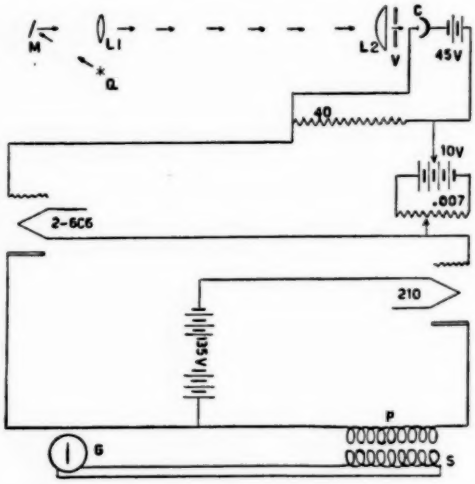

FIG. 2. Diagram of apparatus for amplifying ballistic galvanometer deflections. The resistances are in megohms.

[4] This method of attack on the experimental problem was devised by A. Townsend, Phys. Rev. **47**, 306 (1935).

Q (Fig. 2) is a 108-watt vertical platinum strip filament light source operated from a 60-cycle a.c. transformer in connection with a voltage stabilizer. Light from this source is reflected from the front silvered mirror of the galvanometer and passes through the lens L_1, which forms an image of the filament on a horizontal, V-shaped slit, V, 3.5 meters distant. This slit is affixed to the back of a 6 inch condensing lens, L_2, which brings the transmitted light to a focus on the surface of a photoelectric cell, C. The photoelectric current is amplified and operates, through an air core transformer, a L and N type 2285D galvanometer *used as a fluxmeter*. The primary of the transformer has 36,000 turns and the secondary 3000 turns. The current amplification of the amplifier is 1.8×10^5 and the deflection amplification actually used is about 8. The over-all sensitivity of the system varies between 140 and 220 ergs per cm³ per mm deflection.

Operational procedure

The circuits used for controlling the applied magnetic field intensity are shown in Fig. 3. In the normal operating condition the switches S_1 and S_2 are closed, and those appertaining to the 2 volt circuit are all open. The field is then reduced from its maximum to any chosen value, determined by the resistance R_1, by opening the switch S_3. Any reversed value of the field is obtained by operating the reversing switch, S_4, immediately thereafter. In general the operational procedure consists in first placing the specimen in the state of cyclic magnetization corresponding to maximum applied field, and then noting the change in thermal energy which accompanies a sudden decrease of the field to a preassigned value. Occasionally, however, it is desirable instead to observe the change in thermal energy which occurs when the field is increased from a preassigned to the maximum value, the specimen being in a cyclic state of magnetization as before.

The purpose of the two-volt circuit is to facilitate the elimination of eddy currents, and this is accomplished in the following manner:

Elimination of eddy currents

The inductance L (Fig. 3), effectively 0.4 henry, suffices to render negligible the heat associated with the eddy currents induced in the

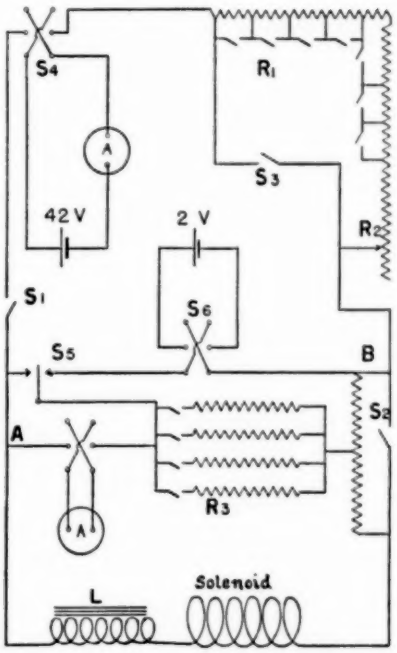

FIG. 3. Circuits for controlling the applied magnetic field intensity.

specimens of unannealed iron, nickel and steel, when these are investigated in the manner described in the preceding paragraph. This is not true of the annealed specimens for two reasons: First, the magnetization curves are steeper, so that dB/dt is larger for a given dH/dt; second, the coercive force is very much smaller, so that the resistance of the 42-volt circuit is large over the steep part of the magnetization curve, and hence the time constant of the circuit is small and dH/dt correspondingly large. The introduction of the 2-volt circuit permits the traversal of the steep part of the magnetization curve of an annealed specimen by the manipulation of a circuit of low resistance, and so, even in such cases, renders negligible the heat contributed by eddy currents. The operational procedure is as follows:

The switch S_2 is opened and the resistance R_2 is adjusted so that the potential difference between the points A and B is equal to that of the two volt storage battery. The switches S_5 and S_6 are closed and S_1 opened. The magnetizing field is then varied in steps by the addition or removal of the resistances R_3.

The investigation at high fields is carried out in the manner previously described.

Calibration

The thermocouple-galvanometer system is calibrated in terms of energy by sending a measured electric current through the specimen for a measured time interval. The resistance of the specimen is measured with a potentiometer and the joule heat calculated accordingly. An exhaustive investigation showed that the calibration is independent of the rate of production of heat in the specimen over the ranges of times and currents employed. Varying amounts of heat up to 20,000 ergs per cm^3 were developed in the specimen in time intervals ranging from 0.067 sec. to 1.23 sec. without detectable variation of the calibration. These experiments were performed with the aid of a commutator mounted on the film-drum shaft of an oscillograph, and gear driven by a synchronous motor. The calibrating current flowed through the oscillograph, and time intervals were measured on the oscillogram.

Experiment showed the energy calibration to be independent of the state of macroscopic magnetization of the specimen, which is to be expected.

A conclusive over-all check on both the magnetic and thermal measurements follows from a comparison of the observed thermal energy change for a complete half-cycle of magnetization with that obtained by graphical integration of the area under the magnetization curve. The thermal energy per half-cycle, calorimetrically measured, should equal exactly one-half the area of the hysteresis loop of the specimen in question. The agreement obtained in the present experiments is shown in Table I, and is seen to be well within the combined precision of the magnetic and thermal measurements.

Therefore, in reducing the data which follow, the small discrepancies were disregarded, and the observed calibration of the thermocouple-galvanometer system was altered in such manner that the hysteresis heat per half-cycle observed calorimetrically would conform exactly with that observed magnetically. In other words, the calibration constant (ergs per cm^3 per cm deflection) of the thermocouple-galvanometer system which was used in reducing the data which follow was obtained from the deflection corresponding to a half-cycle of magnetization together with the observed area of the hysteresis loop of the specimen.

TABLE I. *Hysteresis energy per half-cycle, in ergs per cm^3, as calculated from the thermal and magnetic measurements.*

SPECIMEN	THERMAL DATA	MAGNETIC DATA
Annealed iron	3430	3282
Unannealed iron	18800	18728
Annealed nickel	900	700
Unannealed nickel	21800	21940
Carbon steel	34300	35170

RESULTS

The specimen materials upon which observations are here reported are cold drawn and annealed Armco iron; cold drawn nickel containing the following percentages of impurity: Cu, 0.07; Fe, 0.18; Mn, 0.044; Si, 0.21; C, 0.065;[5] the same nickel annealed; and unannealed carbon steel drill rod containing 1.08 percent carbon.[6] The iron was annealed at 930°C for two hours in an atmosphere of hydrogen, and cooled to room temperature at the rate of about 130° per hour. The nickel was annealed at 1100°C for two hours in an atmosphere of hydrogen and cooled to room temperature at about the same rate.

The magneto-caloric behavior of these materials is shown by the curves labeled T in Fig. 4. The ordinate of a point on one of these curves indicates the change in thermal energy per cm^3 which occurs when the magnetization is altered from the maximum value to the value given by the abscissa of the point. The ordinates of the curves labeled M indicate values of the integral (2), taken between the maximum value of J and those indicated by the corresponding abscissae, and so evaluate the change in internal energy of the medium during the process.

Data which represent the curves of Fig. 4 are given in Table II. In addition this table contains the data which relate J and H for the various materials.

A striking difference is at once evident between the behavior of unannealed iron and nickel. In the case of iron the demagnetization process is accompanied by a decrease in thermal energy far less in amount than the external work

[5] This analysis, together with the specimen material itself, was supplied especially for this research by the International Nickel Company.

[6] This is the material experimented upon by Ellwood, Phys. Rev. **36**, 1066 (1930).

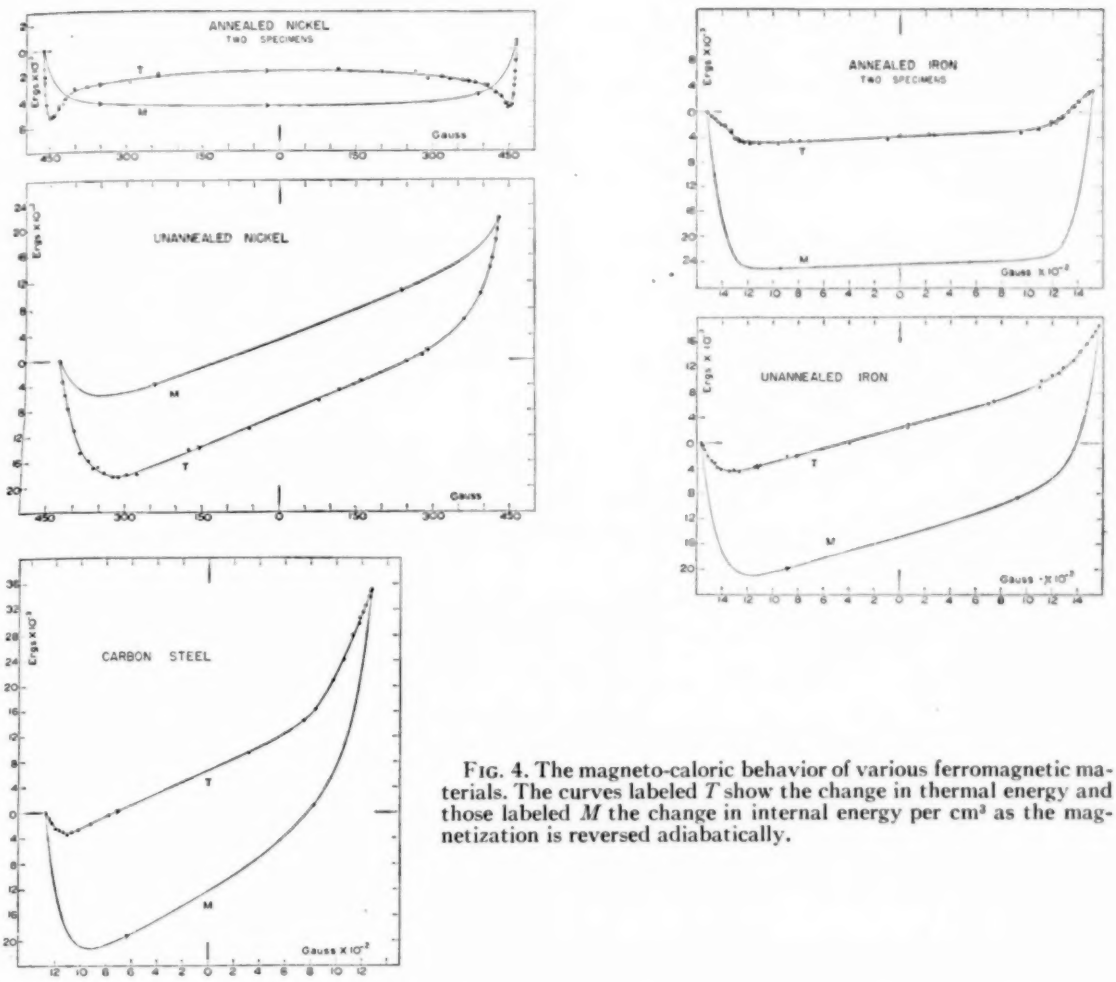

FIG. 4. The magneto-caloric behavior of various ferromagnetic materials. The curves labeled T show the change in thermal energy and those labeled M the change in internal energy per cm³ as the magnetization is reversed adiabatically.

done by the material, and hence involves a *decrease* in internal energy of other than thermal character. In unannealed nickel, on the other hand, the demagnetization process is accompanied by a decrease in thermal energy far in excess of the external work done by the material, and so involves an *increase* in internal energy of another sort. Annealed nickel behaves like unannealed nickel in the region of high magnetization, where the demagnetization process proceeds by continuous rotation of the domain magnetizations, and like iron in the region of low magnetization, where the demagnetization process proceeds by discontinuous reorientation of the domain magnetizations. The writers are, at present, unable to offer any explanation of these phenomena. Further experiments are in progress in this laboratory which, it is hoped, will contribute to their elucidation.

COMPARISON WITH PREVIOUS WORK

The evolution of the comparatively large hysteresis heat in various high coercivity steels has been traced calorimetrically by Adelsberger[7] and Honda, Okubo, and Hirone.[8] The experimental methods employed by these observers were not sufficiently sensitive to permit a study of the phenomenon in magnetically soft materials.

Ellwood,[6] who worked in this laboratory, attempted a detailed examination of 1.08 percent carbon steel. His specimen consisted of 104 rods 1 mm in diameter which, alternately with 104 similar copper rods, were mounted in a Bakelite and brass frame so as to form seven concentric

[7] Adelsberger, Ann. d. Physik **83**, 184 (1927). This work has been discussed theoretically by Gans, Schriften d. Königsb. Gel. Ges. Naturw. Kl. **8**, 31 (1931), and Magnetismus, Leipzig, 1933.

[8] Honda, Okubo and Hirone, Tohoku Univ. Sc. Rep. **18**, 409 (1929).

TABLE II. *The magneto-caloric effect in various ferromagnetic substances. J = intensity of magnetization in gauss; H = magnetic field intensity in oersteds; M = change in internal energy of specimen in ergs/cm³, calculated with integral 2; T = observed change in thermal energy in ergs/cm³.*

J	H	M	T
	(a) Annealed Nickel		
−465	−210	0	0
−461	−156	−700	−3415
−450	−89	−1950	−5120
−425	−31	−3300	−3800
−395	−10.3	−3900	−3000
−325	−2.5	−4200	−2500
−275	−0.50	−4300	−2250
−239	0	−4320	−2000
0	.35	−4300	−1620
155	.75	−4200	−1700
250	1.7	−4100	−1900
300	3.3	−4000	−2050
355	7.0	−3750	−2350
400	14.7	−3300	−2700
435	48	−2250	−3583
450	89	−1200	−4270
461	156	0	−2735
463	190	350	−854
465	210	700	700
	(b) Unannealed Nickel		
−430	−201	0	0
−425	−167	−1000	−3200
−410	−115	−3000	−8800
−390	−65	−4600	−13400
−350	−6.3	−5600	−17600
−315	14	−5400	−18400
−300	20.7	−5100	−18200
−280	25.0	−4800	−17800
−245	27.5	−3900	−16600
−200	28.3	−2600	−15200
−100	29.2	300	−11900
0	30.0	3200	−8600
120	31.0	7000	−4600
220	32.7	10000	−1300
275	35	11900	800
310	38	13200	2600
355	46	15000	5800
395	79	17600	10400
410	114	19000	13600
430	201	21940	21900
	(c) Annealed Armco		
−1518	−210	0	0
−1485	−171	−6800	−700
−1400	−93	−17400	−2100
−1300	−33	−23300	−4150
−1200	−5.3	−24900	−4900
−1150	−2.0	−25000	−4800
−1080	−0.75	−25000	−4800
−800	0	−25000	−4700
−600	.25	−24800	−4600
−300	.50	−24600	−4200
0	.75	−24500	−4000
450	1.25	−24200	−3400
830	1.75	−23900	−3100
1000	2.5	−23700	−2900
1096	4.0	−23400	−2600
1150	6.0	−23200	−2200
1200	10.3	−22800	−1800
1300	38	−20600	−400
1380	83	−16000	1000
1460	150	−7000	2500
1500	190	−400	3000
1518	210	3282	3282
	(d) Unannealed Armco		
−1564	−201	0	0
−1520	−140	−7600	−1800
−1460	−80	−13600	−3400
−1380	−36	−18000	−4400
−1300	−15.8	−20000	−4500
−1200	−3.5	−20900	−4200
−1100	2.0	−20900	−3600
−1000	3.9	−20500	−3100
−900	4.7	−20000	−2600
−500	5.4	−17600	−400
0	6.0	−14800	2400
655	7.5	−10800	6000
900	8.8	−8900	7600
1050	10.5	−7600	9000
1150	14.5	−6400	9900
1245	21	−5000	11100
1310	30	−3400	12200
1400	57	200	14000
1500	121	8200	16600
1564	201	18780	18780
	(e) 1.08% Carbon Steel		
−1278	−202	0	0
−1200	−112	−11848	−2400
−1150	−69	−16044	−3000
−1100	−41	−18706	−3200
−1000	−10	−21000	−2700
−900	1.5	−21300	−1600
−800	6.4	−20797	−700
−650	9.0	−19400	700
−300	11	−15800	3900
0	12	−12270	6600
300	14	−8400	9400
600	19	−3700	12600
800	27	571	15500
900	35	3350	18200
1000	43	7170	22000
1100	73	13026	26000
1200	129	22700	31000
1278	202	35176	35176

cylinders. The lengths of the several cylinders were so adjusted that the envelope of the array was an ellipsoid of revolution. 104 thermocouples connected in series were constructed by joining adjacent rods alternately with short lengths of fine copper and constantan ribbon. The rods were affixed in the frame with wax in order to prevent breakage of the thermocouples, and this circumstance completely vitiated Ellwood's results. The array was constructed at room temperature and experimented upon at a temperature somewhat higher, so that, in consequence of the differential thermal expansion of the specimen rods and frame, all the observations were made with the specimen material under stress. Accordingly the data give a better indication of the magnetostrictive behavior of the material than of its magneto-caloric behavior.[9] The specimen of carbon steel used in the present research was removed from Ellwood's assembly.

Agnes Townsend[4] has published a detailed description of the magneto-caloric effect at low fields in 1 mm rods of cold drawn nickel, and her data are in complete accord with those given in Table II above. It should be noted, however, that in the case of *annealed* materials the constraint imposed on the specimen by Dr. Townsend's method for attaching the thermocouples is sufficient completely to mask the true magneto-caloric behavior of the material. It is for this reason that the specimen mounting herein described was devised.

By far the most extensive research in this field is due to Okamura,[10] who worked with iron, nickel, cobalt, various carbon steels, piano wire, K.S. magnet steel, and iron-nickel alloy. Unfortunate flaws in his experimental method, however, prevent any quantitative comparison of his with the present data. For example, in iron, nickel and 0.2 percent carbon steel Okamura found no agreement whatever between the values of the hysteresis loss per half cycle as calculated from his magnetic and calorimetric measurements. Qualitatively, however, Okamura's results are similar to those given here except in the case of annealed iron, for which he found an initial heating on demagnetization instead of the cooling here reported.

In conclusion the authors desire to acknowledge with thanks the assistance of Dr. Agnes Townsend and Mr. R. J. Walsh during the early stages of the work, and of Dr. H. J. Glaubitz, who aided in the preparation of the data for publication.

[9] The senior author of the present paper was responsible for the failure to detect this error at the time the work was done. The same fault appears in some early work on nickel of Agnes Townsend (Phys. Rev. **40**, 120 (1932)). Credit is due Dr. Townsend not only for discovering the error, but for devising an experimental method which eliminates it.

[10] Okamura, The 363rd Report of the Research Institute for Iron, Steel, and Other Metals.

AUGUST 1, 1938 PHYSICAL REVIEW VOLUME 54

The Ultrasonic Radiation Field of a Quartz Disk Radiating into Liquid Media

FRANCIS E. FOX AND GEORGE D. ROCK
Catholic University of America, Washington, D. C.

(Received May 25, 1938)

The radiation pressure of sound waves on a spherical obstacle is used to determine the distribution of intensity in the sound field of a quartz disk radiating into a liquid medium. The measured distribution of intensity along the axis normal to a crystal face is compared to that to be expected from a plane piston radiating into a semi-infinite medium, and the agreement shows that the theoretical assumptions are fulfilled for the case used and that the "effective area" of the piston is essentially the actual area of the quartz disk.

INTRODUCTION

INVESTIGATIONS conducted with quartz oscillators, or quartz resonators vibrating in gaseous media, have shown that the vibration is very complicated. The face of an X cut resonator maintained at resonance for its fundamental longitudinal mode of vibration exhibits areas both of vigorous motion and comparative rest

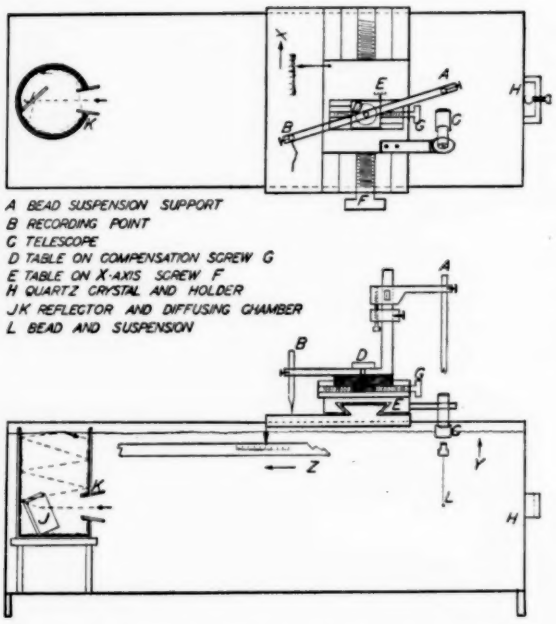
A BEAD SUSPENSION SUPPORT
B RECORDING POINT
C TELESCOPE
D TABLE ON COMPENSATION SCREW G
E TABLE ON X-AXIS SCREW F
H QUARTZ CRYSTAL AND HOLDER
J K REFLECTOR AND DIFFUSING CHAMBER
L BEAD AND SUSPENSION

FIG. 1. Top and side view of tank and carriage.

when examined for nodes either by optical methods or by dusting with lycopodium powder. The extremely small damping in such resonators is responsible for their enormously high resonance amplitudes compared to the static piezoelectric change of dimensions with the driving voltages and makes the amplitude at resonance very sensitive to extremely small variations in the static dimensions of the resonator. At frequencies in the range of several megacycles a variation of thickness of less than a wave-length of visible light is enough to destroy resonance conditions for different parts of the crystal and in these parts the amplitudes fall to a small fraction of the values they would have at resonance. The driving voltage selects those sections of the crystal having dimensions corresponding to resonance and builds up the resonance amplitude, while those portions of the crystal for which the true resonance frequency would be even slightly different from the driving frequency remain comparatively at rest, having little more than the amplitude corresponding to the static deformation to be expected from the driving voltage. If the damping is larger, or if the frequency of the driving voltage does not correspond to exact resonance for any portion of the crystal, the amplitude for slightly different dimensions, although very small compared to resonance amplitudes when vibrating in gases, might be much more uniform. In liquid interferometry the sound source is usually a quartz resonator with at least one side exposed to the liquid, so that the damping of the crystal is much larger than would be the case in air, the resonance amplitudes are correspondingly reduced, and it is possible that the vibration of the resonator is more uniform so that with a sound source radiating into liquid media the assumption of a "piston-like" motion of the source is justified.

METHOD OF INVESTIGATION

It was decided to investigate the distribution of intensity in an acoustic radiation field of such a source in order to see how well this assumption is fulfilled. The sound detector chosen utilizes the acoustic radiation pressure on a small sphere placed in the sound beam. Preliminary work had shown that with a horizontal sound beam of the intensity available, a small sphere suspended on an extremely fine quartz fiber 10–12 cm long could be deflected several centimeters from its rest position by the radiation pressure. While the driving frequency and power input to a quartz crystal radiating into a large trough was maintained constant the intensity distribution was measured by the deflection of the pendulum in various portions of the ultrasonic beam.

APPARATUS

The crystal was a circular X cut quartz disk of 1 cm radius mounted at a nodal plane for its fundamental resonance frequency, which is approximately 2.67 megacycles. The driving voltage was supplied by a transfer tuned LC circuit from a crystal-controlled oscillator at 2.49 megacycles. The current in the lead to the quartz was maintained constant throughout all readings. The

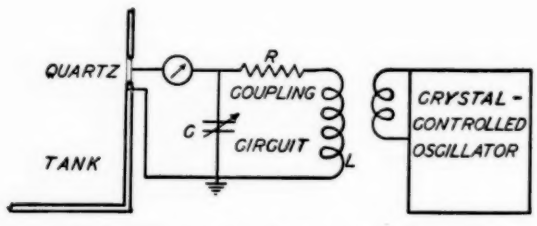

FIG. 2. Arrangement of associated apparatus.

apparatus is shown in Figs. 1 and 2. The sound source was set in the center of one end of a trough $3\times1\times1$ feet with polished plate glass sides and bottom and hard rubber ends. A small lead sphere was attached to the support (A) by means of a fine quartz suspension. The support was an arm of a large vernier caliper with micrometer adjustment, so that the sphere could be raised or lowered in the sound beam (Y direction). To the lower end of the vernier caliper a recording stylus or pencil was attached, and the whole mounted on a table (D) which can be moved by a micrometer screw along the length of the trough (Z direction) to compensate for an observed deflection of the pendulum from the vertical. The micrometer screw was itself on a movable table (E) having another micrometer screw for motion across the trough (X direction) set in a large carriage which could be moved along the length of the trough (Z direction). The center of the coordinate system is taken as the center of the crystal face exposed to the liquid. In making the measurements the carriage was moved to the desired value of Z, the bead adjusted to the desired Y, and then the screw drive used to move the sphere from one side of the trough to the other along the X direction. As the pendulum is deflected, the bead is brought back to its original Z position by the compensating micrometer screw. To keep Z constant and compensate for the deflections that occur the image of the bead is focused on the cross hairs of a telescope mounted on table E so that as the deflections occur and the bead image is displaced it can be restored to its original position by means of the compensating screw. The recorder then traces a curve of X *versus* the "compensating distance" for constant values of Y and Z. The "compensation distance" of course is the deflection of the bead at the point XYZ in question.

Several difficulties arose in insuring the return of the bead to its original Z distance as the (XD) plot was traced. These were caused principally by the bead's moving out of focus if viewed from a stationary telescope pointing along the X axis, while if the telescope were mounted on the table E which moved in the X direction the bead had to be focused through a water-air boundary and due to slight waves on the water surface the image continually flickered. The difficulty was finally overcome by placing a waterproof tube on the telescope with a plane glass window cemented on the end underneath the water level. Surface waves were then no disturbing factor and as the telescope accompanied the bead in the X direction the latter remained constantly in sharp focus at the cross hairs except for the deflection. Another difficulty was that of keeping the bead from being deflected in the X direction when intensity variations were rapid in that direction. The suspension was finally made bifilar, and spread to a separation of about 4 or 5 cm at the top. In the measurements given here the sphere was made of lead to cut down the large deflections obtained with lighter materials and to render unnecessary any compensation for the lift of the bead with deflections. The error in the Y position due to a small deflection D of a pendulum L cm long is $\Delta Y \sim D^2/L$. This error for the suspension used is less than 0.2 mm for the greatest deflection measured. The use of the heavy lead sphere also obviates the effects of the motion of the water. This was evident from the observations of the bead immediately after turning off the sound beam, since the deflection fell quickly to zero even though it was possible to detect by other means (e.g., the motion of small particles suspended in the water) a flow in the liquid in the direction of the sound beam. By using a very light bead the deflection due to this flow could be detected, and persevered for some seconds after the extinction of the sound beam. A further check was the insertion of a very thin collodion film (not thicker than several wavelengths of visible light) in front of the sphere. This prevented the water flow past the bead but allowed the radiation to pass. During the measurements frequent checks were made by obtaining traces for the same YZ values over a period of a month. In all cases these traces were coincident within the accuracy of the measurements. The traces taken in moving across the trough were retraced by the reverse motion.

In the early measurements instability of the bead at some maximum deflection points indicated the presence of standing wave systems in the trough, and attempts to line the trough with absorbing materials were not successful. When materials such as spongy rubber pads were first

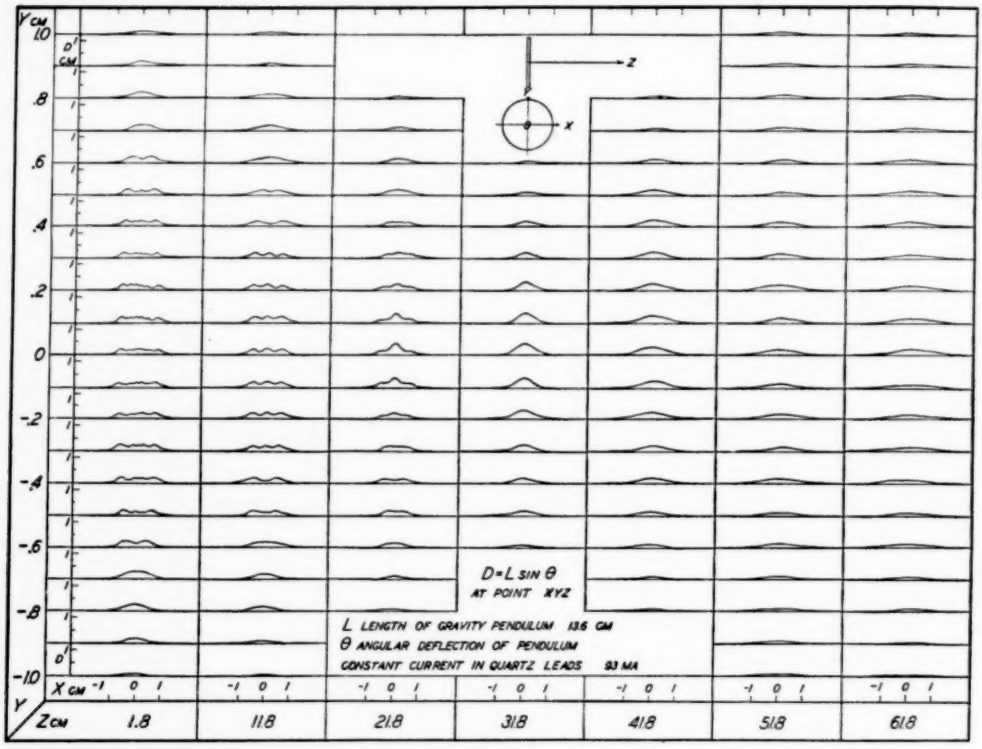

FIG. 3. Deflection along the X axis at constant values of Z and Y. Length of suspension 13.6 cm; mass of lead sphere 0.025 g; radius of sphere 0.081 cm; current in leads to quartz resonator 93 milliamperes.

used, the standing wave systems disappeared; but as the materials became wetted the absorption or diffuse scattering was almost negligible, transmission occurring through water soaked in the rubber almost as well as if the rubber were absent. A "diffuse scattering" and "absorbing" body was then constructed by analogy to the "black-body absorber" used in optics. The beam of sound was transmitted into a large cylinder 20 cm long and 15 cm diameter, through a slightly funnel-shaped opening in the side 6.5 cm wide; the sound beam was at most 4 cm wide at the far end of the trough. Inside was an oblique reflector which directed the reflected waves sideways and upwards so that they strike the container walls at a small angle and make many reflections on a single trip around the container, and because of their upward deflection continue to travel in a helical path to the top of the container where they are reflected downward again. The inside walls of the container were made to assist diffuse reflection, by coating them with a coarse gravel of irregular shape larger than the wave-length of the radiation in the medium, so that the energy entering the container as coherent sound radiation is almost completely diffused and to some extent absorbed in the container. In fact after the sound had been streaming into the container for some time a slight flow of the water around the inside walls could easily be seen—the flow proceeding in the direction of the sound waves. Even with this device the standing wave system did not entirely disappear, but could be detected probably because the first reflector still transmitted a fair portion of the radiation which passed on to the walls and was reflected directly back to form a fairly easily detected standing wave system. Finally the container was made double-walled with an air space completely surrounding the inside cylinder and the reflector made of a prism of brass filled with air to decrease the direct transmission, since the over-all coefficient of transmission at an air-water boundary is several orders smaller than that at a metal-water boundary. In this form the device eliminated

any regular standing wave system that could be detected by either mechanical or optical means and the stability of the bead was all that could be desired.

Measurements

In Fig. 3 traces are given for the values of Z and Y indicated. These give for a fixed distance the X *versus* D trace of the intensity distribution for values of Y one mm apart, and afford for each Z distance chosen a picture of fairly symmetrical distribution of intensity in the XY plane. The regular development of the traces taken at $Y=0$ for increasing values of Z is more strikingly shown in Fig. 4 where the traces for $Y=0$ (i.e., along the horizontal diameter of the crystal) were taken at intervals of 1 cm along the Z axis until at large value of Z the traces become very similar and larger intervals are used as indicated. In the region where the intensity was changing rapidly with Z, traces were made every half-cm, and although not included in the figures, measurements from these traces were used together with those in Fig. 5 to compare the experimental results with the theoretical intensity distribution along the Z axis.

Theoretical Distribution of Intensity Along the Z Axis

The exact expression for the distribution of intensity along the Z axis is easily obtained for a plane piston radiating into a semi-infinite medium. Crandall[1] gives the particle velocity potential along the Z axis of such a piston with radius $R=m\lambda$, where m is some constant and λ is the wave-length of sound as

$$\varphi=-(\dot{\xi}_0/k)\{\sin[\omega t-k(Z^2+m^2\lambda^2)^{\frac{1}{2}}]-\sin(\omega t-kZ)\}. \quad (1)$$

Here the velocity at the piston face is $\dot{\xi}_0\cos\omega t$, and $k=2\pi/\lambda$ or ω/c where ω is 2π times the frequency, and c is the velocity of sound. One can then expand, as Crandall does, the radical for values of $Z>3R$ but since the exact expression is of interest this need not be done. The expression can be written:

$$\phi=(2\dot{\xi}_0/k)\{\sin\tfrac{1}{2}k[(Z^2+R^2)^{\frac{1}{2}}-Z]\times\cos\tfrac{1}{2}[2\omega t-k(Z^2+R^2)^{\frac{1}{2}}-kZ]\}, \quad (2)$$

which yields for the maximum pressure

$$p_{\max}=\rho\dot{\phi}_{\max}=2\rho c\dot{\xi}_0\sin\pi[(Z^2+R^2)^{\frac{1}{2}}-Z]/\lambda \quad (3)$$

and for the intensity

$$I=p^2_{\max}/2\rho c=2\rho c\dot{\xi}_0^2\sin^2\pi[(Z^2+R^2)^{\frac{1}{2}}-Z]/\lambda. \quad (4)$$

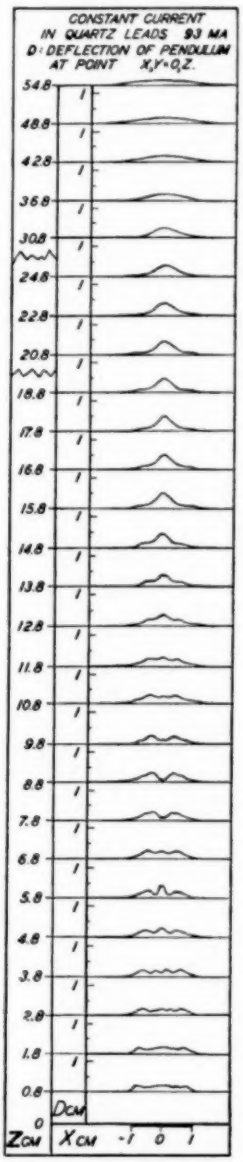

FIG. 4. Deflection along X axis for $Y=0$ and Z as indicated. The scale factor is changed at $Z=20$ and 25 cm to show the traces at large values of Z.

[1] Crandall, *Theory of Vibrating Systems and Sound* (Van Nostrand, 1926) p. 134. See also A. H. Davis, *Modern Acoustics* (Macmillan, N. Y., 1934) p. 61.

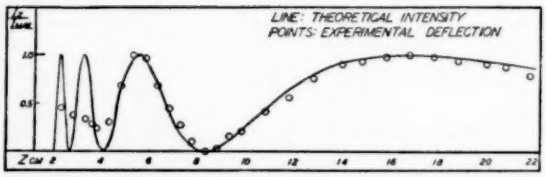

FIG. 5. Distribution of intensity along Z axis. The line is the theoretical distribution given by Eq (4) for $\lambda=0.06$ cm; $R=1.00$ cm; and $2\rho c\xi_0^2=1=$maximum deflection of pendulum. The circles are experimental values from the (XD) curves expressed as the ratio of the deflection at Z to the maximum deflection. The diameter of the circles represent the thickness of the line made by the recorder.

For $Z>3R$ this immediately becomes

$$I\sim 2\rho c\xi_0^2 \sin^2 \pi R^2/2\lambda Z$$

or

$$I\sim 2\rho c\xi_0^2 \sin^2 \pi m^2\lambda/2Z. \qquad (5)$$

The latter is the form given and discussed by Crandall. From (4) or (5) it is evident that for values of Z greater than $m^2\lambda$ the intensity falls continuously as Z approaches ∞. For values of Z less than $m^2\lambda$ the intensity according to (5) passes through successive maxima and minima for values of $m^2\lambda/Z=2, 3, 4\cdots$ the oscillation becoming more and more rapid as Z approaches 0. Although (5) would indicate an infinite number of maxima and minima and an indeterminate value at $Z=0$ it can be seen from (4) that the maxima and minima occur at those values of Z which make the expression $2[(Z^2+R^2)^{\frac{1}{2}}-Z]/\lambda$ equal to integers and that the intensity at $Z=0$ depends on the value of the constant R/λ. If we write $R/\lambda=(n+C)$ where n is an integer and $(n+C)=m$ as formerly defined it is evident that the intensity at $Z=0$ may have any value from zero to a maximum. It is zero for $C=0$ and a maximum for $C=\frac{1}{2}$, and has intermediate values for all other values of C. It is also evident from (4) that as Z varies from 0 to ∞ the angle takes values from $\pi R/\lambda$ to 0, or from $(n+C)\pi$ to 0, yielding n minima, excluding the one at $Z=\infty$, and either n or $n+1$ maxima depending on whether C is less than or greater than $\frac{1}{2}$.

Comparison of Experimental Data with Theory

On the traces made the last maximum occurred at 16.8 cm, the next nearest minimum at 8.3 cm, and the next nearest maximum at 5.3 cm. Although these are clearly defined the exact positions might have occurred within one of the half-cm intervals. By use of these values for Z as those making $m^2\lambda/Z$ equal successively to 1, 2, 3 in (5) the computed values of $R=m\lambda$ are 1.01, 1.00, and 0.98. The value of λ(0.06 cm) was computed from the known velocity of sound in water and the frequency used. The agreement of the computed values of R with the measured radius of one cm is as good as could be expected from the method of determining the Z values used.

We assumed the value of 1 cm for R and used the value of λ as before and plotted the theoretical intensity distribution for values of Z from 2 to 22 cm, the maximum fitted to the value of the maximum deflection. The observed deflections along the Z axis were then plotted as ratios of the deflections at the point Z to the maximum deflection, and are shown in Fig. 5.

The radius of the circles used in marking the experimental points represents the accuracy of the experimental measurements so that again the agreement for large values of Z is all that could be expected. The lack of agreement for small values of Z is probably due to the fact that when the bead is near the crystal there are standing wave systems set up between the bead and the crystal which cannot be neglected, since the bead is not small in comparison with the wavelength. The use of a very small bead, so as both to increase the "resolving power" of the measuring device and minimize the effect of these standing wave systems, would undoubtedly enable one to secure better agreement for smaller values of Z.

The authors wish to acknowledge their indebtedness to Dr. Herzfeld of Catholic University, and Dr. Hubbard of Johns Hopkins University for many suggestions and discussions.

LETTERS TO THE EDITOR

Prompt publication of brief reports of important discoveries in physics may be secured by addressing them to this department. Closing dates for this department are, for the first issue of the month, the eighteenth of the preceding month, for the second issue, the third of the month. Because of the late closing dates for the section no proof can be shown to authors. The Board of Editors does not hold itself responsible for the opinions expressed by the correspondents.

Communications should not in general exceed 600 words in length.

Cosmic-Ray Electron Showers in a Mine 100 Feet Below Sea Level*

The apparatus comprised essentially four trays of cosmic-ray counters, arranged parallel to one another, and separated by distances, so that the whole formed a kind of telescope.

The records were obtained upon moving photographic paper, in which, along the central axis, was recorded in the form of dark lines each "event" which we define as the simultaneous discharge of at least one counter in each of the four counter areas. Above and below the center portion was recorded, in the form of electroscope deflections, a quantity indicative of the number of individual rays passing through the upper and lower of the two central counter areas, and corresponding to an "event." Fig. 1 is a sample of the kind of record obtained; and in all about 300 feet of such records were obtained, covering cases (1), where there was no lead in the apparatus, and (2), where above each of the central trays a slab of lead 6 mm in thickness was inserted.

In the absence of the lead, it was found that, on the average, the number of showers of any size per single ray was practically the same in the mine as in the attic of our Swarthmore laboratory, where the apparatus was covered by thick slabs of marble, to duplicate the conditions in the roof of the mine.

Again in the absence of lead, it was found that, on the average, the total number of rays (as obtained from the showers) passing through the telescope system was 1.6 times the number of "events." It is of profound interest to determine, if possible, whether the extra rays are or are not electrons. In order to obtain information on this matter, we have made use of the experiments with lead. Let A be the upper piece of lead and B the lower. It was found that the ratio of the total number of shower rays emerging from B to the number emerging from A was

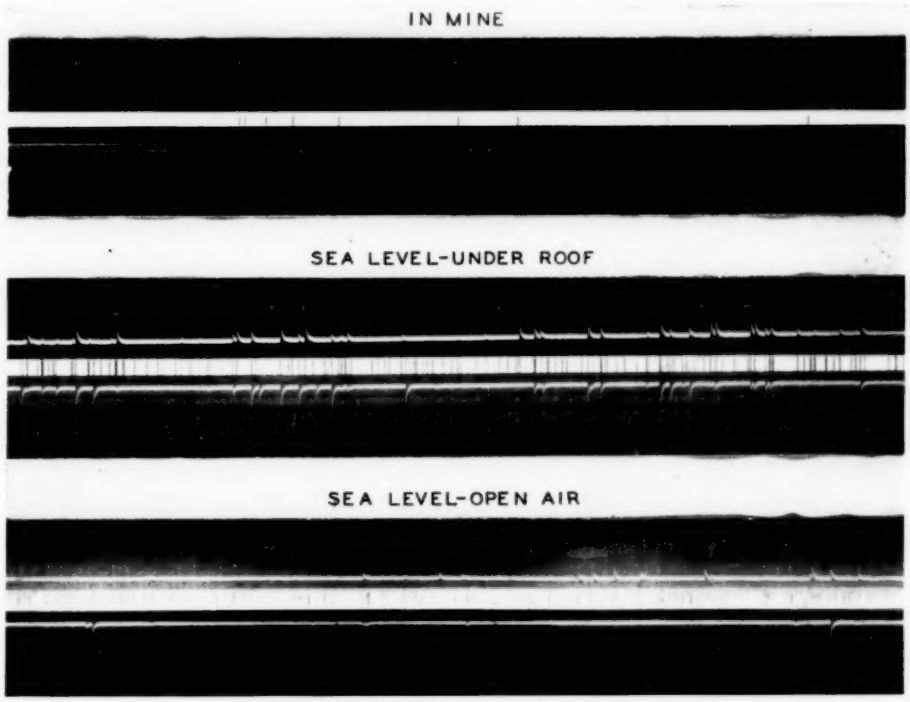

FIG. 1. The heights of peaks indicate numbers of rays. All of these photographs taken without lead in the apparatus.

1.3, where, by the number of shower rays in each case, we mean the number of rays in excess of the number of single rays which are always associated with any recorded "event."

We may now make the tentative hypothesis that the hard component rays do not produce showers appreciably in the lead, and ask what the average energy of a group of electrons would have to be in order that, through the processes of the quantum theory, they would result in the production of showers in the lead such as to give the ratio 1.3 cited above. The answer is 2×10^8 ev. We may then ask how many of such electrons would have to enter the piece of lead A per hour in order to produce, on emergence from that piece of lead, the number of shower rays found per hour. The answer is 7. This is approximately equal to 7.5, which represents the difference between the total number of rays recorded per hour *in the absence of the lead*, and the number of "events" recorded. Thus, there is harmony between the experiments and the assumption that each "event" is associated with one hard ray, which rays themselves produce negligible showers in the lead, but which are accompanied by elecrrons to the extent of 1.6 of their number and of energy 2×10^8 ev.

Although the experiments are consistent, to a first approximation, with neglect of direct shower production by the hard component rays in the lead, we must, nevertheless, assume that it is the showers produced by the hard component in the substance of the earth which, in actuality, represent the electrons found in the mine, since neither primary cosmical electrons of reasonable energy nor their progeny produced by multiplication could penetrate to the depths concerned. It is natural to regard the hard component shower phenomenon as one occurring at rare intervals, possibly with the ejection, on these occasions, of a few or even one particle with high energy. If this particle is an electron, or gives rise to electrons, these electrons, through the ordinary quantum theory processes, may be expected to constitute or to give rise to such shower producing electrons as were to be found in the mine.

The writers wish to express appreciation of the assistance afforded by a grant from the American Association for the Advancement of Science.

W. F. G. SWANN
W. E. RAMSEY

Bartol Research Foundation of the Franklin Institute,
Swarthmore, Pennsylvania,
July 5, 1938.

* The results herein given were presented at the meeting of the American Philosophical Society held in Philadelphia on November 26, 1937.

Production of Highly Vibrating Molecules

On several occasions during the past few years I have called attention to the presence in the spectrum of the auroral afterglow of first-positive bands of nitrogen which originate on very high vibrational levels. Attempts to obtain good photographs of this phenomenon have not been very successful, because of the relative insensitivity of photographic plates in the green. Recently, however, we have been studying a new high pressure afterglow and in its spectrum not only are these bands more intense than in any of the previously observed glows, but their lifetime in the afterglow is much longer. To show the remarkable enhancement of the bands which originate on levels with $v^1=16$ to 21, two spectra are presented (Fig. 1). On each of these spectra the letters l and h mark the bands which originate on low and high levels, respectively. The enhancement of the bands marked h is easily seen. The strip "a" represents the afterglow producing discharge and the strip "b" an ordinary discharge which is not followed by an afterglow. In fact the enchancement of the green sequence is one of the marked characteristics of a discharge which is followed by an auroral or a night sky afterglow. Visual observation of the afterglow shows these bands with about the same relative intensity as that observed in the discharge. This is the reason for reproducing the discharge rather than the afterglow spectrum here.

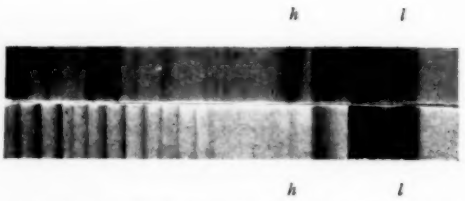

FIG. 1. a, Spectrum of discharge which produces afterglow. b, Spectrum of ordinary discharge.

The afterglow is a marked green in color in contrast to the yellow of the Lewis-Rayleigh glow. When the afterglow is observed at night with well rested eyes, it not only appears to last longer than during the day, but it appears much bluer. Those who have observed this afterglow at night and at the same time looked at a Lewis-Rayleigh glow are definitely impressed by the remarkable difference between the two. The nitrogen is produced by heating $NaNO_2$ in a sealed off evacuated tube; the resulting mixture of nitrogen and oxygen is purified by repeated flashing of the tube. The afterglow is observed only in the wide portion of the tube in which the current density is lowest. The glow is completely missing from the narrow high current density portion of the tube.

This conclusive proof of the enhancement of high vibrations in a nitrogen afterglow, the spectrum of which is a faithful reproduction of the night sky spectrum, should be of considerable interest to students of upper atmosphere phenomena since there are radiations in the light of the night sky which probably correspond to those enhanced first-positive bands. Detailed study of both the night sky and this new afterglow spectrum should clear up this problem.

J. KAPLAN

University of California,
Los Angeles, California,
July 1, 1938.

The Beta-Rays from Radium E

Jauncey[1] has described experiments which suggest that radium E may emit heavy electrons. We have repeated his experiment and obtained similar results and have also tried the experiment with screens between the plates designed to eliminate electrons scattered from the plates which A. H. Compton[2] has suggested may explain Jauncey's results. The screens appeared to stop the line observed by Jauncey so confirming Compton's suggestion.

Our apparatus is similar to that of Jauncey, with the plates 6 cm long and separated by 1.0 mm, and with 5.1 cm between the ends of the condenser plates and the photographic plate. The source was Ra E deposited on a small nickel wire from a solution containing Ra D and its products.

The calculated positions of the lines are shown below the plates.

Plate 1, Fig. 1, shows the line supposedly due to heavy electrons. As well as can be determined the deflection is about 1 mm more than predicted from the theory.

We next, at the suggestion of Dr. H. A. Wilson, placed thin strips of ebonite between the condenser plates as shown in cross section in Fig. 2.

Plates 2, 3, and 4 were obtained with the modified apparatus.

Plate 2 shows by the width of the alpha-particle line that the strips have effectively reduced the width between the condenser plates, and also shows that many ordinary electrons are being recorded with an $H\rho$ of approximately 1750, which is near the maximum of intensity according to O'Conor's table.[3]

We next tried twice to record heavy electrons whose momentum was that of the maximum on the distribution curve, but both times were unsuccessful. The calculated deflection was about 1 cm. The heavy line was eliminated (or at least its intensity was decreased many fold). Plate 3 is one of these attempts. (This plate was also examined with a microphotometer which easily recorded the scratches on the film, but which failed to show any definite indication of the expected line.)

FIG. 2. *A*, Slit between ebonite strips 0.035 cm wide. *B*, Slit between ebonite strip and brass plate 0.065 cm wide. *C*, Ra E source.

Plate 4 shows an attempt to record both the ordinary and the heavy electrons. The fields were selected so that nearly equal numbers of the two should have been present, but there is no indication of a heavy line although the ordinary line is present (but weak).

The apparatus is shown to be recording electrons with $H\rho$ of 1750, but never, after the strips were introduced, were we able to record heavy electrons with this (or any other) value of $H\rho$. The conclusion is that the heavy line is really due to scattering from the condenser plates, and that the strips eliminated this.

We are grateful to Dr. H. A. Wilson, who suggested the experiment, and who directed the work. We wish also to thank Dr. T. W. Bonner for the loan of the Ra D solution.

B. T. WRIGHT
A. W. MCREYNOLDS

The Rice Institute,
Houston, Texas,
June 5, 1938.

[1] G. E. M. Jauncey, Phys. Rev. **53**, 197 (1938).
[2] A. H. Compton, Phys. Rev. **53**, 431 (1938).
[3] John S. O'Conor, Phys. Rev. **52**, 303 (1937).

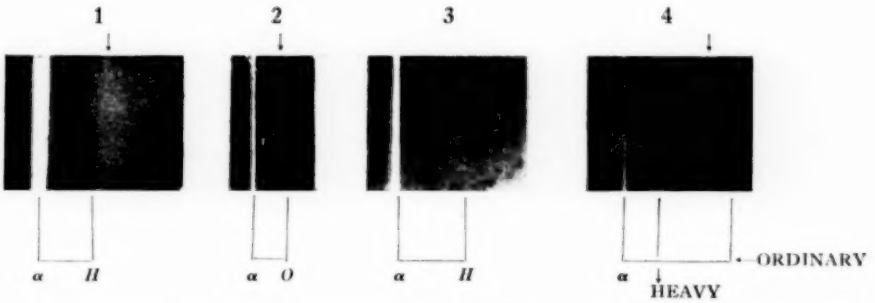

FIG. 1. Photographs taken with β-ray spectrograph. Plate 1 was taken without the ebonite strips. Plates 2, 3, and 4 were taken with these strips introduced. The following table gives the essential data for each plate. Subscripts o and h refer to ordinary and heavy electrons, respectively. s is the calculated displacement from the α-particle line.

Plate	X v/cm	H gauss	β	p	$(H\rho)_o$	$(H\rho)_h$	ρ_o cm	ρ_h cm	s_o cm	s_h cm
1	13700	115	0.40	2.80	730	2050	6.36	17.8	2.5	0.7
2	15000	70	0.71	2.14	1730	3700	24.8	53	0.5	0.2
3	12500	122	0.34	2.90	615	1780	5.1	14.6	5.1	0.9
4	15000	98	0.51	2.63	1000	2630	10.2	26.8	1.4	0.5

The β-Rays of Actinium B and Actinium C'' Partial Spectra

An absorption method has been applied to the β-rays of Ac B and Ac C'' to determine their end points with increased precision. The range of the β-rays of Ac C'' (Ac(B+C)) is 0.68 g/cm² aluminum and the end point 1.47 Mev. This was determined by comparison with Ra E and UX_2, whose end points are known from work with the magnetic spectrometer.[1] It is believed that this method of finding ranges avoids errors due to unequal straggling and unequal γ-ray backgrounds for different radioactive bodies.

Growth curves were followed by the β-activity of the active deposit obtained by exposing aluminum foils to air containing actinon for a few minutes. Care was taken to remove old active deposit from the air by plugs of cotton wool. The β-activity was measured through aluminum up to 0.32 g/cm². From the initial portions of the growth curves for various absorbers the absorption curve for the β-rays of Ac B was obtained. By comparison with the curves for Ra E and Ac C'' the range of the β-rays of Ac B is about 0.64 g/cm² and the end point 1.40 Mev. This confirms Lecoin's result,[2] obtained with a cloud chamber, that the main portion of the Ac B spectrum is much more penetrating than has been believed for 28 years.

Lecoin's observations[2] and previous work by the writer[3] agree in showing that a soft component of small intensity is also present in the spectrum of Ac B. By these two different methods a minimum in the distribution curve is found to occur at about 300,000 electron volts. (The present work suggests that this value may have to be increased to 400,000 electron volts.) The intensity of the low energy peak is at least 1 in 10 for the main spectrum. While it occurs in the region of a number of secondary β-ray lines Li[4] has found only 3.3 secondaries per 100 disintegrations. The writer believes that the primary β-ray spectrum of Ac B is complex and consists of two main components. On account of overlapping the end point of the soft component must be greater than the minimum of 300,000 electron volts in the combined distribution curve, and 500,000 electron volts may be taken as an estimate. Further, on account of overlapping the ratio of the intensities of the soft to hard components must be increased from 1 : 10 given above to 1 : 7, and it may be as high as 1 : 5. Both the energies and intensities are in fair agreement with Ellis and Mott's hypotheses[5] and Li's work[4] on the γ-ray intensities.

The Ac B nucleus may transform into Ac C in the ground state in two ways. (1) By the less frequent way, a β-particle of 0.5 Mev energy is emitted, and the resulting excited nucleus of Ac C falls to the ground state with the emission of one γ-ray of 0.829 or two γ-rays of 0.404+0.425 Mev energy. (2) By the more frequent way, a β-particle of 1.40 Mev energy is emitted.

From the β-intensities given above the excitation probability of the uppermost level of the C nucleus is at least 0.12 and may be as high as 0.17 Mev. In order to obtain a similar value from the γ-ray intensities it is necessary to assume that the γ-rays are electric quadripole instead of electric dipole radiation. This assumption is supported by their very small ionization relative to the primary β-ionization in the present work. The excitation probability of the uppermost level of the C nucleus for γ-rays is then found to be 0.197 from Li's results.

If the explanation presented here can be confirmed it provides a striking example in favor of the use of maximum energies instead of average energies. The average energy of a β-ray spectrum is here assumed to be one-quarter of the maximum energy. We have, when average energies are used, by one path 0.12+0.83=0.95 Mev and by the alternative path 0.35 Mev. The discrepancy is more striking than that in the well-known Th C branching, where the large α-ray energies mask the disagreement.

The difficulty of Ac B in the log-log plot of end points against transformation constants[6] is now partly removed. If one takes partial transformation constants he finds that the soft component falls on the curve for permitted transitions, and the hard component between the two curves, but probably it belongs to the permitted transitions.

The work summarized here will soon be published in full. The β-spectra are now being investigated by other methods.

B. W. SARGENT

Queen's University,
Kingston, Ontario, Canada,
July 15, 1938.

[1] A. G. Ward and J. A. Gray, Can. J. Research **15**, 42–44 (1937).
[2] M. Lecoin, Comptes rendus Acad. Sci. Paris **202**, 1057–59 (1936).
[3] B. W. Sargent, Proc. Camb. Phil. Soc. **25**, 514–521 (1929); **29**, 156–160 (1933).
[4] K. T. Li, Proc. Roy. Soc. **A158**, 571–580 (1937).
[5] C. D. Ellis and N. F. Mott, Proc. Roy. Soc. **A141**, 502–511 (1933).
[6] B. W. Sargent, Proc. Roy. Soc. **A139**, 659–673 (1933).

"Radio"

The word "radio" appeared in the title ("Radio Isotopes of Nickel") of a Letter to the Editor by J. J. Livingood and G. T. Seaborg on page 765 of the May first issue of the *Physical Review*. It is obviously intended as an abbreviation of the word "radioactive," since the complete form "radioactive isotope of nickel" appeared in the text of the letter.

A second case of the same sort and over the same signatures appears on page 847 of the May 15th issue. The title is "Long-Lived Radio Cobalt Isotopes" and the text contains the more conventional form "radio-cobalt." It may be noted that the hyphen has been dropped already from the analogous "radiolead."

The use of "radio" as a combining form is so well established that it is admitted by dictionary makers. As a separate word its utility lies in the abbreviation it affords for the extremely awkward terms: "radiotelegraphy and (or) radiotelephony." The use of the same word in a new sense seems unnecessarily confusing.

L. W. MCKEEHAN

Sloane Physics Laboratory,
Yale University,
New Haven, Connecticut,
July 5, 1938.

Fluctuations of Residual Ionization Current at Great Depths

Recently there appeared in the *Physical Review*[1] a paper by Volney C. Wilson on cosmic-ray intensities at great depths. Wilson has determined these intensities in a copper mine by means of a fourfold Geiger-Müller tube telescope, down to the depth equivalent to 1106.7 m of water. He has not found the very sharp decreases of intensity of cosmic rays at the depths of 250 m and 500 m water equivalent, which were found by Clay[2] and Corlin[3] with ionization chambers. To be sure, when determining the shower intensities by means of Geiger-Müller tube coincidences, Wilson has found slight decreases of intensity at the depths indicated by Clay and Corlin, but in view of possible statistical errors, he is not very positive as to these anomalies.

We believe we are able to indicate a possible explanation of the anomalies found by Clay and Corlin. We have measured residual currents in ionization chambers filled with argon or with air under pressures up to 34 atmospheres. These observations were made in a rocksalt mine (at Wapno, province Poznań, Poland), at a depth equivalent to 900 m of water; the salt was nearly free from potassium contaminations. We have found that the residual current at this depth shows very marked fluctuations, when measured during relatively short time intervals (not over 30 min.). The conditions of work in the mine were very favorable: very constant temperature, nearly total absence of moisture and very low intensity of local radiation (only 0.01 of that found usually in closed spaces at sea level); moreover, the local radiation was cut off by lead 10 cm thick.

At the depth of 406 m under the earth surface (equivalent to 900 m of water) the residual current in the ionization chamber filled with argon under pressure of 29 atmospheres amounted to 1/320 of the value observed at the earth surface. This corresponds to the lowest intensity found by Clay in the Gulf of Aden at a depth of 270 m of water.

S. Szczeniowski

Institute of Theoretical Physics of the Stefan Batory University, Wilno, Poland, (S. S.)

St. Ziemecki

Physical Laboratory of the Main School of Agriculture, Warsaw, Poland, (S. Z.)

July 5, 1938.

[1] V. C. Wilson, Phys. Rev. **53**, 337 (1938).
[2] J. Clay, Physica **1**, 373 (1934).
[3] A. Corlin, Nature **133**, 63 (1934).

The Physical State of Chromium Impurity in Corundum

It is well known that the intense red fluorescence shown by ruby when excited by blue light is due to the chromium impurity included in the crystalline ground material corundum Al_2O_3. The spectrum of the fluorescence light at low temperatures shows a sharp intense red doublet at λ6920 and 6934A. Previous observers have pointed out that this sharp doublet is due to the chromium ion Cr^{+++}, and arises as a result of the transitions ${}^2G_{7/2} \rightarrow {}^4F_{7/2}$ and ${}^2G_{9/2} \rightarrow {}^4F_{9/2}$. But the exact physical state of these fluorescent Cr^{+++} ions, in relation to their surrounding ground material is still a matter of doubt and uncertainty.

I came across an old and neglected observation of Mendenhall and Wood[1] which when interpreted throws some light on the question in a striking manner. They found that under the action of a magnetic field each line of the doublet is split up into four components. As the transitions concerned here are between states with $J = 7/2$ or $9/2$, the Zeeman pattern in usual circumstances would consist of 18 or 14 components. Actually it is observed that there are only four components for each line of the doublet.

This fact can be satisfactorily explained only on the assumption that the fluorescent ions of chromium actually replace the aluminum ions of the lattice of the crystalline ground material Al_2O_3 and that they are not scattered at random in the body of the corundum as stray impurity in the form of Cr_2O_3 having no definite relationship with the surrounding ions and atoms. For, the chromium ions considered here are paramagnetic and following Bose and Stoner we can suppose that the L moment of the ion is unable to respond to the external magnetic field as it tends to assume a definite orientation with respect to the neighboring ions and atoms. Only the spin moment is free to orientate and this alone will be quantized under the magnetic field. Thus the upper as well as the lower energy level which gives either line of the doublet will be split up into two sublevels, according as the spin is parallel or antiparallel to the direction of the magnetic field, H. The transitions from the two upper levels to the two lower ones will then give four Zeeman components, for each line of the doublet.

The components in the Zeeman pattern are sharp. All the fluorescent Cr^{+++} ions scattered in the ground material must, therefore, have their L moments orientated in a like manner with regard to the surrounding ions and atoms, so that they will all be in identical energy states. This equivalent inability of the L vectors in all the Cr^{+++} ions to respond to the magnetic field is possible if it is assumed that the Cr^{+++} ions replace the Al^{+++} ions of the ground material and are thus constituents of the regular crystal lattice.

The interval between the outermost two components of the Zeeman pattern can be calculated if the Landé factor g is taken to be 2, as only the spin is quantized.

$$\begin{aligned}\Delta\nu &= (\Delta m - \Delta m') \times g \times L \times H. \\ &= 4 \times 2 \times 4.674 \times 10^{-5} \times 22000. \\ &= 8.23 \text{ cm}^{-1}.\end{aligned}$$

The interval actually observed is about 10.4 cm^{-1}, i.e., of the same order of magnitude as the one calculated above.

A detailed account of this and other aspects of the question will appear elsewhere.[2]

B. V. Thosar

College of Science, Nagpur, India.

May 30, 1938.

[1] Mendenhall and Wood, Phil. Mag. **30**, 316 (1915).
[2] To be published in Phil. Mag.

The Nature of the Ionosphere Storm

Comprehensive observations of ionosphere storms over a period of nearly three years have resulted in the following tentative picture of an ionosphere storm. The ionosphere storm, like the magnetic storm, has two phases, a turbulent phase and a moderate phase.

The turbulent phase[1, 2] consists of a violent boiling or turbulence of the entire ionosphere in the auroral zone, and results in irregular motion of small clouds of ionization and a disintegration of the normal stratification of the ionosphere from the E layer on up. Whatever causes the storm has apparently plunged into the ionosphere at auroral zone latitudes, and literally torn it up. Preceding the turbulent phase, on several occasions when the auroral zone extended as far south as Washington, an increase in F layer ionization has been observed. This is consistent with the idea that the carrier of the energy of the ionosphere storm, when it first entered the high ionosphere, caused an increase in ionization. No consistent increase in F layer ionization has been observed to precede the less severe storms, when Washington was considerably south of the auroral zone.

The turbulent phase is followed by the moderate phase[1–4] of the ionosphere storm. This phase is characterized by an expansion and diffusion of the higher F region in latitudes fairly well removed from the auroral zone. The effect lasts much longer than the turbulent phase and is felt in latitudes which are nearer the equator in storms of great intensity. This phase is the one usually observed at Washington and has been found to lag behind the severe effects of the associated magnetic storm by several hours. During this phase the ionosphere gradually returns to normal conditions.

The experimental data suggest that the first phase of both the ionosphere storm and the associated magnetic storm occurs only in the auroral zone, and is a direct result of the turbulence of the ionosphere in this region. Whatever may be the current systems assigned to account for the magnetic effects of the first phase, they must have their origin in the turbulence of the auroral zone and perhaps in the consequent interference with the normal circulation of currents in this zone. For example, a turbulence in the E region or below might well decrease the electrical conductivity in this region of short free paths for the ions, and cause a resultant decrease in the westward daylight current in the auroral zone and the observed increase in H.

The phenomena observed during the second or moderate phase seem to indicate some kind of heating effect in the high ionosphere which spreads out from the auroral zone. During this phase the turbulence of the ionosphere in the auroral zone has ceased and the stratification has returned, although the ionosphere is still more diffused here than elsewhere. The expansion of the ionosphere in this phase may produce the resultant westward current necessary to account for the decreased value of H during the latter part of the associated magnetic storm.[5]

S. S. Kirby
N. Smith
T. R. Gilliland

National Bureau of Standards,
Washington D. C.
July 15, 1938.

[1] T. R. Gilliland, S. S. Kirby, N. Smith and S. E. Reymer, Proc. I. R. E. September, 1937, to date.
[2] S. S. Kirby, T. R. Gilliland, N. Smith and S. E. Reymer, Phys. Rev. **50**, 258 (1936).
[3] S. S. Kirby, T. R. Gilliland, E. B. Judson and N. Smith, Phys. Rev. **48**, 849 (1935).
[4] S. S. Kirby, N. Smith, T. R. Gilliland and S. E. Reymer, Phys. Rev. **51**, 993 (1937).
[5] E. O. Hulburt, Rev. Sci. Inst. **9**, 44 (1937).

Proceedings of the American Physical Society

Minutes of the San Diego Meeting, June 22–24, 1938

THE 221st regular meeting of the American Physical Society was held in San Diego, California, on June 22, 23, and 24, 1938. Except for the afternoon session of June 23, which occurred at the Scripps Institution of Oceanography at La Jolla, all sessions were held in quarters at Balboa Park.

The three morning sessions were devoted to the presentation of the 38 contributed papers abstracted below. Of these papers 5, 6, 16, 32, 34, and 35 were read by title.

The symposium of Wednesday afternoon, June 22, held jointly with the Astronomical Society of the Pacific, was concerned with Nuclear Transformations and their Astrophysical Significance. Speakers were:

W. A. Fowler, *California Institute of Technology*
J. R. Oppenheimer, *University of California and California Institute of Technology*
R. Minkowski, *Mt. Wilson Observatory.*

On Thursday afternoon, there was held at La Jolla a symposium on Physical Problems of the Ocean with the following speakers:

H. U. Sverdrup, *Scripps Institution*
F. P. Shepard, *University of Illinois*
Roger Revelle, *Scripps Institution*
W. E. Allen, *Scripps Institution*
G. F. McEwen, *Scripps Institution*
R. D. Gordon, *Scripps Institution*

Maximum attendance at each session was 60 ± 5 persons.

Paul Kirkpatrick
Local Secretary for the Pacific Coast

Abstracts of Contributed Papers

1. Collimated, Variable Energy Beam of Pure Thermal Neutrons. Luis W. Alvarez, *Radiation Laboratory, University of California.*—The cyclotron beam has been modulated at 120 cycles per second, giving almost square pulses of neutrons lasting about 0.004 second each. The sensitivity of a linear amplifier has been modulated at the same frequency, but with opposite phase, so that no fast neutrons are recorded. If a Li lined chamber is placed 8 meters from the source, thermal neutrons will just reach it in 0.004 sec., and therefore be registered. With Cd sheets on sides and back of the chamber, and Cd diaphragms in front, no neutrons but thermal ones directly from the source can be counted, giving a collimated beam. (No other neutrons can live long enough in the free state.) This fact has been confirmed experimentally. If the chamber is moved toward the source, the effective temperature of the recorded neutrons drops with the square of the distance, while their number remains constant (until the breakdown of the Maxwellian distribution, the $1/v$ detection law, or the inverse square law sets in). With a BF_3 chamber, the number of slow neutrons is too great for the collecting voltage at present available. Descriptions of the modulating circuits will be given together with reports of preliminary absorption and scattering experiments.

2. Excited State of He^3. L. I. Schiff,* *California Institute of Technology.*—Bonner's recent experiments indicate the existence of a bound excited state of He^3 about 2 Mev above the ground state. Since this is probably a P state, it involves interactions that are not determined by the normal state energies of the light nuclei or by existing data on scattering. The variational method with a two-parameter wave function yields no bound excited state when the usual saturating forces are used. Since this method with a similar wave function gives 0.75 of the ground state energy of He^3, and since the excited state is well bound (3.5 Mev below the continuum of a deuteron plus a proton), one would expect the variational method to yield fairly accurate results. In order to obtain a state in roughly the indicated place with two-body non-spin orbit interactions, it is necessary to use strongly non-saturating forces between both like and unlike particles; these forces just avoid binding the ^1P and ^3P deuteron and ^3P di-neutron and di-proton. Such interactions would probably cause serious difficulties with the systematics of nuclei.

* National Research Fellow.

3. The Electrical Axis of the Heart by Direct Observation. W. H. Jordan, *University of South Dakota.*—The usual method of finding the direction of the heart axis is to analyze the electrocardiograms taken with three successive connections to the body. Now a circuit has been developed whereby the direction of the heart axis can be seen directly by observing the trace of the electron beam on a standard cathode-ray tube. The customary three leads to the right arm, left arm, and left leg are employed. The bioelectrical potentials developed are amplified by three amplifiers star connected. The amplified voltage can be connected to a special triple axis cathode-ray tube

as shown by Hollman[1] or to the usual type of cathode-ray tube containing only horizontal and vertical deflecting plates. The connections necessary to maintain proper magnitude and phase relationships in the latter case are described.

[1] Hollman, Electronics, Jan. (1938).

4. Vitrification and Crystallization of Living Cells at Low Temperature. ALEXANDER GOETZ AND S. SCOTT GOETZ, *California Institute of Technology.*—The conditions which determine whether a liquid when cooled far below its melting point will enter the crystalline or the vitreous state are studied on live organic cells (Saccharomyces Cerevisiae). Substantial evidence has been found that the capacity for life ceases with crystallization of the cell plasma and that it is preserved when the physical conditions of cooling favor vitrification. The cooling rate (dT/dt) was varied from 10°–10^4 deg. sec.$^{-1}$ down to final temperatures (T_0) of −185°C and −252°C. It was found that for the same T_0 the cooling rate controls the death rate (δ) almost completely, as δ is larger than 75 percent when crystallization is favored, whereas it can be decreased down to 3 percent under vitrifying conditions. The duration of exposure (τ) does not affect δ at −185°C if τ is varied by 10^3. The temperature T_0 below −185°C does not affect δ, although a considerable influence of τ was found at −50°C. Repeated exposures of the same cells under conditions not especially favoring vitrification were studied and the integral death rate (δ_n) after the nth exposure was checked against the expectancy for an invariance of δ with n. It appears that $\delta(n)$ is not controlled by simple probability relations and that factors of biological nature enter.

5. Constitution of the Solfataric Gases at Kilauea Volcano, Hawaii. STANLEY S. BALLARD, *University of Hawaii.*—A preliminary analysis of the gases emanating at the Sulfur Bank near Kilauea Volcano has been completed. The purpose was to establish the identity of all constituents other than the obvious steam and sulfur vapor. Chief collections were made in September, 1936, and August, 1937. A combination of chemical and spectroscopic methods of analysis was used. The chief constituent (other than steam) proved to be sulfur dioxide, which constituted as much as 90 percent of some samples. Carbon dioxide was present in amounts equal to about one-twelfth the sulfur dioxide content. Oxygen and nitrogen were present always approximately in the normal atmospheric ratio, but in absolute amounts which varied widely from sample to sample. Argon was present in the nitrogen residues, but no other rare gases were detected. No significant trace of the combustible gases ordinarily associated with volcanism was detected in any sample. In general these results do not seem to be incompatible with the partial analyses of Allen[1] made in 1922, although it may be that the sulfur dioxide content has increased since that time. Acknowledgment is made of the collaboration of Professor John H. Payne in the chemical aspects of the analysis.

[1] E. T. Allen, Bull. Hawaiian Volcano Observatory **10**, 89 (1922).

6. Alterations in the Near Infra-Red Absorption Spectra of Water and of Protein Molecules when Water is Bound to Gelatin. JOSEPH W. ELLIS AND JEAN BATH, *University of California at Los Angeles.*—The absorption spectrum of a 0.20 mm oven-dried gelatin specimen consists entirely of two CH bands (1.72 and 2.28 μ) and three NH bands (1.50, 2.05 and 2.18 μ) in the 1–2.5 μ region. A similar specimen, having absorbed from a saturated atmosphere water equal to 35 percent of the total weight, shows the CH bands unaltered but the NH bands diminished in intensity. Another specimen similarly swollen with 99.9 percent D_2O shows the NH bands more nearly obliterated. In the $(\nu_\sigma+\nu_\pi)$ band of light and heavy water (1.44 and 1.99 μ, respectively) and in the $(\nu_\sigma+\nu_\delta)$ band of light water (1.91 μ), portions of both the high and low frequency sides are missing, indicating the absence or diminution in number of both vapor-like and the most highly perturbed water molecules. The $(\nu_\sigma+\nu_\delta+\nu_R)$ band of light water at 1.79 μ (ν_R=hindered rotation frequency) is sharpened in the swollen gelatin spectrum. An analogous band $(\nu_\sigma+\nu_\pi+\nu_R)$ at 1.35 μ appears for the first time. All the alterations cited in the water and protein bands indicate, or are consistent with the hypothesis, that the water molecules taken on by the gelatin from a saturated atmosphere are bound to NH or NH_2 groups by means of hydrogen bridges.

7. α-Particles from the Disintegration of Lithium by Deuterons. H. STAUB* AND W. E. STEPHENS, *W. K. Kellogg Radiation Laboratory, California Institute of Technology.*—Using an ionization chamber and linear amplifier with high differentiality the number-range curve of α-particles arising from disintegration of Li by deuterons was taken at 800 kv peak. The continuous distribution due to the reaction:

$$Li^7+D^2\rightarrow n^1+Be^8;\ Be^8\rightarrow 2He^4 \qquad (1)$$

was observed, ranging up to about 7.7 cm. On it was superimposed a homogeneous group agreeing in its 7.6 cm mean range, within the limits of error and when corrected to the same voltage, with one observed by Williams, Shepherd and Haxby[1] and ascribed by them to the reaction

$$Li^7+D^2\rightarrow He^4+He^5. \qquad (2)$$

This leaves the He^5 unstable by 0.8 Mev. In our experiment the peak at 7.6 cm is, as in reference (1), somewhat wider than the peak observed at 13.0 cm, due to the reaction

$$Li^6+D^2\rightarrow 2He^4, \qquad (3)$$

which has a width of about 0.9 cm at half-maximum. An estimate based on the theory of Bethe and Livingston[2] shows that this width is entirely due to the deep penetration of the deuterons at the high bombarding voltage of 0.8 Mev. The numbers of disintegrations at 0.8 Mev for the three processes are found to be in the ratio 50 : 10 : 1 for (1), (2) and (3) respectively. Similar ranges and intensity ratios were obtained when the counter was biased low to give the integral number-range curve.

* International Exchange Fellow.

[1] Williams, Shepherd and Haxby, Phys. Rev. **51**, 888 (1937); **52**, 390 (1937).

[2] Bethe and Livingston, Rev. Mod. Phys. **9**, 286 (1937).

8. Neutrons from the Break-Up of He^5. W. E. Stephens and H. Staub,* *W. K. Kellogg Laboratory, California Institute of Technology.*—We have reinvestigated[1] the energy spectrum of the neutrons from the disintegration of lithium by 0.8 Mev (a.c.) deuterons in the region from 2 Mev to 6 Mev. A sharp drop in the number of neutrons at 3.8 Mev is interpreted as the high energy limit of the continuum of neutrons from the two stage reaction

$$Li^7+D^2\rightarrow He^5+He^4+Q_1 \quad (1)$$

$$He^5\rightarrow He^4+n^1+Q_2. \quad (2)$$

Williams, Shepherd and Haxby[2] have established the existence of reaction (1) and have determined the value of Q_1 to be 14.3 Mev. Using this value and the known masses, the value of Q_2 is calculated to be 0.8 Mev. For a bombarding energy of 0.8 Mev for the deuterons, the neutron continuum can be calculated to extend from 0.1 Mev to 3.8 Mev. Since this continuum is superimposed on the neutrons from the reaction

$$Li^7+D^2\rightarrow Be^8+n^1+Q_3 \quad (3)$$

and probably some from Li^6, all that can be observed with certainty is the high energy cut off. From the value of 1 to 5[3] for the relative yield of reaction (1) to reaction (3) at our bombarding voltage, we can estimate that reaction (2) accounts for most of the neutrons giving the sudden rise. It may be, however, that some of them are due to the reaction

$$Li^6+D^2\rightarrow Be^7+n^1+Q_4 \quad (4)$$

as suggested by Roberts and Heydenburg.[4]

* International Exchange Fellow.
[1] Bonner and Brubaker, Phys. Rev. **48**, 742 (1935).
[2] Williams, Shepherd and Haxby, Phys. Rev. **52**, 390 (1937).
[3] See preceding abstract.
[4] Abstract 78, Washington meeting (1938).

9. Radiative Losses by Particles of Anomalous Magnetic Moment. Samuel B. Batdorf and Erich W. Beth, *University of California.*—The fact that the absorption of the penetrating constituent of cosmic radiation is intermediate between expected values for electrons and for protons is generally explained by the assumption of an intermediate mass. It is difficult to draw conclusions about the mass due to the possibility of writing a Dirac type equation for a particle with arbitrary magnetic moment; a suitable choice of magnetic moment might render such a particle highly penetrating. The radiative losses were accordingly calculated by the von Weizsäcker method, the bremsstrahlung being first treated in the reference system in which the cosmic-ray particle is originally at rest and the results then transferred by a Lorentz transformation to the coordinate system at rest with respect to the nucleus. We find that, while we can choose the magnetic moment so that the radiative losses increase by any desired amount, they can be decreased by only a very small fraction by choice of the magnetic moment. We conclude that a particle of this type must have a mass much larger than the electron mass in order to account for the penetrating constituent of cosmic radiation.

10. Mass of Cosmic-Ray Particles. R. M. Langer, *California Institute of Technology.*—A wide range of heavy electron masses in the cosmic radiation would lead in a particular cloud chamber to a distribution of measurable values of mass in a restricted region according to the upper limit of $H\rho$ measurable in the apparatus. For a limiting $H\rho$ equal to 10^5 the favored mass is about 10^2 electron masses. For smaller $H\rho$ neither the heavy nor the light electrons will be very penetrating. This can be shown easily with the help of curves connecting energy, energy loss, mass and $H\rho$. Moreover chambers with higher limiting $H\rho$ will get measurable tracks much faster than those with lower limits and heavy tracks due to lighter masses will remain relatively rare. For lighter masses other forms of detection are advantageous. The lighter electrons may appear in showers and account for the narrow pencils of straight tracks sometimes observed. The second maximum in shower frequency at about 20 cm of lead is just what would be expected if most of the electrons producing the showers had a mass of about 3 electron masses. A particularly interesting estimate of mass can be made from data published by Ehrenfest[1] who mentions a particle whose change in $H\rho$ indicates a mass of about 7 electron masses.

[1] P. Ehrenfest, Jr., Comptes rendus **206**, 428 (1938).

11. Measurements of the Mobility of Potassium Ions at High Field Intensity and Low Pressure. Allen V. Hershey, *University of California (Introduced by Leonard B. Loeb).*—The mobility of potassium ions at high field intensity and low pressure has been measured by the Townsend deflection method in the gases H_2, He, N_2, and A. The product of mobility and pressure should be a function of the ratio of field intensity to pressure. Thus, at a given value of E/p (E=field intensity in volts per cm; p=pressure in mm Hg), the product kp (k=mobility in cm per sec. per volt per cm) should be the same at all pressures. This was found to be true at the highest pressures investigated but not at the lowest, apparently because of a breakdown in the method, rather than a true variation in mobility. At a small value of E/p, the results agreed to within a few percent with the measurement by Tyndall and Powell[1] and by Powell and Brata.[2] As E/p is increased, the mobility at first rises, passes through a peak, and then diminishes. The initial rise in nitrogen has been reported by Mitchell and Ridler.[3] Pronounced peaks were obtained in H_2, N_2, and A, but not in He.

[1] Tyndall and Powell, Proc. Roy. Soc. **136A**, 145 (1932).
[2] Powell and Brata, Proc. Roy. Soc. **138A**, 117 (1932).
[3] Mitchell and Ridler, Proc. Roy. Soc. **146A**, 911 (1934).

12. Resonance Broadening of Spectral Lines. W. V. Houston, *California Institute of Technology.*—The radiationless transfer of excitation energy from one atom to another during a collision is one cause of the broadening of spectral lines. It can be shown that the broadening produced in this way is the same for all members of a multiplet, in agreement with the observations, but considerably less in magnitude than that observed. Another source of broadening can be found in the coupling between the motion of the whole atom and the electronic motion. This also is the same for all members of a multiplet, and broadens a line to about the same extent as the first cause.

13. Absorption of Sound in Carbon Dioxide and in Carbon Disulphide. V. O. KNUDSEN AND E. FRICKE, *University of California at Los Angeles.*—Sound absorption measurements in pure CO_2 at atmospheric pressure and 22°C have been conducted which, together with measurements by Curtis, confirm the collision theory of anomalous absorption as developed by Einstein, Kneser, and others. The absorption coefficient is appreciable at frequencies as low as 2000 cycles, and increases to a maximum of 0.317 per wave-length at 77,000 cycles. This maximum is higher than values obtained by previous workers, and indicates that both the deformation and symmetrical valence vibrations participate in the exchanges between translational and vibrational energy. Small impurities, as water or alcohol vapors, affect the absorption greatly; the entire absorption band is shifted to higher frequencies. Measurements in mixtures of CO_2 in O_2 and CO_2 in N_2 indicate that neither the O_2 nor N_2 is appreciably excited by collisions with CO_2. Measurements in CS_2 reveal an absorption similar to that for CO_2 except that the absorption begins at about 10,000 cycles. In mixtures of CS_2 and O_2, the observed absorption at frequencies below 10,000 cycles is accounted for by assuming that only the vibration of O_2 molecules is excited by collisions with CS_2 molecules; at higher frequencies the CS_2 molecules also are excited, principally by collisions with other CS_2 molecules.

14. A Probe Investigation of Anode Spots. J. E. HENDERSON AND S. M. RUBENS, *University of Washington.*—Anode spots are readily produced in a glow discharge maintained in the chamber formed between two concentric copper spheres of diameters 53.4 and 5.08 cm, the inner sphere being anode. These spots are striking in appearance, especially since they arrange themselves in symmetrical patterns over the surface of the anode. Pressure, current density, and surface conditions of the anode determine the number and size of the spots in agreement with earlier work.* Similar conditions prevail when the inner sphere is replaced by a thin disk, the spots first appearing near the edge where the field is greatest. Space potentials, electron concentrations, and electron temperatures measured in the plasma surrounding the spots with a cylindrical Langmuir probe indicate that the spots are sheaths possessing a positive space charge. This accounts for the symmetrical arrangements observed. A spot having the same properties as the others could be formed at will on a small insulated disk mounted flush with the anode surface if the potential of the disk was raised to a suitable potential above the anode depending on the gas, pressure, and current density.

* C. H. Thomas and O. S. Duffendack, Phys. Rev. **35**, 72 (1930).

15. Spherical Ground Joints for Vacuum Systems. S. M. RUBENS AND J. E. HENDERSON, *University of Washington.*—The problem of providing for a universal type of motion of a probe employed in some glow discharge investigations was solved by using a ground glass joint of which the surfaces in contact were sections of spheres. Such surfaces are readily formed by blowing the glass into simple molds. The grinding is easily accomplished by rotating and rocking the convex surface within the concave one with a random motion. The closeness of contact between the surfaces is far superior to that of the ordinary conical ground joint. Joints of this type exhibit unusual flexibility and seem to have numerous applications besides the one indicated. A five way stopcock has been constructed on this principle. Samples of these devices will be exhibited.

16. The Probable Ionization of High Speed Electrons in Nitrogen. ROBERT B. BRODE AND DALE R. CORSON, *University of California.*—The ionization due to high speed electrons has been measured by counting the drops in the cloud chamber tracks. By delaying the expansion about $\frac{1}{2}$ second after the passage of the ionizing particle the tracks were broadened by diffusion so that counting was easy and reliable. The energy of the particle was obtained from the deflection of the track in a magnetic field. Tracks from 10 to 30 cm in length were counted in fields from 800 to 2500 gauss. The ionization as determined by these drop counts decreased rapidly from about 100 drops per cm in 1 atmosphere of nitrogen at an energy of 10^5 ev to a minimum of 50 drops per cm at 2×10^6 ev. With increasing energy the ionization increased to about 70 drops per cm at 10^8 ev. These measurements are in good agreement with the theoretical prediction for the variation of ionization with energy for electrons in this energy range.

17. The Beilby Layer on Thin Ground Quartz Crystals. F. R. HIRSH, JR., *California Institute of Technology.*—A ground quartz crystal with the two sides of unequal roughness was found to give spuriously double spectral lines, the stronger component of which came from the rougher side, i.e. the reflection here is apparently a surface phenomenon alone due to a disturbed (Beilby) layer of a crystalline nature. With light etching by use of H_2F_2 these surface reflections weaken and reflection starts from the Bragg planes in the crystal body; this is evidenced by the filling in of the space between the spurious double components with reflected x-ray energy. If the crystal is etched heavily (42 hours in 50 percent H_2F_2) the two spurious spectral line components disappear, leaving between their former positions a single line of true Laue reflection origin. This result supports the idea that the ground crystal is covered by a crystalline Beilby layer of atoms aligned by the external fields of the crystal itself. If the curved crystal distorted elastically throughout its entire radial thickness, the two surface layer reflections would merge due to exact focussing. That it does not occur, is evidence that the surface (Beilby) layer differs in physical nature from the crystal body.

18. Evidence for Surface Layers in Cleaved Calcite Crystals. V. L. BOLLMAN AND JESSE W. M. DUMOND, *Occidental College and California Institute of Technology.*—In a continuation of earlier work[1] radiation from a molybdenum target x-ray tube was passed through a slit of a precision transmission spectrometer and then through a thin cleaved calcite crystal. The spectral lines obtained on a photographic film were found to be double and to exhibit marked fluctuations in intensity along the lines. From the geometry of the arrangement it was concluded that the

radiation producing the double lines came from the entrance and exit surfaces of the calcite crystal. Other tests led to the conclusion that the intensity fluctuations along the lines were produced by disturbances on the surfaces of the crystal. Recently another series of tests has been made with the same apparatus. A cleaved crystal exhibiting the properties mentioned above was etched one face at a time and exposures taken to ascertain the nature of the reflections. Mild etching with 0.7 *N* HCl according to a technique worked out by Manning[2] failed to affect the nature of the photographic pattern. Prolonged etching, however, removed the sharp line reflections, coming from the surfaces. A less well-defined fainter line then appeared in a position between the "surface" lines. This latter trace showed no sign of intensity fluctuation along the length of the line.

[1] DuMond and Bollman, Phys. Rev. **50**, 97 (1936).
[2] K. V. Manning, Rev. Sci. Inst. **5**, 316 (1934).

19. Photoelectric Long Wave-Length Limit of Magnetized Iron. DONALD H. LOUGHRIDGE AND N. KERMIT OLSEN, *University of Washington.*—The photoelectric current from a cylindrically shaped piece of iron is measured with a FP-54 bridge circuit when the iron is subjected to field strengths from zero to 5000 gauss. These readings are taken for different wave-lengths and plotted on Fowler curves to obtain the threshold frequency of the iron. Acceleration potentials always in excess of that required for saturation are used on the photo-cell. The effect is most pronounced near the long wave-length limit of the iron, and the change in the threshold frequency of the iron due to the magnetic field is derived from proper treatment of the Fowler curves. The effect is of the order of a few angstroms for the data taken up to date. Alternate readings of photoelectric current, with magnetic field on and off, are taken to minimize the effect of such unavoidable sources of fluctuation as arc intensity, electrometer tube adjustments, and temperature changes. The threshold frequency of the iron is about 2600 angstroms, which checks the value given by Cardwell.

20. Spark Breakdown Potentials in A, N_2 and H_2 for Pt and Na Cathodes. FLORENCE EHRENKRANZ, *University of California (Introduced by Leonard B. Loeb).*—Curves were obtained for sparking potentials between fixed plane parallel electrodes in pure mercury-free argon, nitrogen and hydrogen for Pt and Na cathodes as a function of the pressure times the plate separation. The effect of heated Pt and Na cathodes on the sparking potentials in hydrogen was investigated. The presence of Na lowers the sparking potentials near the minimum by 50 percent, 28 percent, and 30 percent in A, N_2 and H_2, respectively. The percentage lowering is 7.5 for $p\delta$ equal to 240 mm×cm in A, 20 for $p\delta$ equal to 360 in N_2, and 11 for $p\delta$ equal to 320 in H_2. Predischarge currents with Pt cathodes were less than 10^{-9} amp.; with Na cathodes, currents of 360 microamperes at $p\delta$ equal to 356 in N_2 and of 8 microamperes at $p\delta$ equal to 320 in H_2 occurred. Sparking potentials in H_2 with heated Pt and Na cathodes are identical within the limits of experimental accuracy. The probable explanation of this result is that the formation of NaH removes all of the Na and destroys the volatile substance which causes the lowering in the cold Na experiments.

21. Angular Distributions of Recoil and Photoelectrons Produced by 300 to 800 kv X-Rays in Nitrogen. HAROLD TRUEBLOOD AND DONALD H. LOUGHRIDGE, *University of Washington.*—By the use of an automatically controlled cloud chamber, and the 800,000-volt x-ray tube of the Swedish Hospital, Seattle, a large number of photographs have been made of the effects of high voltage x-rays passing through nitrogen. A magnetic field of about 400 gauss enabled the energies to be measured. Recoils were distinguished from photoelectrons by the criterion of the maximum energy allowable from Compton's formula as a function of the angle. Curves plotted with total electrons, at a given ejection angle, against energy show a definite break at the calculated value of the Compton energy. The experimental angular distribution curves for the recoils fit well with the Klein-Nishina distribution. The gradual shift in the most probable angle of ejection for photoelectrons, as a function of the energy, checks well with the Sommerfeld calculations in this region.

22. Long Period Radioactive Zinc. J. J. LIVINGOOD AND G. T. SEABORG, *Radiation Laboratory, University of California.*—A chemically identified radioactive zinc isotope, produced by irradiating zinc with 8 Mev deuterons, has been found to have a half-life of 7 months. Positrons are emitted, which definitely identifies the activity with Zn^{65}. Electrons are also observed, as well as an anomalously high ratio of gamma-rays to particles; this indicates *K* electron capture as an alternative method of decay. An activity with this period and similar characteristics of radiation has recently been reported[1] after proton bombardment of copper; this is consistent with the above isotopic identification.

[1] S. W. Barnes and George Valley, Bull. Am. Phys. Soc. **13**, No. 2, 40 (1938).

23. Normal Modes of Vibration of a Body-Centered Cubic Lattice. PAUL FINE, *California Institute of Technology.*—The frequencies of the normal vibrations of a body-centered cubic lattice have been calculated for atomic constants obtained from the elastic constants of tungsten. The results suggest an approximation to the frequency distribution which takes into account the atomic nature of the crystal. The vibrations are found to fall into three groups, each having the same kind of distribution, which is characterized by a frequency of maximum probability computed from the elastic constants. From these frequency distributions the specific heat due to the atomic vibrations is calculated. The model used, in which elastic forces between atoms are assumed, leads to the Cauchy relations between the macroscopic elastic constants, and these are satisfied only approximately for tungsten and not at all for many other substances. According to Fuchs,[1] the failure of the Cauchy relation for monovalent metals is due solely to the influence of the electrons on the compressibility of the crystal. If then the compressibility is determined from the other elastic constants by means of the Cauchy relation and this value is used in calculating the characteristic frequencies, the

specific heat obtained differs from that observed by an amount which may be attributed to the electronic contribution.

[1] K. Fuchs, Proc. Roy. Soc. **A153**, 635 (1936).

24. Magnitude of Accelerated Current in the Cyclotron. ROBERT R. WILSON, *Radiation Laboratory, University of California.*—The magnitude and distribution of the ion currents accelerated in the Berkeley cyclotron have been measured by means of a water-cooled probe introduced between the accelerating electrodes or dees and noting the heating of the water. As the probe is moved inward, this current is found to increase linearly from zero at the outside edge of the dee to a large value of about one-half of a milliampere of deuterons when the probe is in about one-sixth of the distance into the center. At this position apparently all the beam is being intercepted, and moving in farther does not give an appreciable increase of current. Measurements on the initial ionization at the center indicate that approximately all the available ions are being accelerated. Under more favorable running conditions, it is expected that there is easily as much as one milliampere of six to nine million volt deuterons circulating within the dees. Of this only ten percent is withdrawn by the deflector; henceforth the large circulating current will be used, especially for long bombardments, by introducing targets directly into the circulating beam at various positions which will not seriously interfere with the deflected beam.

25. The Objective Quantitative Definition of the Graininess of Photographic Emulsions. A. DEMBER, A. GOETZ AND W. O. GOULD, *California Institute of Technology.*—Methods to determine the graininess of photographic emulsions objectively have only been developed recently and consist so far in measuring the average transparency fluctuation. The method analyzed here bases on the evaluation of a microphotometric record representing the relative transparency fluctuations ($\Delta T/T_m$) of a uniformly exposed area of the emulsion. Besides the sum of the fluctuations, the distribution of the areas they occupy as a function of their magnitude can be determined. The graininess (G) is defined from the distribution (probability) function $\pi = C/G \cdot \exp -[\Delta T/(T_m G)]^n$; it indicates the inverse rate of decline of the occurrence of relative transparency fluctuations with the deviation from the average transparency (T_m). For evaluating the microphotometric records an analyzer is used, allowing the direct reading of the probability integral function. Thus the numerical value of G is obtained; furthermore the distribution law, determined by the exponent n, is checked with each measurement, accidental disturbances in the emulsion can thus be eliminated. The value of n is found $\leqq 2$; therefore a Gaussian (statistical) distribution gives a close representation. The numerical value of G depends on the scanning area (α) of the microphotometer, so for obtaining comparable values this area has to be kept constant. Otherwise a correction according to the function $G(\alpha)$ has to be applied.

26. An Instrument for the Objective and Quantitative Determination of Photographic Graininess. W. O. GOULD, A. GOETZ AND A. DEMBER, *California Institute of Technology.*—The instrument consists of a microphotometric recorder and a photoelectric integrator. In the former unit the relative transparency fluctuations ($\Delta T/T_m$) of a uniformly exposed section of an emulsion are recorded under high resolving power and magnification by means of a photo-cell, the amplified output of which is traced with a high frequency galvanometer on 35 mm film. The motion of the latter is coordinated with that of the emulsion. A variable area record is thus produced which represents truly $\Delta T/T_m$ of the emulsion area scanned (0.2 mm^2). This record is analyzed by the integrator as follows: It is placed on a revolving drum and scanned by an illuminated slit. The light transmitted falls upon a photo-cell. Its current is thus proportional to the average occurrence of $\Delta T/T_m$ for a value of transparency determined by the lateral position of the slit on the record. As the slit is moved slowly across the record the shape of the transparency distribution function is obtained. The current is measured with a scale consisting of a family of distribution curves plotted in polar coordinates for different graininess parameters. The scale is rotated synchronously with the slit motion. The indicating light beam selects and follows a particular distribution curve as the slit is moved, thus evaluating numerically the graininess.

27. A Search for an Electrostatic Analog to the Red Shift. H. T. DRILL, *University of Washington (Introduced by J. E. Henderson).*—The existence of a gravitational red shift suggests the possibility of a like dependence of frequency upon electrostatic potential. A search for such an effect was carried out by Kennedy and Thorndike[1] in 1931. The frequency shifts quoted by them, although within their quoted probable error, were very close to their probable error, suggesting the possibility that further refinements might yield positive results. As the interferometer used by them was available and not easily improved, an increase in sensitivity was most readily obtained by increasing the potential difference between the light source and interferometer. This was accomplished by mounting the mercury arc used as a source within the sphere of a Van de Graaf generator. The generator was operated at 300 kilovolts, both positive and negative with respect to the interferometer. This is approximately six times the potential difference used by Kennedy and Thorndike. The frequency changes observed were well within the probable error for the light source at both positive and negative potentials, indicating a frequency change of less than one part in 10^{15} per volt. This is clearly a null result.

[1] R. J. Kennedy and E. M. Thorndike, Nat. Acad. Sci. **17**, 620–622.

28. The Separation of Radioactive Substances Without Use of a Carrier. D. C. GRAHAME AND G. T. SEABORG, *University of California.*—Carefully purified gallium-free zinc was bombarded with 8 Mev deuterons in the Berkeley cyclotron to form radioactive gallium. It was found possible to extract radioactive gallium chloride with pure ether from an aqueous solution[1] (6N in HCl) without the addition of inactive gallium chloride as a carrier. The partition coefficients between the liquid phases for the chlorides of Ga^{68} (1 hr.)[2] and Ga^{67} (83 hr.)[3] were found to be identical

with those observed for gallium chloride in ordinary amounts. Long lived radioactive cobalt isotopes are formed by the bombardment of iron with 6 Mev deuterons.[4] The minute amounts of cobalt thus formed were found to be distributed between liquid phases in the same manner as cobalt in larger amounts. The distribution of minute quantities of cobalt chloride between water and ether was not changed by the presence of relatively large amounts of inactive ferric chloride. The use of extraction methods offers a simple means of separating completely and in the most concentrated form the radioactive isotopes of many elements.

[1] Noyes and Bray, *Qualitative Analysis for the Rare Elements* (Macmillan Co., 1927), p. 151.
[2] Livingood, Phys. Rev. **50**, 425 (1936).
[3] Alvarez, Phys. Rev. **53**, 606 (1938).
[4] Livingood, Seaborg and Fairbrother, Phys. Rev. **52**, 135 (1937).

29. On the Viscosity of Nonpolar Liquids. S. KYROPOULOS, *California Institute of Technology* (*Introduced by A. Goetz*).—The phenomenon of viscosity drop by flow orientation (mechanical orientation in a Couette apparatus) with nonpolar, extremely dissymmetrical molecules, points to a marked influence of the dissymmetry of polarizability on this phenomenon and on viscosity in general. In such liquids the forces of interaction are practically confined to the dispersion forces and there are very definite states of minimum mutual potential energy. This results in the temporary formation of complexes of higher saturation of those residual fields of force which interact in the phenomenon of viscosity. An analogous case is represented by long chain hydrocarbon molecules with polar head, where dipole forces are eliminated to a great extent, insofar as viscosity is concerned, by association, resulting in a viscosity behavior similar to corresponding paraffins. With small molecules, even small permanent moments tend to suppress the influence of the optical anisotropy, resulting in a type of complexes which is ultimately, even temporarily, strongly determined by the dipole forces.

30. A Search for Temperature Changes Accompanying Field Emission at High Temperatures. G. FLEMING AND J. E. HENDERSON, *University of Washington*.—In work previously reported[1] a search was made for temperature changes of a field emitter at room temperature; no temperature change of as much as 1°C was observed. Using similar apparatus this same type of investigation has been extended up to the thermionic region. Gold and platinum thermocouples fashioned into points (one sharp and one dull) were placed in opposition and used as emitters up to the melting point of gold. Similar measurements were made to approximately 1600°K using tungsten-platinum thermocouples. Heating was accomplished by 500-cycle currents from which the d.c. instruments were protected by high inductances. Total field currents as large as three milliamperes were used. Even up to temperatures at which a minute thermionic emission occurred, there was found no temperature change of more than 2°C, the estimated uncertainty in the measurements. The result indicates that below the temperature at which thermionic emission sets in strongly only a small portion of the total number of electrons emitted partake of the thermal energy of the metals studied.

[1] J. E. Henderson and G. M. Fleming, Phys. Rev. **48**, 486 (1935).

31. The First and Second Townsend Ionization Coefficients for Pure H_2. DONALD H. HALE, *University of California* (*Introduced by Leonard B. Loeb*).—Experiments were made to determine the Townsend coefficients for ionization by collision in pure H_2. Precautions were taken to exclude Hg vapor from the ionization chamber. The experiments were carried out using the method developed by Bowls.[1] The values of α/p plotted as $f(X/p)$ show wide variations from a similar curve plotted from the values of Townsend and Hurst[2] for experiments carried out in H_2 which was contaminated with Hg. The values of α/p for the Hg free H_2 are lower by as much as thirty percent for values of X/p below 300. The curve of β/p plotted as a $f(X/p)$ shows a well-defined peak at an X/p of 100. It then decreases reaching a minimum at an X/p of 200 and shows a gradual increase at the higher values of X/p. The curve of values of γ $(=\beta/\alpha)$ plotted as $f(X/p)$ shows a similar peak at an X/p of 100. These peaks are much like those found by Bowls[1] for pure N_2. However, in H_2 they occur at slightly lower values of X/p and are less pronounced.

[1] Bowls, Phys. Rev. **53**, 293 (1938).
[2] Townsend and Hurst, Phil. Mag. **8**, 738 (1904).

32. Motion Picture Polarigraph for Sky Light Investigations. WILLI M. COHN, *Berkeley, California*.—An instrument has been developed for replacing visual measurements of polarization, transmission, etc., by permanent records. A modified Martens polarization photometer is connected with a motion picture camera. The Nicol prism rotates, and the photometric field is photographed every ten degrees. The position of the Nicol prism is indicated on each record. The intersection of the density curves for the two halves of the photometric field is determined. A set-up is presented for the rapid determination of the polarization of the entire vault of the sky. It is outlined that the polarization of sky light seems to be a very sensitive supplement to routine measurements of radiation from sun and sky and of the turbidity of synoptic air masses. It seems desirable to find out if, for instance, the approach of typhoons may be predicted from polarization measurements, since changes in the polarization of sky light seem to occur a long time before any clouds, etc., appear. Further applications of the instrument are obvious for polarimetric work in the laboratory and in the plant, whenever visual determinations should be replaced by permanent records, for instance in connection with sugar analysis, biological, and medical work, etc.

33. Where Does the Light of the Night Sky Originate? JOSEPH KAPLAN, *University of California at Los Angeles*.—It is generally agreed that the light of the night sky originates higher in the atmosphere than do most auroral displays. Cabannes and Dufay, by an experimental procedure of not great accuracy, place this level between 200 km and 300 km. The writer has produced afterglows in very weakly excited nitrogen, at low pressures, which agree with the light of the night sky and give evidence of its

high origin. Recent experiments on afterglows in nitrogen at pressures around 30 mm indicate an origin of some of this light as low as the lowest auroral displays. In fact, the best laboratory reproduction of a night sky spectrum has been produced in these high pressure glows. Such features as the Vegard-Kaplan bands, first positive bands originating on very high vibrational levels, second positive bands, cyanogen tail bands, the new 3471 line of nitrogen, and absence of the first negative bands, are prominent in these afterglows. These are all definite or highly probable characteristics of the light of the night sky. Although the two red lines of oxygen probably originate at higher levels, it seems reasonable to suggest that most of the radiation originates in the lower regions of the upper atmosphere.

34. On Neutron Stars. F. ZWICKY, *California Institute of Technology.*—(a) Collapsed neutron stars,[1, 2] according to present knowledge, represent *states* of *lowest energy* that matter may assume without being completely transformed into radiation. (b) The transformation of stellar matter into the neutron state may occasionally proceed very rapidly. The stupendous rate at which energy was liberated in some of the recently observed super-novae may thus find an explanation. (c) The relative change of frequency due to the gravitational redshift of light originating on the surface of neutron stars tends in limiting cases toward unity. Such redshifts may be observable in super-novae and in their remains. (d) According to the general theory of relativity the mass of a star of given density cannot surpass a certain critical value (Schwarzschild limit). At this limit the energy liberated because of gravitational packing is $(1-4/3\pi)Mc^2=0.58Mc^2$, where M is the *proper mass* of the star. The derivation of this result which was obtained in discussion with Professor R. C. Tolman will be communicated elsewhere. For neutron stars the *limiting* proper mass is approximately $M_L=R^{3/2}m_N=1.8\times10^{35}$ grams, where $R=e^2/\Gamma m_P m_e=2.29\times10^{39}$ is the ratio of the electrical to the gravitational attraction between a proton and an electron and m_N is the mass of a neutron.

[1] W. Baade and F. Zwicky, Phys. Rev. **45**, 138 (1934) and **46**, 76 (1934). Proc. Nat. Acad. Sci. **20**, 259 (1934). See also F. J. M. Stratton, *Handbuch der Astrophysik*, Vol. 7 (1936), p. 671.
[2] F. Zwicky, The Scientific Monthly **40**, 461 (1935).

35. The Diurnal Variation of Atmospheric Condensation Nuclei. N. E. BRADBURY AND H. J. MEURON, *Stanford University.*—Continuous records of the diurnal variation of the density of atmospheric condensation nuclei have been obtained over a period of four months. The apparatus employed consists of a Wilson cloud chamber with an expansion ratio of 1.15. At regular intervals the air in the chamber is replaced by a fresh sample, saturated with water vapor, and subjected to an expansion. A beam of light passing through the chamber is diminished in intensity by the resulting fog, and the degree of extinction may be related to the nuclei density. The diurnal variation in nuclei density shows a definite forenoon and evening maximum with a pronounced minimum prior to sunrise and a mid-day minimum of lesser extent. Such a variation might be expected in the normal daily convective cycle. The average hourly values of nuclei density have been compared with the hourly averages of the local component of the diurnal variation of the earth's electric field for this station. The results indicate that in a large measure, if not entirely, the variations in the local component of the earth's potential gradient arise out of variations in the nuclei density.

36. A New Radiation Pyrometer for the Measurement of Low and High Temperatures. JOHN STRONG, *Astrophysical Observatory, California Institute of Technology.*—An instrument will be described which uses a thermopile to measure energy emitted at various wave-lengths in the spectral region between 6 and 35μ. The various monochromatic bands employed are obtained by successive reflections from crystal surfaces. The instrument may be used to measure the surface temperature of cold or hot solids. Also, it may be used to measure the temperature of gases, vapors and liquids, including clouds. The atmosphere is particularly transparent for the residual rays of quartz (8.9μ) and carborundum (12μ). Accordingly, these wave-lengths are useful for observation of temperatures where a long air path is involved. A resume of astronomical and meteorological observations will be given.

37. The Mechanism of the Positive and Negative Point Coronas in Air at Atmospheric Pressure. GERVAIS W. TRICHEL, *University of California (Introduced by Leonard B. Loeb).*—The current fluctuations in positive and negative point to plane corona have been studied by coupling a radio receiver and oscillograph to the corona circuit. Negative points supply sufficient electrons by secondary processes at the point. The ionization by electron avalanches builds a space charge which in $\sim10^{-8}$ sec. chokes off the discharge. As the region is cleared of positive ions the current falls exponentially until the fields are restored to the firing value. The discharge frequency is regular, increases with applied potential, and is proportional to the current. The positive point corona consists of positive space charge streamers emerging from the whole point composed of electron avalanches propagated outward by photo-ionization in the gas. The diffusion of positive space charge eventually extinguishes the streamer and the arrival of a *negative ion* is required to start a new streamer. To do this, $X/p>90$ near the point to ionize the ion. The frequency of the streamer bursts for a fine point is from 3×10^5 to 2×10^6 per second. The mechanism of spark breakdown in positive point corona may be explained on this basis.

38. The Mechanism of the Positive Ion Emission from Catalysts. ALLEN V. HERSHEY, *University of California (Introduced by Leonard B. Loeb).*—It has been possible to draw some definite conclusions concerning the mechanism of the emission of positive ions from Kunsman catalysts as a result of experiences gained in a search for a pure source of ions. The catalysts are known to contain Fe, and a few percent each of Al_2O_3 and an alkali oxide, for example, K_2O. Since the potassium is present in chemical combination with oxygen, it cannot be emitted as an ion

without either the emission of O_2 or the removal of oxygen by some reducing agent. The iron effectively furnishes this reducing agent, and FeO is probably the product formed in accordance with the reaction

$$Fe+K_2O \rightarrow FeO+2K^+ +2e^-.$$

The metallic iron also facilitates the escape of the liberated electrons. The accumulation of FeO around the crystals of K_2O tends to block the emission of ions by preventing the passage of oxygen from the K_2O to the more distant Fe, and by obstructing the electrons. Variation in the emission under various conditions from an impure catalyst containing both sodium and potassium could be interpreted in terms of the inhibitory effect of the FeO.

Author Index to Abstracts

Alvarez, Luis—No. 1

Ballard, Stanley S.—No. 5
Batdorf, Samuel B. and Erich W. Beth—No. 9
Bath, Jean—see Ellis, Joseph W.
Beth, Erich W.—see Batdorf, Samuel B.
Bollman, V. L. and Jesse W. M. DuMond—No. 18
Bradbury, N. E. and H. J. Meuron—No. 35
Brode, B. and Dale R. Corson—No. 16

Cohn, Willi M.—No. 32
Corson, Dale R.—see Brode, B.

Dember, A.—see Gould, W. O.
——, A. Goetz and W. O. Gould—No. 25
Drill, H. T.—No. 27
DuMond, Jesse W. M.—see Bollman, V. L.

Ehrenkranz, Florence—No. 20
Ellis, Joseph W. and Jean Bath—No. 6

Fine, Paul—No. 23
Fleming, G. and J. E. Henderson—No. 30
Fricke, E.—see Knudsen, V. O.

Goetz, A.—see Dember, A.
——see Gould, W. O.
—— and S. Scott Goetz—No. 4
Goetz, S. Scott—see Goetz, A.
Gould, W. O.—see Dember, A.
——, A. Goetz and A. Dember—No. 26
Grahame, D. C. and G. T. Seaborg—No. 28

Hale, Donald H.—No. 31
Henderson, J. E.—see Fleming, G.
——see Rubens, S. M.
—— and S. M. Rubens—No. 14
Hershey, Allen V.—No. 11; No. 38
Hirsh, F. R., Jr.—No. 17
Houston, W. V.—No. 12

Jordan, W. H.—No. 3

Kaplan, Joseph—No. 33
Knudsen, V. O. and E. Fricke—No 13
Kyropoulos, S.—No. 29

Langer, R. M.—No. 10
Livingood, J. J. and G. T. Seaborg—No. 22
Loughridge, Donald—see Trueblood, Harold
—— and N. Kermit Olsen—No. 19

Meuron, H. J.—see Bradbury, N. E.

Olsen, N. Kermit—see Loughridge, Donald H.

Rubens, S. M.—see Henderson, J. E.
—— and J. E. Henderson—No. 15

Schiff, L. I.—No. 2
Seaborg, G. T.—see Grahame, D. C.
—— see Livingood, J. J.
Staub, H.—see Stephens, W. E.
—— and W. E. Stephens—No. 7
Stephens, W. E.—see Staub, H.
—— and H. Staub—No. 8
Strong, John—No. 36

Trichel, Gervais W.—No. 37
Trueblood, Harold and Donald Loughridge—No. 21

Wilson, Robert—No. 24

Zwicky, F.—No. 34